The momentum spectrum of cosmic ray muons above 300 GeV/c in the vertical direction

Piggott, J. L.

The Momentum Spectrum of Cosmic Ray Muons above 300 GeV/c in the Vertical Direction

by

J.L. Piggott, B.Sc.

A Thesis submitted to the

University of Durham for the

Degree of Doctor of Philosophy

November, 1975

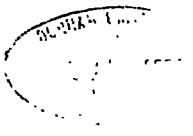

ABSTRACT

The sea-level vertical muon momentum spectrum has been measured in the momentum range 100 GeV/c to 3000 GeV/c, using the MARS spectrograph in Durham. The various instrumental effects which affect either the shape or the absolute intensity of the measured spectrum have been studied in detail.

The analysis procedure has been discussed in detail including the accuracy of the analysis technique and the criteria for rejection of certain events.

A simple muon production and propagation model has been used to predict the pion and kaon production spectra using the muon spectrum derived from the results of this experiment. It has not been found possible to predict the ratio of the number of kaons to the number of pions produced at production and an estimate of this ratio (0.106) has been used to fit a constant exponent power law spectrum.

The present results have been compared with those of other workers and are found to yield a smaller value of the exponent for the fitted power law production spectra. This result suggests that the pion and kaon production spectra are somewhat flatter than previously measured for momenta above 100 GeV/c by previous MARS experiments (Ayre et al., 1975). The present results on the muon spectrum, however, agree, within the limits of the statistical accuracy, with other spectrograph data. Comparison with surveys of indirect measurements of the muon momentum spectrum suggest that the present results give a higher absolute intensity for the muon momentum spectrum above 1000 GeV/c.

PREFACE

The results presented in this thesis represent the research carried out in the period 1972 - 1975 while the author was a research student under the supervision of Professor A.W. Wolfendale in the Cosmic Ray Group of the Physics Department of the University of Durham.

The MARS spectrograph had been constructed when the author joined the group in 1972. However, the author has played a part in the assembly of some of the flash-tube trays used in the present experiment. The author has been responsible for the running of the instrument for the purpose of the work described in this thesis, and has also played a part in developing the computer analysis technique used to analyse the data. The interpretation of the results of the computer analysis has been the sole responsibility of the author. The work described in this thesis in fact represents the first stage of the experiment, and data is being collected continuously and will eventually be analysed and combined with the results described in this thesis to yield statistically more accurate results.

Preliminary results have been presented at the XIV International Cosmic Ray Conference in Munich, Germany, by Baxendale et al., 1975*. The alignment procedure described in this thesis has been presented by Ayre et al., 1975.**

* Baxendale J.M., Daniel B.J., Hawkes R.C., Piggott J.L., Thompson M.G., Thornley R., 1975, P.I.C.C.R., (Munich), 3, 2011.

** Ayre C.A., Baxendale J.M., Daniel B.J., Goned A., Piggott J.L. and Thompson M.G., 1975, Nucl. Inst. and Meth., 124, 335.

CONTENTS

CHAPTER 1

INTRODUCTION

1.1 HISTORICAL INTRODUCTION

Cosmic ray studies have been an important branch of physics since the discovery by Hess (1912) of "another source of the penetrating radiation in addition to the γ- radiation from the radioactive substances in the earth's crust". This statement was made as a result of a series of balloon flights up to 5000m using two Wulf radiation detectors to measure the amount of ionisation present in the air as a function of height above sea level. This was found first to decrease and then increase with increasing height. Further confirmation that the radiation came from above was obtained when the ionisation was found to decrease with depth in snow-fed lakes (Millikan and Cameron, 1926), indicating that the radiation was not coming from the earth's crust. The significance of the lakes being snow-fed was to ensure that the water was not contaminated with any solid radioactive material.

It was first thought that the radiation was high energy gamma rays because this type of radiation was the only radiation known at that time, which would penetrate matter to the same extent as the cosmic radiation.

The first observation of individual cosmic rays was made in a cloud chamber set up between the poles of a magnet (Skobelzyn, 1929). The cloud chamber was actually being used to study the energy spectrum of β- particles from radioactive decays, when extra tracks were seen which were not deflected in the magnetic field. These tracks were attributed to high energy Compton recoil electrons produced by the cosmic γ- radiation.

The conclusion that the cosmic radiation itself was charged

and particulate was arrived at by Bothe and Kolhorster (1929). In their classic experiment they surrounded two Geiger-Muller tubes with lead (which was checked to ensure that it was non-radioactive) and placed various thicknesses of lead between the tubes. They found many coincidences between the two counters indicating that the radiation was traversing the lead. They also found that the absorption coefficient was similar to that of the cosmic radiation, thus they concluded that the cosmic radiation itself consisted of charged particles. Further experiments revealed a variation of intensity with latitude (Clay, 1932) and that more particles came from west of the zenith compared with easterly directions indicating that the radiation was charged and interacting with the earth's magnetic field (Johnson, 1933). Since this time many studies have been made of the cosmic radiation and many of the elementary particles were first discovered in the cosmic ray beam (eg positron (Anderson, 1932) and Λ° hyperon (Rochester and Butler, 1947)).

1.2 THE PRIMARY RADIATION

The primary radiation consists mainly of protons (88%) and helium nuclei (11%), the remainder being heavier nuclei. It is interesting to note that the heavy nuclei (1% of the total) carry approximately 30% of the total incident cosmic ray energy. There are three main areas of study in this field, a search for anisotropies, a measurement of the energy spectrum and an investigation of the composition of the primary radiation. The energy spectrum of primary protons and nuclei is shown in figure 1.1. The various methods of measurement are also shown in the corresponding energy regions. Satellite and balloon-borne experiments have been used to measure the incident spectrum directly and also give an indication of the nature of the particles (ie their charge).

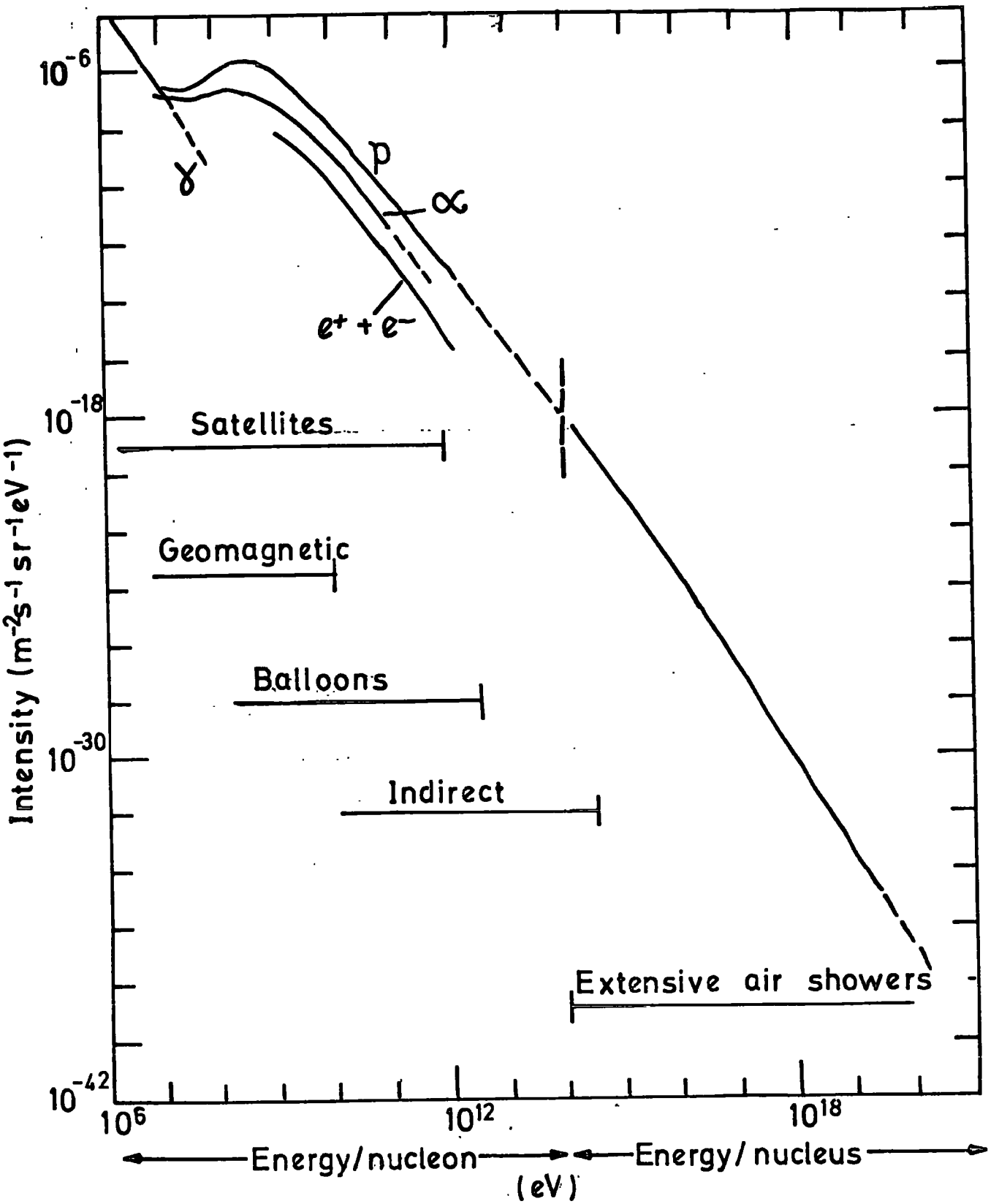

Figure 1.1 The primary energy spectrum of cosmic ray particles (after Wolfendale 1973)

The tracks of the particles are observed in photographic emulsions, and the nature of the particles deduced from the grain intensities of the tracks. The other methods of measuring the energy spectrum involve the knowledge of the propagation of a primary particle through the atmosphere and its subsequent interactions with the air nuclei, so that the primary spectrum can be deduced from measurements made at sea level. Attempts are also made to deduce the arrival directions of the primaries from sea level data from air shower studies.

1.3 THE PROPAGATION THROUGH THE ATMOSPHERE

For a proton the complete atmosphere represents about twelve interaction lengths. Therefore the probability of a primary proton reaching sea level is small (approximately 1 in 10^4). Figure 1.2 shows schematically the passage of a typical primary proton with an energy of approximately 10^{13} eV through the atmosphere. On the initial collision with an air nucleus many pions and kaons will be produced together with short-lived baryons and mesons, which subsequently decay into pions, kaons and nucleons. The charged pions and kaons will either interact with a second air nucleus producing more secondary particles or will decay in flight via various decay modes eventually to muons and neutrinos. The muons have a relatively longer lifetime than the pions and kaons and many will reach sea level without decaying and can easily be detected. The neutrinos will also reach sea level. However these particles are very difficult to detect because of their very small interaction cross-sections. The zero charged pions decay into two gamma-ray photons, which can in turn produce an electron-positron pair (pair production). The electrons and positrons can produce more γ-rays by Bremsstrahlung. In this way an electron-gamma-ray shower is initiated. These showers

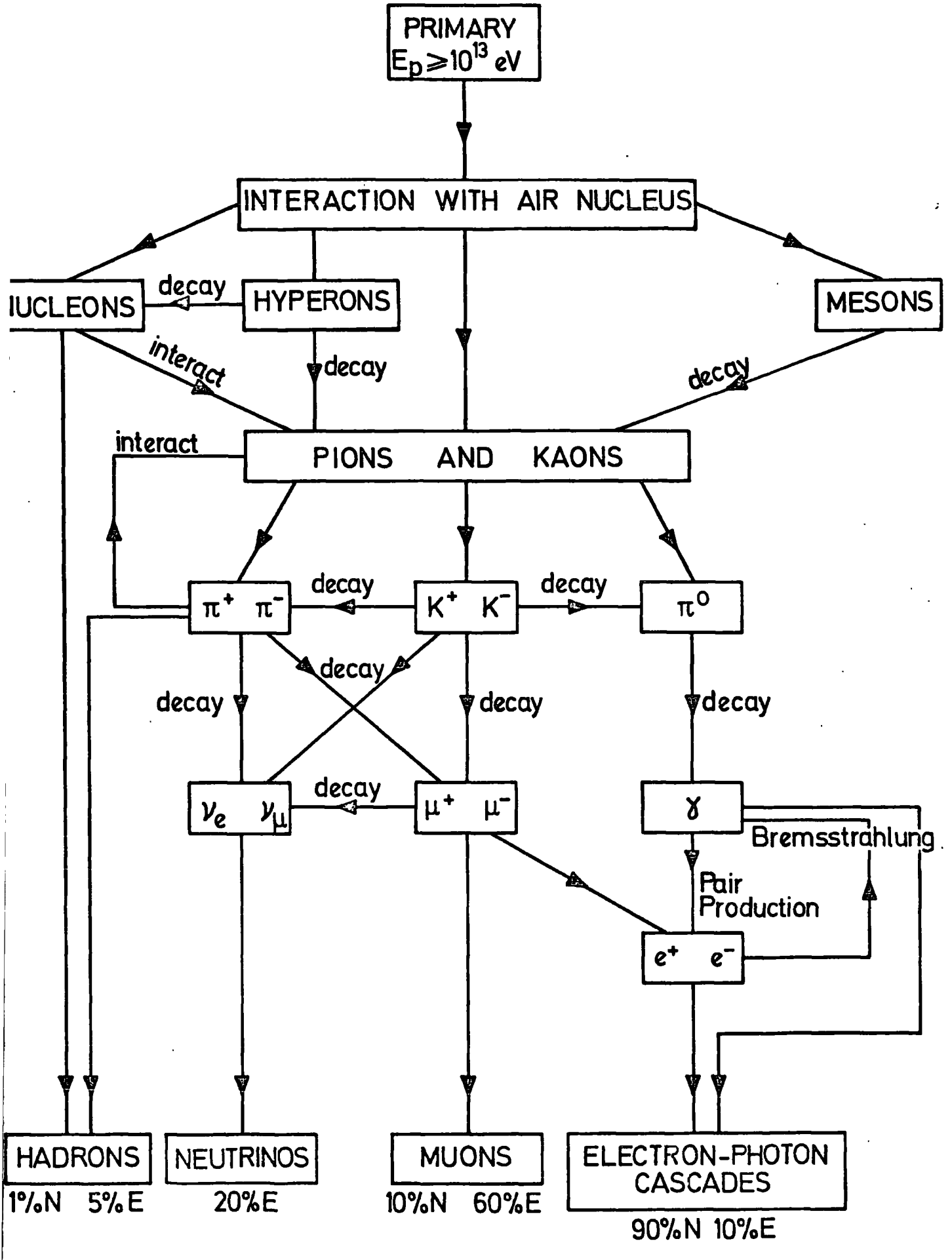

Figure 1.2. A schematic diagram to show production processes for the cosmic radiation arriving at sea level.

however, do not in general have enough energy to traverse the whole atmosphere, since when the mean energy of the electrons reaches 84 MeV (the critical energy for air), absorption by the air nuclei will dominate and the shower will decrease in size (ie in number of particles).

As can be seen from figure 1.2, the largest amount of energy arriving at sea level is carried by the muonic component, but the largest number of particles occur in the electron-photon cascades. For very high energy primaries large showers of particles are produced in the atmosphere resulting in the arrival of many millions of particles covering large areas at sea level. These are called extensive air showers. To detect such showers from high energy particles large arrays of particle detectors have been built covering typically 10 km^2 (for example Haverah Park covers 12 km^2). From a measurement of the number of particles (particle density) arriving at sea level in a shower, the primary energy of the particle producing the shower can be estimated, by making detailed model calculations of the propagation of the particle through the atmosphere. In order to do this it is important to have a model of the nuclear interactions occurring in the atmosphere. A problem associated with the measurement of air showers arises due to the fluctuations that can occur in the sea level component of showers initiated by similar particles of the same energy, depending on how quickly the shower developed on traversing the atmosphere. Thus even if the nuclear physics is completely understood it is still not possible to calculate the primary energy to any degree of certainty.

1.4 NUCLEAR INTERACTIONS

As mentioned previously, interactions of cosmic ray nuclei with an atmospheric nucleus are important in the field of measuring

the primary spectrum. Nuclear interactions have been studied at CERN using the two colliding proton beams (the ISR facility). Although these interactions are of a much simpler nature than those occurring in the atmosphere, the energies reached at CERN are the highest which are at present available from accelerators, and these interactions must be used in order to obtain some information as to the nature of such collisions. A proton is found to interact with an elasticity of approximately 0.5 and therefore about half of the available energy is used in producing secondary particles (mainly pions).

The number of secondaries produced has been calculated by several workers using various models of the interactions. The CKP model (Cocconi, Koerster and Perkins, 1961) predicts that the number of secondaries is proportional to $E_p^{\frac{1}{4}}$ (E_p being the energy of the incident particle). This model is based on accelerator measurements up to an energy of 30 GeV and assumes an exponential distribution of energy among the secondaries, with a mean energy depending on the energy of the incident particle. The scaling model (Feynman, 1969) predicts that the number of secondaries is proportional to the logarithm of the energy of the incident particle. This model assumes that the distribution of energies for the secondaries is the same for all incident particle energies, when the energy distribution is expressed as a function of the actual energy divided by the maximum energy possible for the secondary. Another importamt factor is the number of kaons produced in the interactions. The ratio of kaons to pions produced in nuclear interactions affects the shape of the sea level muon spectrum, because the kaons have a shorter lifetime than the pions. The kaons are correspondingly more likely to decay before they interact, thus producing more muons at higher energies and hence decreasing

the slope of the muon spectrum. The ratio has been measured at CERN as 0.15 up to 1000 GeV/c.

1.5 ORIGIN OF COSMIC RAYS

The problem of the origin of cosmic rays has not been fully resolved at the present time. There appear to be very energetic sources in the galaxy capable of providing the acceleration required to produce the very highest energy cosmic rays (approximately 10^{20} eV). The large energy release of supernovae (Ginzburg et al., 1964) and their remnants are possibilities, as are the pulsars (Cooke et al., 1969) and the galactic nucleus (Kulikov et al., 1969). It is not certain whether the sources are wholly galactic, extragalactic or a mixture of both. Any search for discrete cosmic ray sources is hampered by the interaction of the particles with the galactic magnetic field resulting in the impossibility of equating the arrival direction at the top of the atmosphere with the direction of its source. For primary particles with energies above 20 GeV the incoming arrival directions are isotropic.

1.6 THE PRESENT WORK

The muon spectrum at sea level has been measured by many workers (for example Allkofer et al., 1971, Nandi and Sinha, 1972, Ayre et al., 1975 a). Figure 1.3 shows the measured spectra obtained by various workers. The spread of the measured intensities above 100 GeV/c reflects two main points, the first being the point at which the particular spectrum is normalised (important if the measured spectrum is not an absolute one) and the second being the small number of particles recorded with momenta above 500 GeV/c. Several of the points shown in the figure correspond to measurements taken at or above the maximum detectable momentum of the respective instruments, thus making them suspect. The present experiment provides experimental data up to 3000 GeV/c, and the rate of

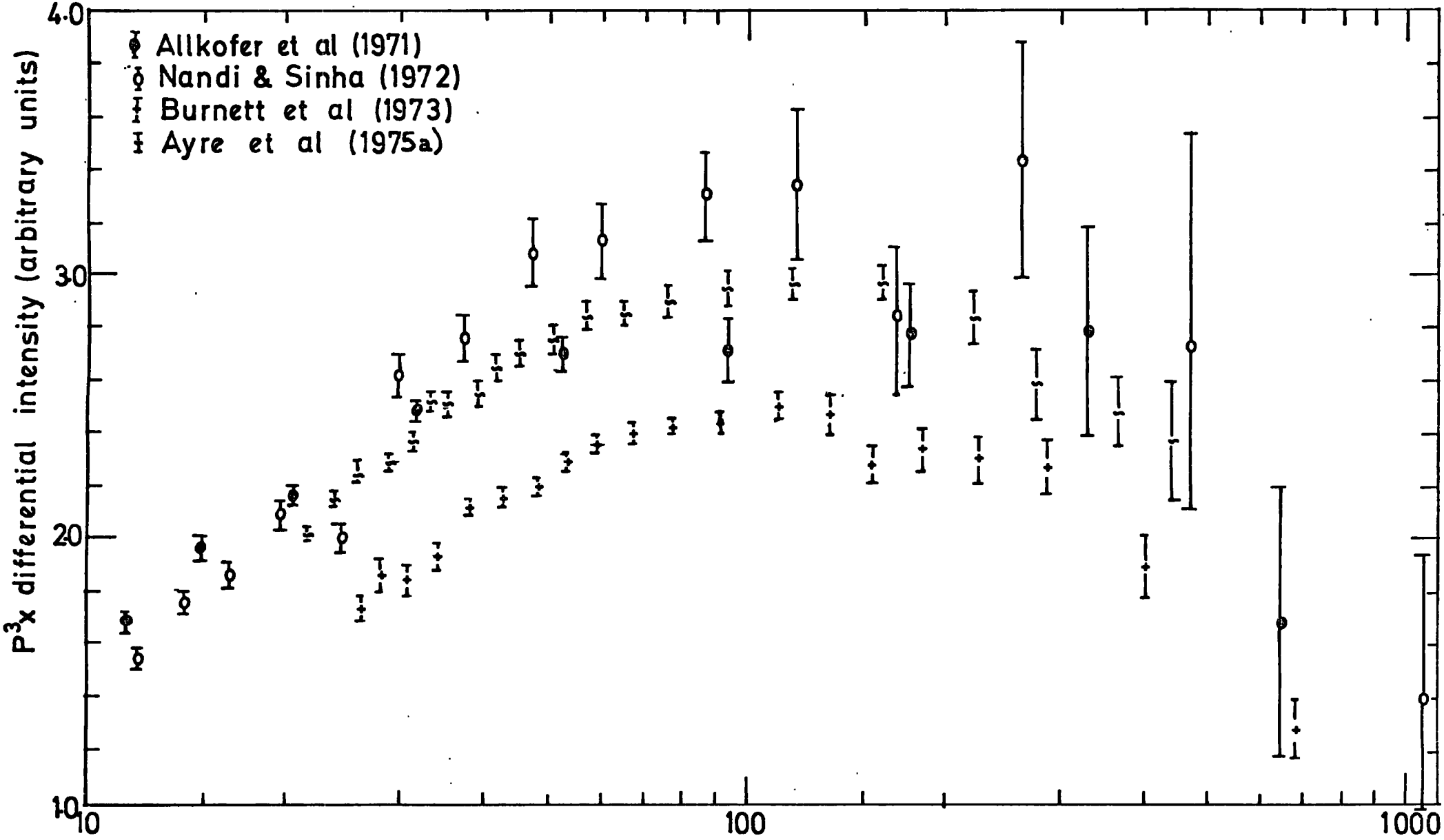

Figure 1.3 The muon momentum spectrum.

particles traversing the instrument with momenta above 500 GeV/c is high enough to ensure good statistics up to and beyond momenta of 1000 GeV/c. The absolute muon spectrum and the charge ratio (the ratio of the number of positive to the number of negative muons in the same momentum interval) have been measured and the results are given in chapter 5. The comparison of this measured spectrum and charge ratio with those of other workers is discussed fully in chapter 6. The measured muon spectrum is used to obtain an estimate of the slope of the primary spectrum (section 5.7).

The apparatus used in the experiment is described in chapter 2. Chapters 3 and 4 deal with the analysis of the data collected and the subsequent corrections applied in order to obtain the absolute spectrum.

The author has been responsible for the running of the apparatus during the eighteen month period over which the data were collected and for the subsequent interpretation of the results obtained from the computer analysis of these data.

CHAPTER 2

THE MARS SPECTROGRAPH

2.1 INTRODUCTION

The spectrograph which is known as MARS (Magnetic Automated Research Spectrograph) is a solid iron magnetic instrument designed to measure the momentum spectrum of cosmic ray muons at energies up to 5 TeV. At such high energies a spectrograph must have an acceptance that is large enough for there to be a statistically significant number of high energy muons traversing the instrument in the envisaged running time of the apparatus, consequently such instruments are physically large. The large acceptance also results in a high number of low energy muons traversing the instrument. Thus MARS includes a momentum selector, which preselects particles of high momentum, and these high energy events are analysed at a later date.

High energy muons are often accompanied by electron-photon cascades generated by electromagnetic interactions in or above the apparatus (for MARS, interactions occur in the iron blocks). Such cascades, or bursts, make accurate track location in the detector containing the burst impossible, rendering the information from such a detector unusable. To combat such a problem MARS contains five measuring levels so that the curvature of a muon's trajectory can still be measured even if two detectors are unusable.

A full description of MARS has been given by Ayre (1971), Ayre et al. (1972 (a), (b)). However the parts of the instrument relevant to this work are described briefly below.

2.2 GENERAL DESCRIPTION

As mentioned before, MARS is a multilayer solid iron magnetic

spectrograph. There are four iron electromagnets interleaved with a series of particle detectors. There are two main types of detector employed, scintillation counters and trays of flash-tubes. Trays of Geiger-Muller tubes are used as subsidiary counters. Figure 2.1 shows the relative positions of all the detectors used in MARS. Two sizes of flash-tubes are used, large diameter tubes (internal diameter 1.5cm) in the momentum selector trays located at levels 1, 3 and 5 and small diameter tubes (internal diameter 5.5mm) in the measuring trays located at all five levels. The scintillation counters, also located at levels 1, 3 and 5, provide the initial trigger for the spectrograph. The momentum selector trays determine whether or not a trigger is likely to have been caused by a high momentum particle and the measuring trays are used to locate the actual trajectory. Only the data from the flash-tubes of the measuring trays are stored for analysis. The Geiger-Muller trays are used at the top and bottom levels to locate approximately the trajectory in the back plane of the spectrograph (ie along the lengths of the flash-tubes).

The spectrograph is divided into two separate halves, defined as the blue side or the red side of the instrument. For the purposes of this work, only the blue side contained flash-tube detectors and the red side contained scintillation counters which were used for checking purposes only.

All the flash-tubes on the blue side are digitised and the system is automatic, the data from the measuring trays being stored in a computer connected on-line to the apparatus when a high momentum event is detected by the momentum selector. The apparatus runs continuously and to remove any instrumental biases due to the field direction, the magnet current is reversed every twenty-four hours. The data stored on the computer are

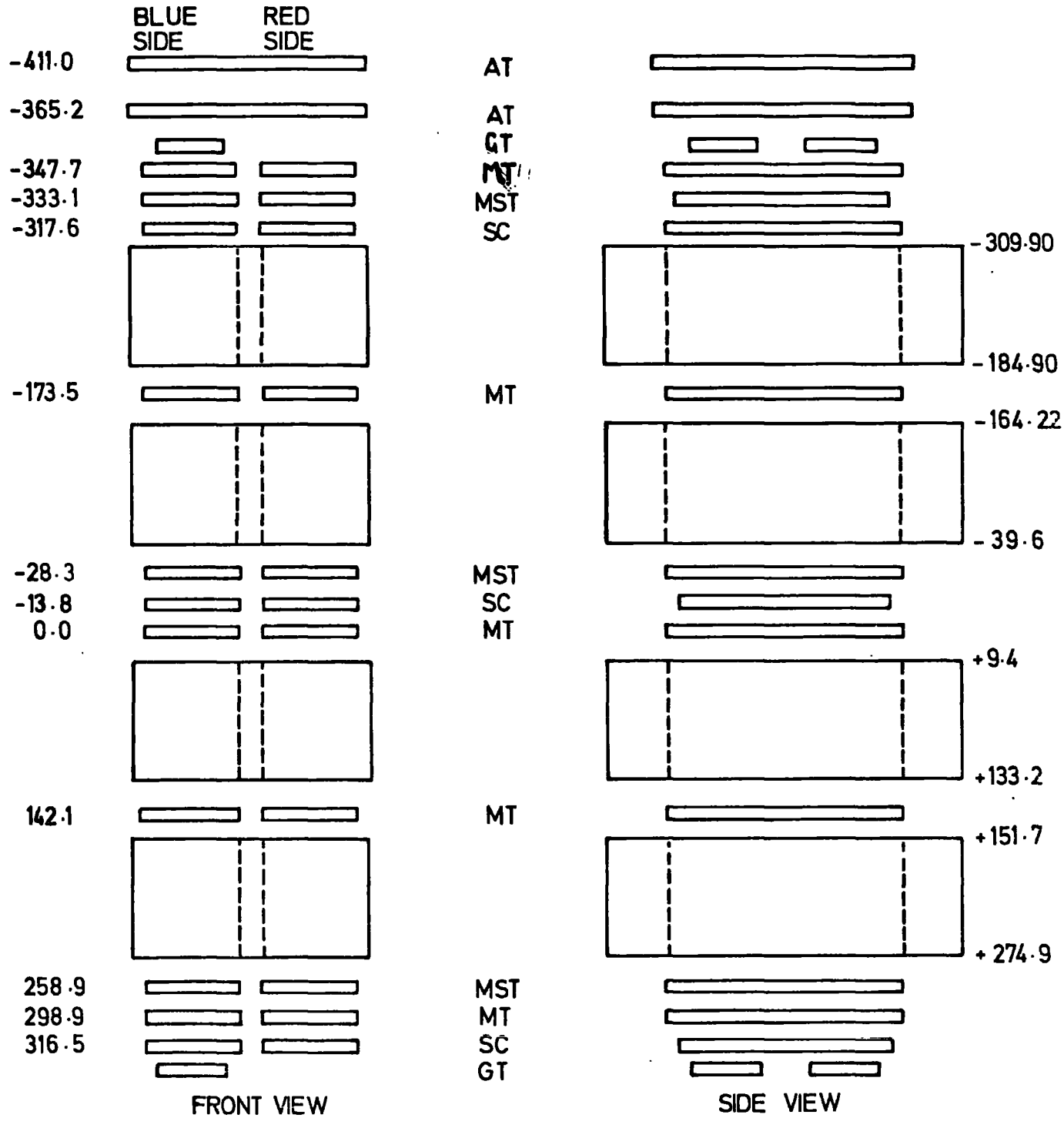

AT - AZIMUTHAL TRAY
MST - MOMENTUM SELECTOR TRAY
SC - SCINTILLATION COUNTER
GT - GEIGER TRAY
MT - MEASURING TRAY
ALL DIMENSIONS ARE IN cms.

Figure 2·1. The MARS Spectrograph.

also checked twice daily to ensure that no electronic faults have developed.

2.3 THE MAGNET

The magnet provides the force which bends the trajectory of a charged particle traversing MARS. A particle of mass m, charge e, velocity v travelling through a magnetic field of flux density B experiences a Lorentz force F given by

$$\underline{F} = e\,\underline{V} \times \underline{B} \qquad 2.1$$

As a consequence (neglecting the particle's energy loss) the particle's trajectory is a circle of radius r in the end plane of the spectrograph where

$$r = \frac{P}{Be} \qquad 2.2$$

and r is proportional to the momentum of the particle provided that the field is uniform.

The magnetic field is generated in MARS by current flowing in coils around the iron blocks in the manner shown in figure 2.2. To enable the momentum of a particle to be measured accurately, the field must be known accurately. Both the uniformity and the magnitude of the field have been measured, the former by small search coils distributed throughout the magnet and the latter by using a large loop of wire around an arm of the magnet block. The field is 16.3 ± 0.1 kG with a non-uniformity of approximately 4% (Ayre, 1971). However, since the mains supply voltage varies by up to 7% and the magnet power supply is unstabilised, the field is found to vary by about 1% due to variation in the 50 A supply current. Consequently the field has a value of 16.3 ± 0.16 kG.

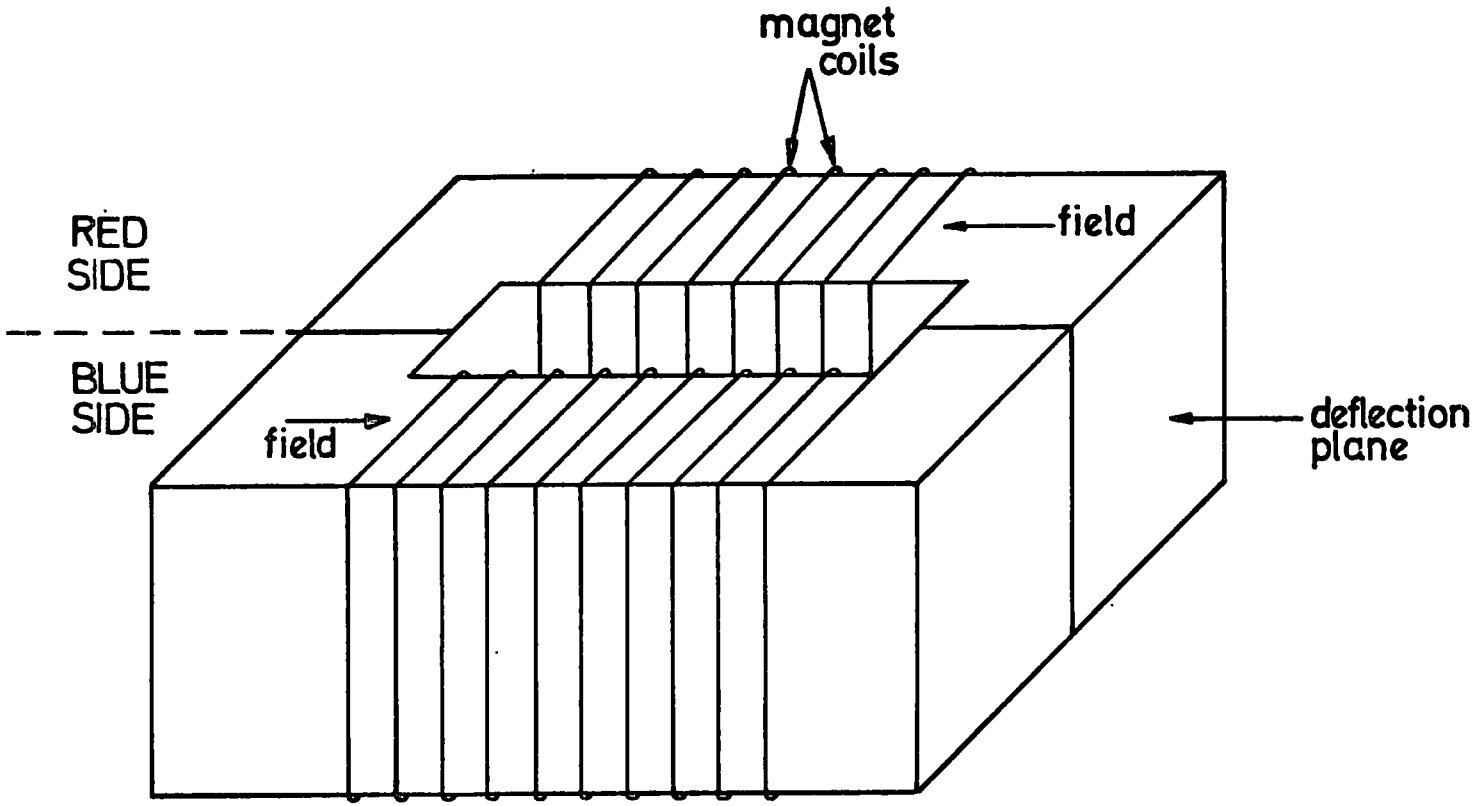

Figure 2.2. Schematic diagram of a magnet block.

2.4 THE PARTICLE DETECTORS

The three types of particle detector used in MARS will be briefly described, and the manner in which the data from each of the detectors are used.

2.4.1 THE SCINTILLATION COUNTERS

The phosphors of the counters are plastic (Ne 102A) and each phosphor is viewed by four photomultiplier tubes. The outputs from the two diagonally opposite photomultipliers are added together, the resultant being amplified before passing via discriminators to a coincidence circuit which produces a pulse on the passage of a particle through the instrument (figure 2.4).

The counters are located in the top, middle and bottom layers of both sides of the magnet. A coincidence between the three blue side scintillation counters is used as the trigger for the spectrograph. Figure 2.3 shows their construction schematically. Each counter is approximately 5cm deep, 75cm wide and 176cm long.

The three scintillation counters also define the overall acceptance of the spectrograph, which varies with momentum, because of the bending of the trajectories of low momentum particles out of the magnet by the magnetic field. However, for energies greater than 100 GeV the acceptance has reached its asymptotic value.

2.4.2 THE NEON FLASH-TUBES

The neon flash-tubes as introduced by Conversi and Gozzini (1955) used in MARS are 2m glass tubes filled with neon gas. Two sizes of tubes are used, large (internal diameter 1.5cm) and small (internal diameter 0.55cm). On the passage of a particle, the gas inside the tubes is ionised and on the application of a high voltage pulse across the tube a discharge occurs inside

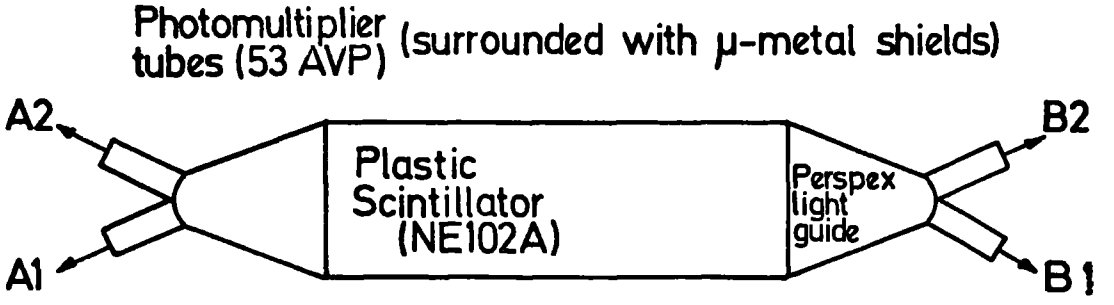

Figure 2·3. Plan view of scintillation counter.

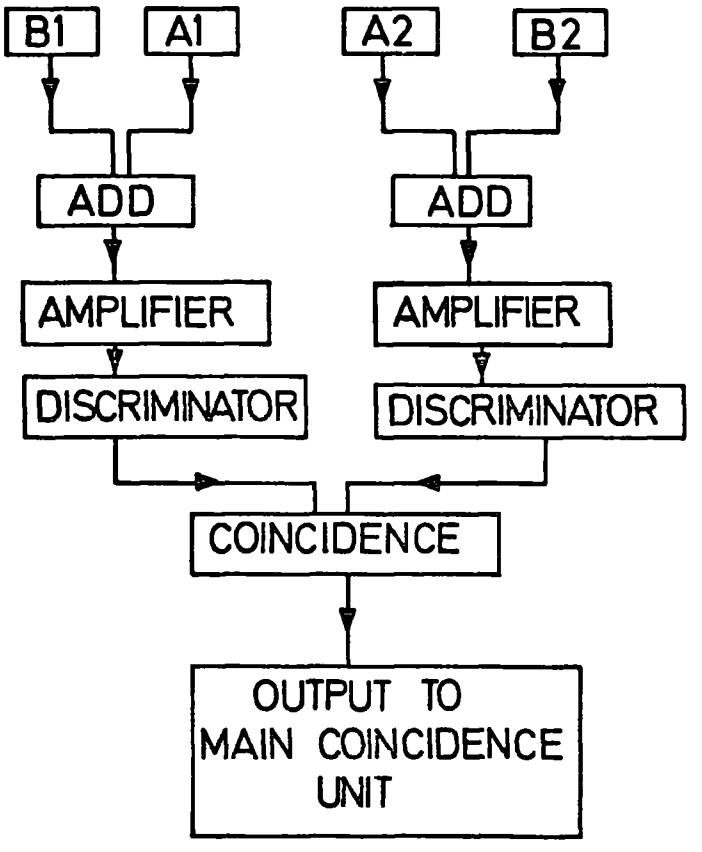

Figure 2·4. Sequence of events following the passage of any charged particle through a scintillation counter.

the tube. Each tube in the blue side of MARS is digitised following the method of Ayre and Thompson (1969) and Ayre (1971). When a tube discharges, a small voltage pulse is picked up by a probe attached to the end of each tube and an electronic memory associated with the tube is 'set'. All the memories are 'reset' at the beginning of each event and during the leading 'edge' of the high voltage pulse. This is to prevent spurious 'pick-up' causing memories to be set incorrectly. Flash-tubes are used in both the momentum selector trays and measuring trays described below. The high voltage pulse is obtained in the same way for both types of tray. The pulse is approximately 5 kV and 3.5 μs in length and is produced by causing the discharge of a delay line across a resistor.

2.4.3 THE MEASURING TRAYS

The measuring trays contain 712 small diameter flash-tubes arranged in 8 rows forming 89 columns. The tube pattern is shown in figure 2.6. The data from each of the memories are read off separately, so that only the actual tubes which fired are recorded. The data format from each tray contains 96 columns, the first containing the tray identifier (ie 1 to 5) the last 6 containing dummy information (subsequently used for storing the results of the analysis of the event).

Pulses to abstract information as to which flash-tubes have discharged are sent to each tray and column in turn. The column numbers are stored each in two bytes together with the patterns of tubes fired. Each tube is assigned one of eight binary bits, hence the column number and the tube data are completely contained in four bytes. Columns containing no discharged tubes are ignored thus reducing the amount of data to be stored. The tray identifier and dummy columns serve to define the beginning

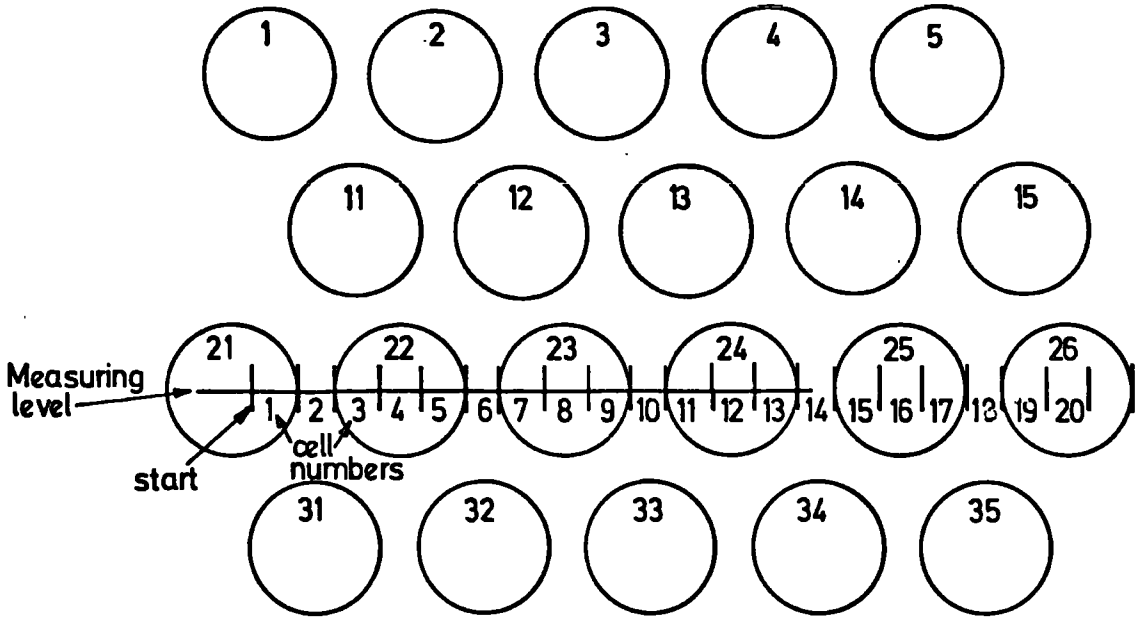

Figure 2·5 Momentum selector tray tube pattern.

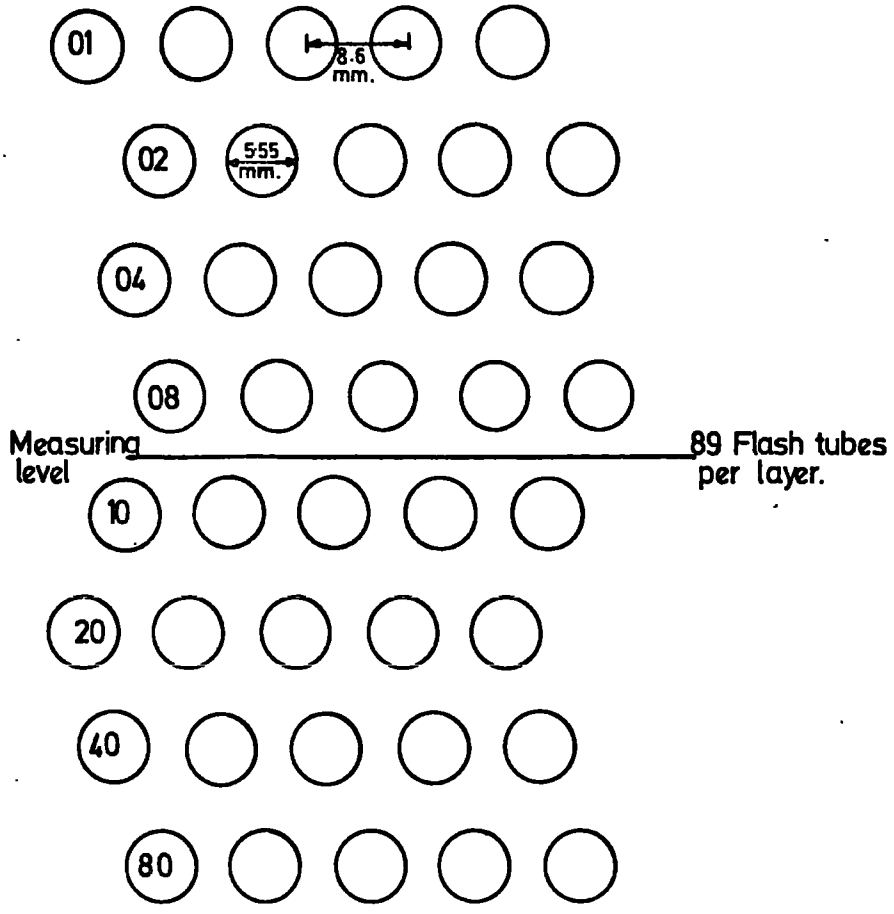

Figure 2·6 Measuring tray tube pattern

and end of the data from each tray.

During the course of the experiment the original momentum selector in the apparatus (ie Mark I instrument) was replaced (ie Mark II instrument). Initially for every event the small diameter tubes were pulsed but when the event was deemed not to be a high momentum event the memories were reset without being read. When the replacement momentum selector was operational the flash-tubes were only pulsed for possible high momentum events.

2.4.4 THE MOMENTUM SELECTOR TRAYS

The momentum selector trays are each divided into 152 $\frac{1}{2}$cm cells. Each tray contains 155 large diameter flash-tubes, which are arranged in four rows in the staggered pattern shown in figure 2.5. For each combination of flash-tubes discharged, a particular $\frac{1}{2}$cm cell is allocated.

On the passage of a particle and the application of a high voltage pulse across the flash-tubes, the electronic memory for each discharging flash-tube is set in the same way as for the measuring trays. On the subsequent application to the tray of a gating (or read) pulse, the trajectory is allocated electronically to a cell. The relative positions of the first four cells with respect to the first columns of tubes are also shown in figure 2.5. Table 2.1 shows the cells allocated for various combinations of tubes in figure 2.5. For any tube combinations for which two cells are possible, the one with the greater probability is allocated.

TABLE 2.1

RELATION BETWEEN PREDETERMINED FLASH-TUBE CONFIGURATION AND ALLOCATED CELLS (for notation see figure 2.5)

CELL NO	LAYER			
	1	2	3	4
	TUBES DISCHARGED			
1	1		21	31
1	1	11	21	31
1	1		21	
2	1	11		31
2		11		31
2	1			31
3	1	11	22	31
3		11	22	31
3	2	11	22	31
4	2	11	22	
4		11	22	
4		11	22	32
4	2	11	22	32

2.4.5 THE GEIGER-MULLER TUBE TRAYS

Each tray contains 23 60cm Geiger-Muller tubes. Pulses are received whenever a particle traverses a tray. The tubes are positioned so that two layers of tubes completely cover the area of the tray in the horizontal plane. Each tray measures 49cm x 60cm and covers approximately 2/9 of the scintillation counter area.

The output pulses from the Geiger counters are put in coincidence with the spectrograph trigger pulse and memory circuits are set if a coincidence is recorded. Each tray is assigned a number 1,2,4, or 8 and the

various combinations of trays can be recorded in 1 byte in the event header (see section 2.6). Thus a four fold coincidence is recorded as 1111 and a single coincidence as 1000, 0100, 0010 or 0001. These trays are used in the setting up of the measuring trays and in determining the relative skewness of the trays. They determine whether a particle has traversed the front or back of the instrument or has traversed the spectrograph at a large azimuthal angle.

2.5 THE MOMENTUM SELECTION SYSTEMS

In this work two momentum selection systems have been employed. The original momentum selector (Mark I) was very inefficient in data collection due to the long recovery time of the small diameter flash-tubes (approximately 30 s). A second momentum selector (Mark II) is now employed, which does not require the small diameter tubes to be pulsed for each event. Throughout this account, wherever possible, the two systems will be considered together so that comparisons can be made.

2.5.1 THE MARK I MOMENTUM SELECTOR

Each of the 152 cells in each tray has associated with it, in the momentum selector, a shift register bit. The momentum selector essentially determines the magnitude of the deflection which a particle has undergone in passing through the spectrograph. The deflection (Δ) is defined by the mathematical expression

$$\Delta = (a + c - 2b) \times 0.5\text{cm}$$

where a, b and c are the points of intersection of the trajectory with the measuring levels of trays 5, 3 and 1 respectively. Figure 2.7 shows this diagramatically. Δ is the distance between the intersection of the straight line joining a and b with tray 1 and the intersection of the real trajectory with tray 1. This

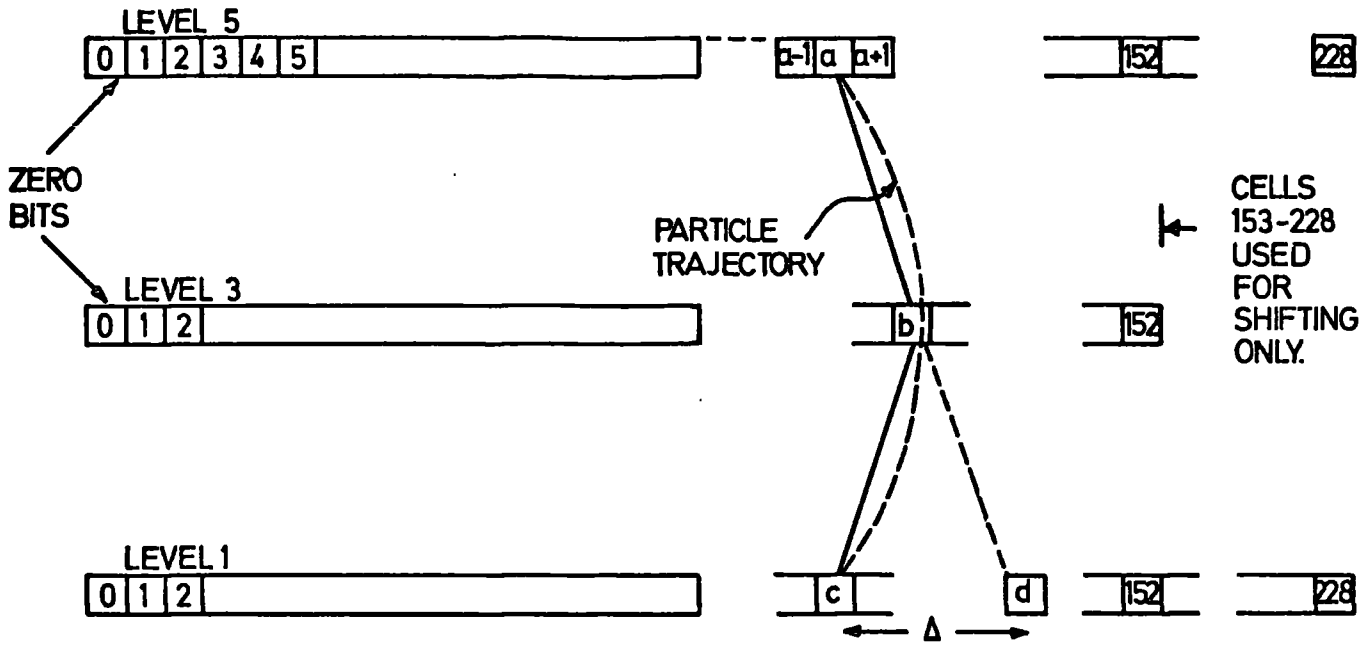

Figure 2·7. Principle of operation of Mk.1. momentum selector.

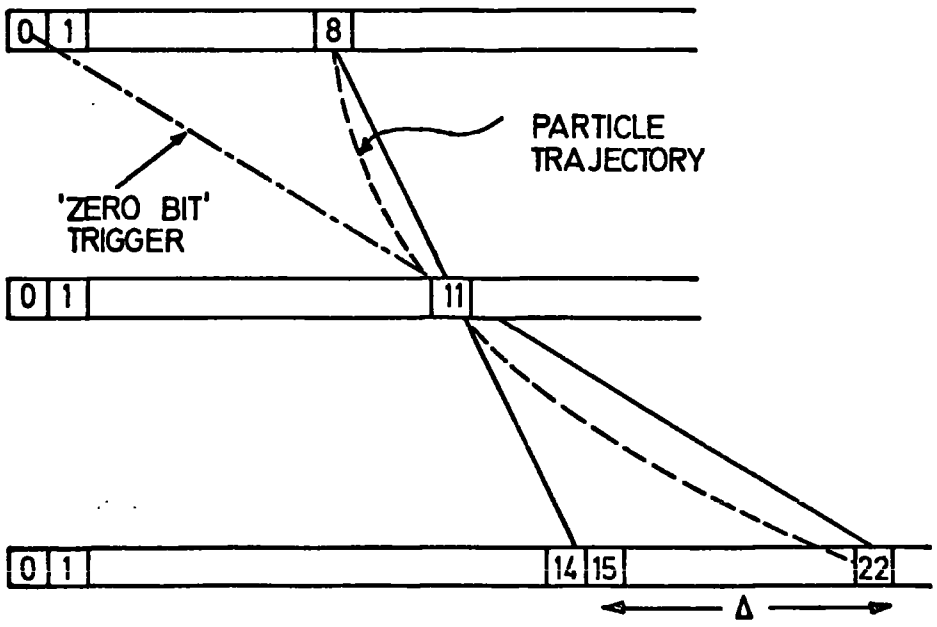

Figure 2·8. Example of how a trajectory with deflection 8 triggers the momentum selector by means of zero bit.

assumes that the two arms of the spectrograph are equal, which is not in fact the case. Subsequently a correction is made for this.

The momentum selector consists of three shift registers A, B and C. A and C have 228 bits and B has 152 bits. For the last cell in B (152) coincidence gates are set up so that all possible combinations of cells a and c with b = 152, having a deflection less than or equal to two cells, give a 'high momentum event' pulse. Any event with $\Delta \geq 3$ is rejected as being of too low a momentum. The bits are shifted all three levels together, one bit at a time until all the bits have been shifted 152 times. The extra cells in A and C are for those high momentum events for which a or c is bigger than b. The time taken for a pulse indicating an event of high momentum depends on the frequency of the shifting procedure and takes 75 μs. It is this long time delay which makes it impossible to pulse the measuring trays after a decision on the momentum of the event has been reached. Thus the measuring trays are pulsed together with the momentum selector trays, but data from the former is only used if a high momentum event is indicate

Incorporated in the momentum selector is an automatic checking system. This sets the '0' bit at the beginning of each set of shift registers and checks that all three bit '0's reach the end of the shift registers at the same time. A fault is registered if their arrival is not simultaneous. A complication in the data interpretation arises due to these '0' bits. Figure 2.8 shows a trajectory which would trigger the momentum selector due to these zero bits. In this case a high momentum event is recorded even though the real deflection is 8 ie $(8 + 22 - (2 \times 11))$. In fact any trajectory with

$$a - 2b \leq 2 \qquad \text{or} \qquad c - 2b \leq 2$$

is registered as a high momentum event. Most of these events are rejected during the analysis as being of too low a momentum and

a correction is made for the remaining few. A flow chart showing operation of the spectrograph when the Mark I momentum selector was in use is shown in figure 2.9.

2.5.2 THE MARK II MOMENTUM SELECTOR

In order to speed up the momentum selection process, a series of coincidence gates are used in the Mark II momentum selector. The cells are combined in groups of four in levels 5 and 3. In level 1 the cells are combined in groups of six overlapping so that each cell is in two groups. Table 2.2 shows the original cell numbers and the group numbers in the three momentum selector trays.

TABLE 2.2

ORIGINAL CELL NUMBERS AND NEW GROUP NUMBERS

CELL	A,B	C
1	1	1
2	1	1
3	1	1 and 2
4	1 and 2	1 and 2
5	2	1 and 2
6	2	2 and 3
7	2 and 3	2 and 3
8	3	2 and 3
9	3	3 and 4
10	3 and 4	3 and 4
11	4	3 and 4
12	4	4 and 5
13	4 and 5	4 and 5
14	5	4 and 5
15	5	5 and 6
16	5 and 6	5 and 6

The deflection Δ is defined in the same way as before using the new group numbers, and coincidence gates are set up so that any combinations of three cells for which $\Delta = 0$ gives a high

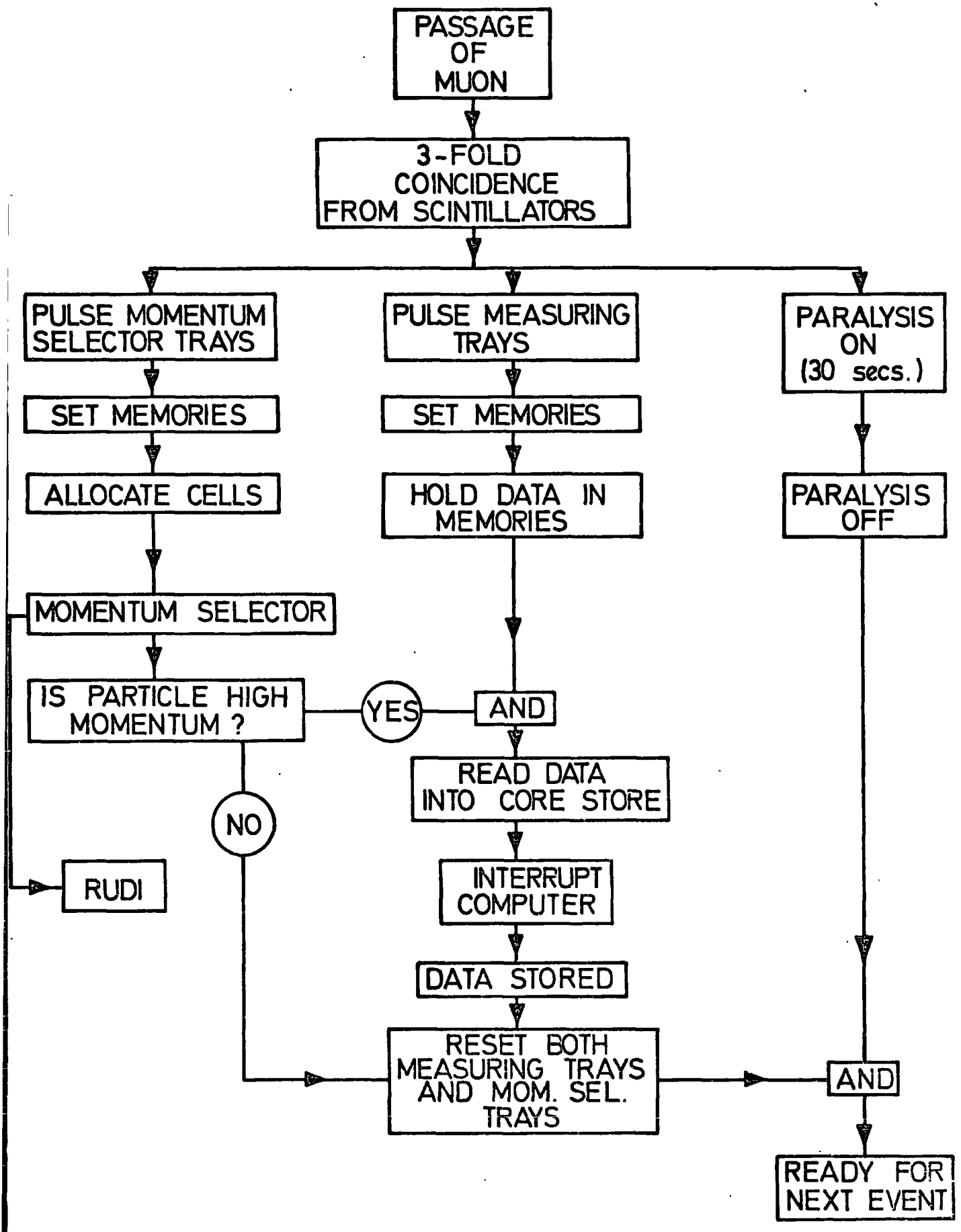

Figure 2·9 Operation of MARK 1 Momentum Selector.

momentum pulse.

The timing sequence is important when using the Mark II momentum selector, as it is essential for efficient operation of the small diameter flash-tubes that the measuring trays are pulsed as soon as possible after the passage of a particle. The high voltage pulse is applied to the momentum selector trays within 0.5 μs and the pulse is 4 μs long. The gating pulse (1 μs) is applied after 5 μ s and the momentum selector decision pulse is produced after 6 μ s. Thus the total delay in determining whether or not the event was due to a high momentum particle is 6 μ s. It is found that this time delay does not affect the measuring tray tube efficiencies. Figure 2.10 is a flow chart showing the operation of the spectrograph whilst the Mark II momentum selector was in use.

2.6 THE DATA FORMAT AND STORAGE

The data for each event is stored in a specific format. The data is preceded by the event header which contains the event number, the date, the time, the magnet current, the magnetic field direction, the trigger mode (blue in the case of this experiment), the geiger counter data and the atmospheric pressure. The header is followed by the measuring tray data. All the information pertaining to an event is assembled in a magnetic core store before the on-line computer is interrupted. The use of the core store minimises the transfer time of the data to the computer, which is required for other tasks at the same time.

The computer is an IBM 1130 with two associated magnetic disc drives and it is used to control two experiments, MARS and the High Energy Nuclear Physics Group's bubble chamber film analysis. The second disc drive of the computer is used to store

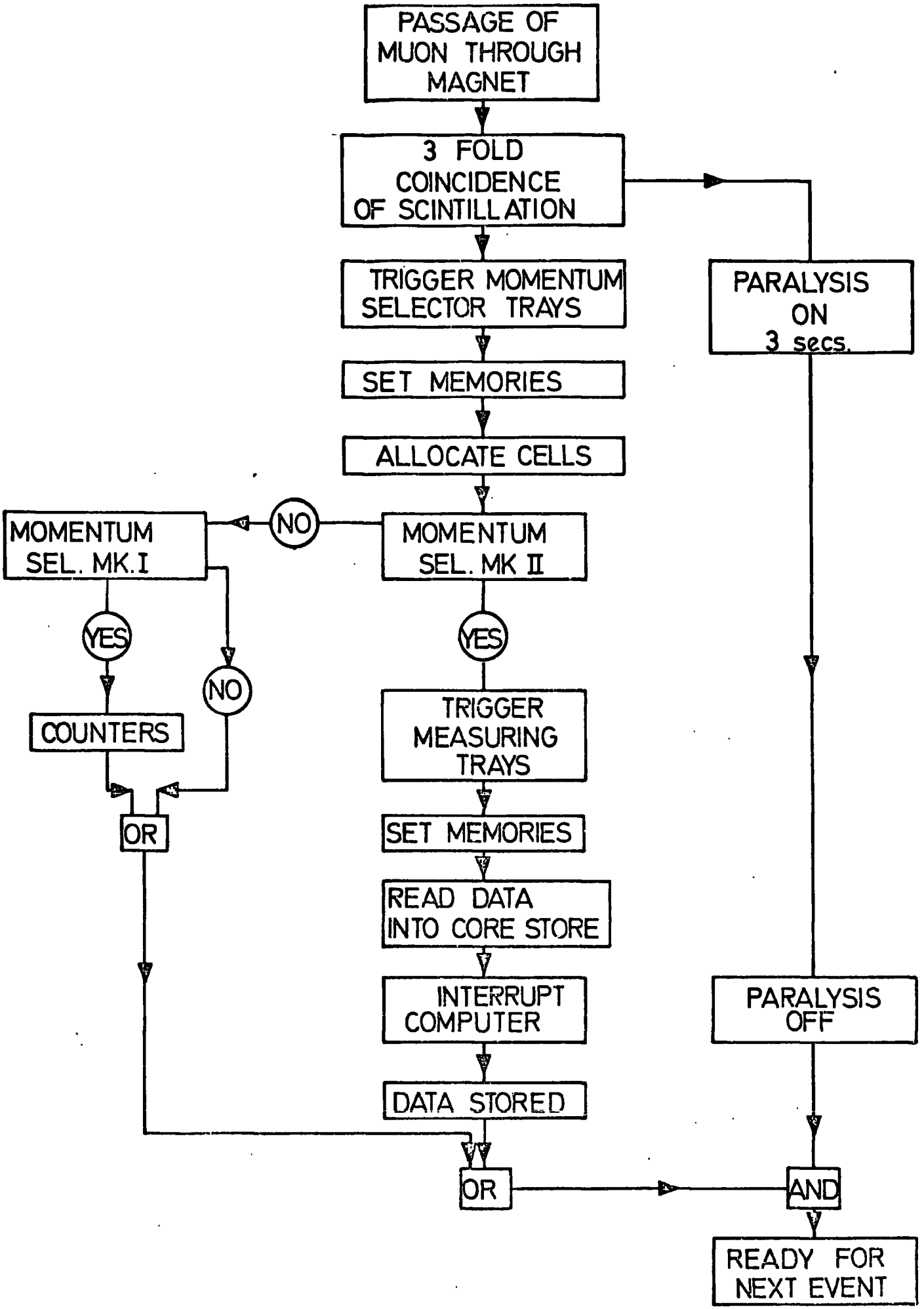

Figure 2·10 Operation of MARK II Momentum Selector.

the MARS data at all times and the first disc drive is used for the bubble chamber analysis during the day and for the MARS analysis at night. The storage and format of the data have been described in detail by Wells (1972).

The actual method of analysis will be described in chapter 3.

CHAPTER 3

THE ANALYSIS TECHNIQUE

3.1 INTRODUCTION

For an instrument such as MARS which collects a large volume of data each day, it is necessary to devise an automatic method of analysis. This is achieved in the case of MARS by using computational techniques. The computer programme is described briefly together with the types of event which are rejected before and after the analysis of the event has been completed. The reanalysis of the initially rejected events is also described. The analysis programme has been described more completely in several other publications (Wells, 1972, Thompson and Wells, 1972).

3.2 THE COMPUTER PROGRAMME

3.2.1 FITTING A TRAJECTORY

The aim of the programme is to locate and identify the correct track in each tray and hence to calculate the momentum of the particle. A good approximation of the trajectory of a particle losing energy as it traverses the iron magnet blocks is a parabola and this can easily be determined from the experimental data.

If a parabola of the form $y = ax^2 + bx + c$ is fitted to the coordinates of the track in each tray then the momentum of the muon is proportional to the radius of curvature of the trajectory, which can be found from the coefficient of the x^2 term. Using equation 2.2 and substituting the characteristics of MARS then

$$P = \frac{0.2445}{a} \text{ GeV/c} \quad \text{for } x \text{ and } y \text{ in m.} \qquad 3.1$$

In the programme this formula is modified to take account of the gaps between the magnet blocks (where the trajectory is straight).

Thus the equation used by the programme is

$$P = \frac{0.1949}{a} \text{ GeV/c} \qquad 3.2$$

The method of fitting uses a 'least squares' fitting technique where the standard deviation of the experimental data points around the fitted curve is minimised. The standard deviation of the fitted trajectory is subsequently used to select wrongly analysed events. Such events have in general a large standard deviation.

3.2.2 IDENTIFICATION OF TRACKS

Initially the tracks of the particles in each tray have to be identified. Each tray consists of 712 flash-tubes arranged in 8 rows. The first tube in each row is defined to be the first column. Thus the data is arranged in 8 rows of 89 columns. To locate a track, the programme searches for groups of two or more discharged flash-tubes in the same or adjacent columns of tubes. the majority of events have only one group per tray and the analysis of such an event is described below. However if a tray does contain more than one group all the possible combinations of groups are analysed individually.

A group of discharged tubes may consist only of the actual tubes traversed by the particle. It is quite likely, however, that knock-on electrons trigger adjacent tubes, or because the tubes are not one hundred per cent efficient that tubes actually traversed by the particle are not discharged. For these reasons, it is necessary to provide, within the programme, a method by which the flash-tubes can effectively be switched on or off. The various options available to the programme (shown in figure 3.1) enable a track to be fitted through the tube information by taking account of possible knock-on electrons or tube inefficiencies.

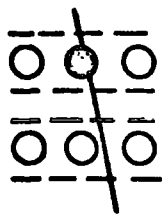

OPTION 0

Good fit - no information has to be assumed.

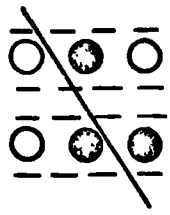

OPTION 6.

One single knock-on and and one double knock-on are assumed in different layers.

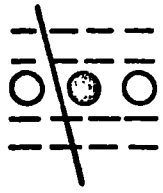

OPTION 1.

A knock-on electron is assumed (a discharged tube is neglected).

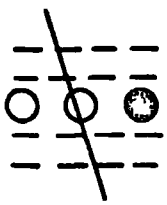

OPTION 7

A tube inefficiency and a knock-on in the same layer are assumed.

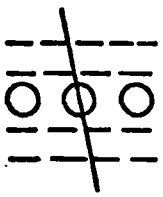

OPTION 2.

A tube inefficiency is assumed (an undischarged tube is assumed to have discharged).

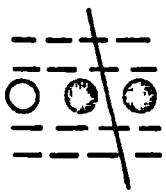

OPTION 8.

Two knock-ons in the same layer are assumed (muon passed between them).

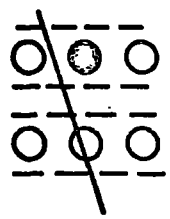

OPTION 3.

A knock-on electron and a tube inefficiency in different layers are assumed.

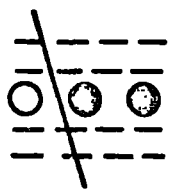

OPTION 9.

Two knock-ons in the same layer are assumed (muon passed to one side of them).

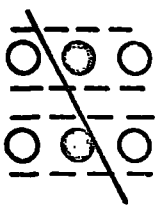

OPTION 4.

Two knock-on electrons in different layers are assumed.

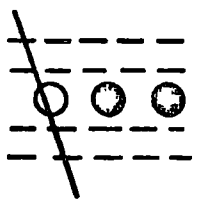

OPTION 10.

An inefficiency and a double knock-on are assumed in the same layer.

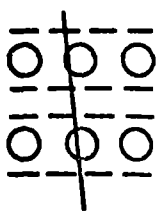

OPTION 5.

Two inefficiencies in different layers are assumed.

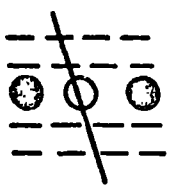

OPTION 11.

Assumes an inefficient tube between two knock-ons.

Figure 3.1. The fitting options available to the computer.

A track is fitted through the flash-tube data of the group to be used in each tray, using the option having the lowest possible number as defined in figure 3.1. The options with the lower numbers are those which are more likely to occur and thus are used in preference to the higher numbered options. The coordinates of the track so obtained are taken for the initial fitting of a parabola to the complete event. Should there be more than one track in a tray with the same option number then the mean coordinate of the tracks in the tray is taken. This procedure is carried out for each of the five trays. Any group of two tubes is not used in the fitting procedure since the options provided are not sufficient to fit this unambiguously. Also any group comprising either more than five adjacent columns of data or more than ten discharged tubes is defined as a burst and is not considered in the subsequent fitting of the parabolic trajectory, as it probably comprises two or more particles. Groups which consist of four or five columns of data are taken three columns at a time since it is unlikely that a muon will traverse a tray at such an angle that tubes in more than three columns are discharged.

At this stage in the analysis a parabolic curve is fitted to the located points in the flash-tube trays. If there are less than three such points available for consideration the event cannot be analysed and is regarded as a failed event. The angle of the fitted parabola at each of the trays is compared with the angle of the track defined by the flash-tube data and the fitted option in that tray. If the two angles are incompatible further tray fit options are considered until the angles are compatible. If this proves to be impossible the track is not used in the subsequent analysis. These considerations generally result in new more precise coordinates for the trajectory in each tray.

A second and final parabola is then fitted to the new coordinates. From this parabola the momentum of the particle is calculated together with the standard deviation of the fitted parabola to the points. Table 3.1 summarises the various error codes associated with the reasons for not using the data from a flash-tube tray during the analysis.

TABLE 3.1

ERROR CODES FOR UNUSED TRAYS

ERROR CODE	ERROR
20	No track can be fitted through the data without violating the flash-tube information
30	No group of discharged flash-tubes within one tube spacing of the fitted trajectory in an unused tray
40	No group of three discharged flash-tubes in a tray
60	No discharged flash-tube in the column indicated (ie electronics fault)
70	Trajectory failure due to the angle of the trajectory and the tube pattern in the tray being incompatible

At this point the analysis is complete for the particular combination of groups tried. If there are other groups in any of the trays the answers so far obtained are stored and a further combination of groups is analysed. When all the possible combinations of groups have been analysed the successful combination using data from the greatest number of trays is taken as the muon trajectory. If there is more than one such combination that

with the lowest standard deviation is taken as the most likely muon trajectory.

The programme now searches for the trajectory of a possible second muon. The only group combinations considered are those which do not use any of the groups associated with the first muon. The exception is where one of the groups associated with the first muon is a burst and since a burst contains at least two tracks this is thought admissible. If there are one or more group combinations remaining then the second muon trajectory is located in the same manner as the first by taking the group combinations with the greatest number of used trays and the smallest standard deviation. If there are still combinations of groups remaining which contain none of the groups associated with the first two muons, the event is 'flagged' as a possible multiple muon event using error code 96 (see table 3.2).

A further check concerning the trajectory and the experimental data is made with respect to the distance between the fitted trajectory and the nearest group in each unused tray. The initial requirement of the programme is that there is such a group within one tube spacing of the trajectory in each of the unused trays. Further limitations are imposed on the value of the standard deviations of the fitted trajectories. These requirements are momentum dependent, having maximum values of 0.25×10^{-2}m for momenta above 20 GeV/c and 0.1×10^{-1}m for momenta below 20 GeV/c. These limitations are described in detail in section 3.5.4.

3.3 THE AMENDED ANALYSIS PROGRAMME

The amended analysis programme provides a method of analysing certain events which fail the main analysis programme. The flash-tube data in the trays can be edited column by column. Thus it is possible to split or remove groups from a tray. The requirement

that there must be a group within one tube spacing of the track and that the standard deviation of the fitted trajectory must be small are waived, this being recorded as an error code (see table 3.1). This programme does not consider any group of less than three discharged flash-tubes or any tray with three or more groups, hence the group to be used in the analysis must be closely defined. A particular advantage of this programme is that it does not require a group in each tray. Therefore events can be analysed omitting one or more trays and consequently many confused events can be reclaimed.

3.4 PRELIMINARY MOMENTUM SELECTION OF THE EVENTS TO BE REANALYSED

Before any event is studied manually or reanalysed by the programme, a preliminary momentum selection is performed by the computer programme. This is primarily designed to decrease the time required for the reanalysis of the events with many group combinations or with contamination due to showers. The momentum selection system is designed such that all particles with a possible momentum above 50 GeV/c are reanalysed together with as small a number as possible of the particles with momenta less than 50 GeV/c. This is achieved by considering only combinations of groups in the trays producing relatively straight trajectories. The momentum selection process considers each discharged flash-tube as a track so that no event is rejected which may be attributed to a particle of high momentum. The selection scheme has been tested and checked to ensure that it selects all events with momenta above 50 GeV/c.

As stated earlier this experiment is only concerned with penetrating particles with momenta greater than 300 GeV/c, thus by reanalysing as few events as possible below 50 GeV/c, the analysis time is decreased by a factor of three. Any event subsequently found to have a momentum of less than 50 GeV/c is rejected. This

technique is only used during the reanalysis of the failed events.

3.5 EVENTS NOT ANALYSED OR WHICH FAIL ANALYSIS

Several types of event are not analysed at all at the first attempt, others are failed after the analysis. Table 3.2 shows the error codes associated with these failed events.

TABLE 3.2

ERROR CODES FOR WHICH THE ANALYSIS PROGRAMME FAILS THE EVENT

ERROR CODE	ERROR
91	One or more flash-tube trays with no group in it
92	More than thirty columns of flash-tube data in tray 5 (ie incident extensive air shower)
93	More than ten group combinations successfully analysed
94	All the combinations of groups in the trays fail
95	Combination of groups fails the standard deviation or group-trajectory separation criteria
96	Possible multiple muons (3 or more successfully analysed independent combinations of groups)
99	More than twenty-five groups in all the trays combined

Error codes 91, 92 and 99 are generated before the analysis procedure commences, the remainder being generated after the analysis is complete. The reasons for failing to analyse an event are described below together with the method of reclamation for each separate type of failure. As many events as possible have been reclaimed in order to decrease the corrections that subsequently have to be applied to the data to allow for the unanalysed events. Figure 3.2 shows schematically the main parts of the analysis programme

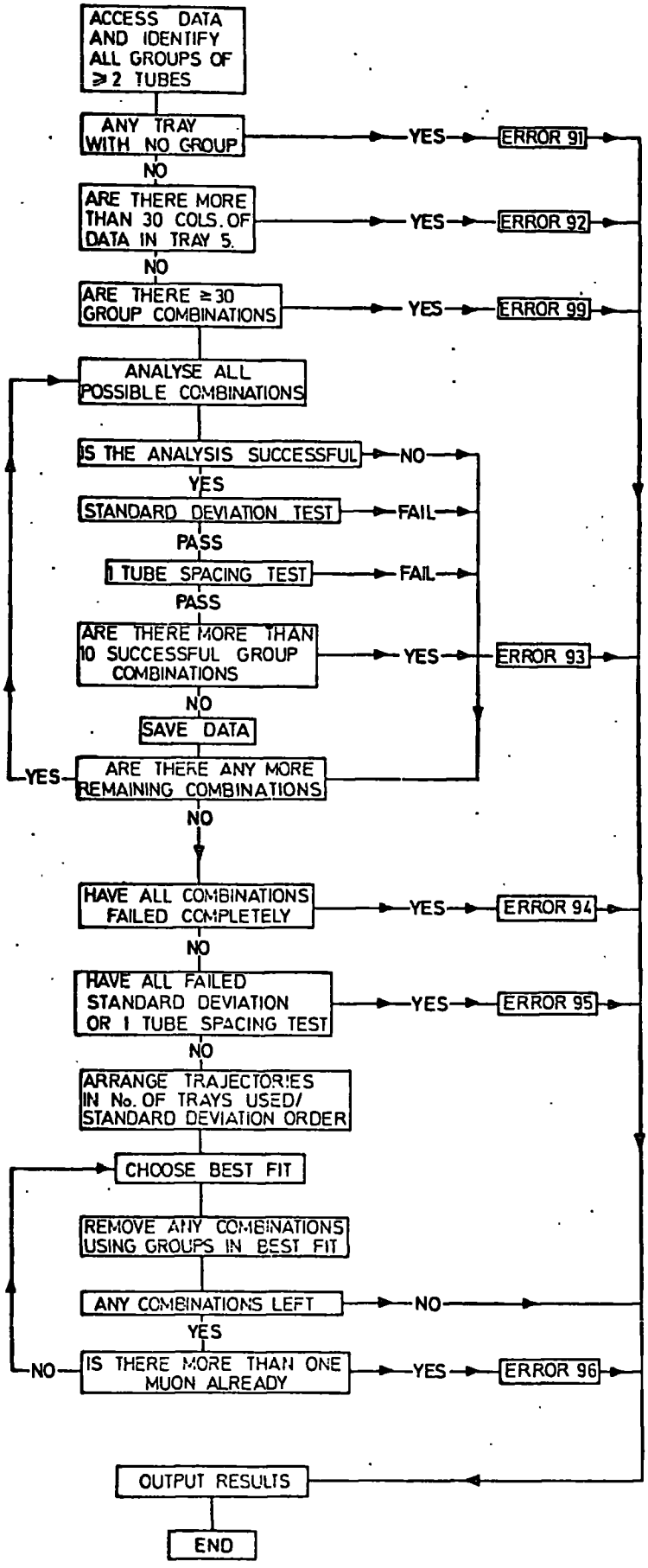

Figure 3.2. A flow chart showing the essential features of the analysis programme.

and illustrates at which points the error codes arise.

3.5.1 NO GROUP IN A TRAY (Error Code 91)

For the data obtained using the Mark II momentum selector the average number of tubes discharged is 4.58 taken over the five trays. Table 3.3 shows the separate layer efficiencies for each layer and the average layer efficiency for each tray. It should be noted that the maximum expected layer efficiency is 65%.

TABLE 3.3

LAYER EFFICIENCIES FOR EACH TRAY (Mark II data)

LAYER	TRAY 1	TRAY 2	TRAY 3	TRAY 4	TRAY 5
1	58.4	49.9	63.0	57.3	54.4
2	58.0	63.8	59.1	58.9	57.6
3	58.1	56.3	33.7	57.6	58.0
4	61.6	60.3	61.6	58.5	54.7
5	56.8	57.0	41.6	57.9	51.3
6	58.9	58.5	55.7	60.4	55.5
7	59.5	60.4	59.4	53.7	58.9
8	60.1	57.6	57.9	61.6	58.9
AVERAGE	58.9	58.0	54.0	58.2	57.3

A calculation has been made of the expected number of events for which only one tube would be discharged in a tray due to the inefficiencies of the flash-tubes. Each individual layer efficiency was considered in each tray for the Mark II momentum selector data. This showed that the number of events lost due to the discharge of single tubes only in any tray is 1.12%. Such a loss is considered small and no attempt to retrieve such events is made. However a correction is applied to the final results of the experiment to allow for these events. Table 3.4 shows the

expected frequency distribution and the calculated frequency distribution of the number of tubes per track for each tray. (Each tray is different due to the different layer efficiencies for each tray.) The total number of particles considered is 10000.

TABLE 3.4

TUBE POPULATION DISTRIBUTIONS FOR EACH MEASURING TRAY

		EXPECTED NUMBER OF EVENTS				
No OF TUBES PER TRACK	PER TRAY FOR 100% EFFICIENT FLASH-TUBES	ALLOWING FOR THE INEFFICIENCIES TRAY 1	TRAY 2	TRAY 3	TRAY 4	TRAY 5
8	3	1	1	1	1	1
7	689	346	306	169	319	247
6	2356	1567	1599	897	1419	1278
5	5361	4126	4186	2499	3891	3552
4	1574	2979	3012	3455	3154	3393
3	17	854	801	2255	1041	1283
2	0	116	92	653	161	228
1	0	8	4	67	12	19
0	0	0	0	2	0	0

It can be seen from table 3.4 that 112 events out of 10000 are expected to cause one tube or less to discharge in one of the trays. The actual figure is slightly lower than this due to knock-on electrons and bursts close to the track triggering adjacent tubes which would not have been triggered by the actual particle.

For the data obtained using the Mark I momentum selector the measured layer efficiencies are substantially lower, namely 48.4%, 52.5%, 43.8%, 58.1%, and 53.8% for trays 1 to 5 respectively, and the probability of there being only one discharged tube

on the track in any tray is much higher. Therefore the Mark I data events having only one tube on the track are included and labelled as such so that the actual number of such events is known. These events were located by searching for events with one discharged tube within one tube spacing of the fitted trajectory in an unused tray.

3.5.2 TOO MANY GROUPS (Error Code 99)

So as to decrease the overall time required for the analysis of the data on the first analysis run, events which have more than twenty-five possible group combinations are labelled as such and only analysed at the reanalysis stage. Most of these events are side showers and can be identified as such by studying a computer 'picture' of each event. Figure 3.3 shows a computer picture of such a side shower from which it can be seen that all the tracks are incident at large zenith angles. It should be noted that each tray is separated by approximately 1.25m of iron and hence the particles only traverse relatively small amounts of iron and need only to be of low energy. In the diagram, each 'star' represents a discharged flash-tube and the crosses at the edge of each tray indicate the extremities of that tray. It should also be noted that neither the tubes in each tray nor the trays themselves are directly underneath each other nor are the trays equally spaced in the vertical direction. Hence the computer picture is somewhat distorted.

The 'cut' at twenty-five group combinations means that any event including two or more muons will be rejected at this early stage of the analysis and can be analysed later. By rejecting all these complex events initially it is ensured that only 'good' (clear) events pass the initial analysis procedure and therefore such events do not need extensive individual checking.

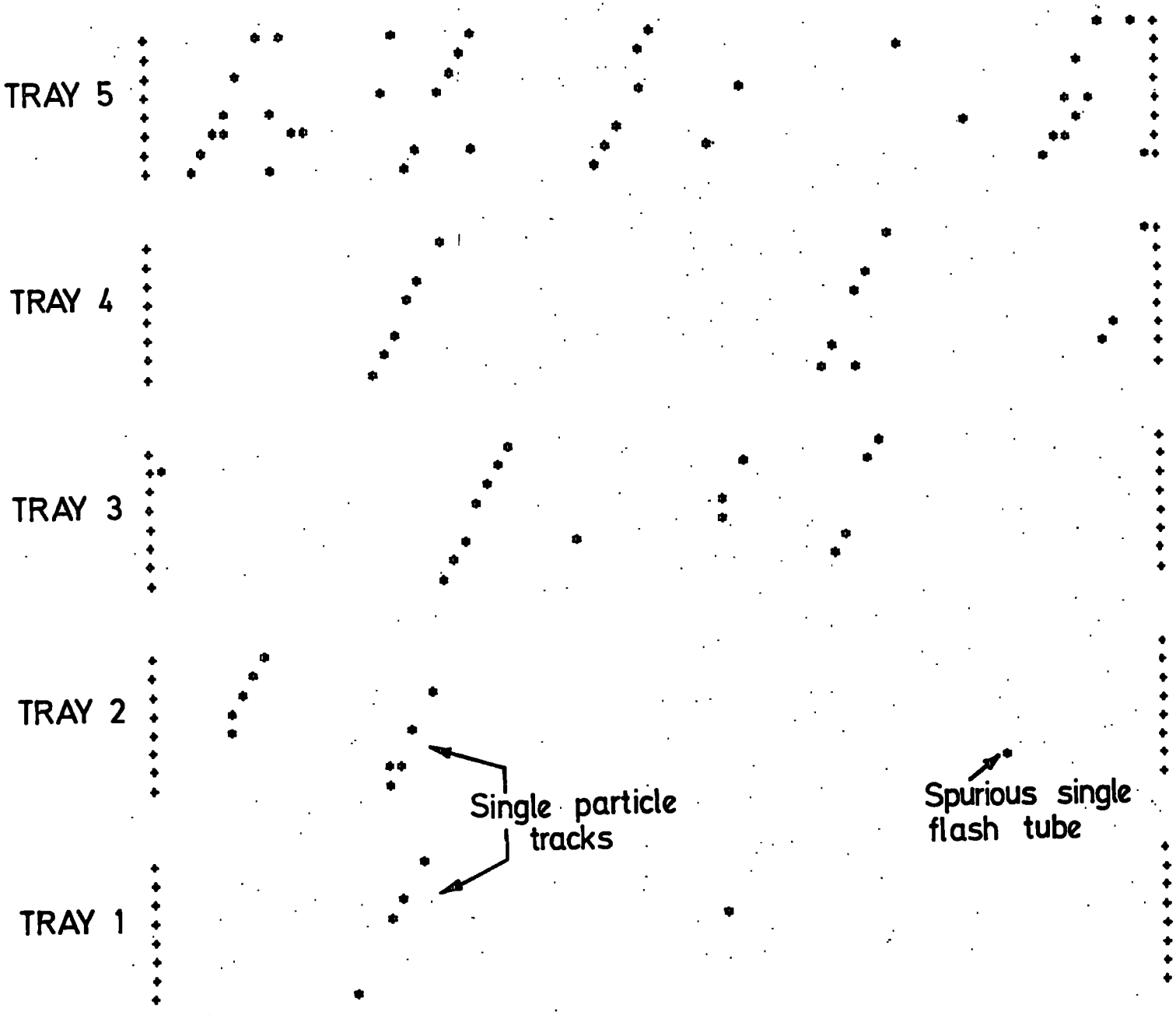

Figure 3.3.
A computer picture of a side shower.

The failed events in this category are reanalysed later as a separate group using the main analysis programme with the maximum number of groups set at infinity and incorporating the computer momentum selector (section 3.4).

3.5.3 SHOWERS (Error Code 92)

Any event with more than thirty columns of data in tray 5 is regarded as an air shower and as such is not analysed. The 'cut' at thirty columns was used after a study had been made of the frequency distribution of the number of columns of data in each event for trays 1 and 5 (see figure 3.4). For any event with so much tube information in tray 5, it is impossible to say whether the particle actually passed through the tray or whether the tubes were discharged purely by the accompanying particles (figure 3.5). The cut also decreases the analysis time since there may be up to thirty groups in tray 5 to consider.

In order to estimate the number of accompanied muons actually traversing the whole magnet all the shower type events are reanalysed omitting tray 5. The momentum spectrum so obtained is that for particles traversing the bottom four measuring trays with an air shower triggering the top scintillation counter. The acceptance for these particles is much larger (figure 3.6) than that for the whole spectrograph and the spectrum must be reduced by multiplying by the ratio of the acceptance of the spectrograph for the bottom four measuring trays to the acceptance for all five measuring trays. The acceptance of the spectrograph is discussed in detail in chapter 4.

The need to analyse such shower events arises since it is uncertain whether the momentum spectrum of muons accompanied by air showers is the same as that for the unaccompanied muons. It is therefore necessary to estimate the numbers of muons traversing

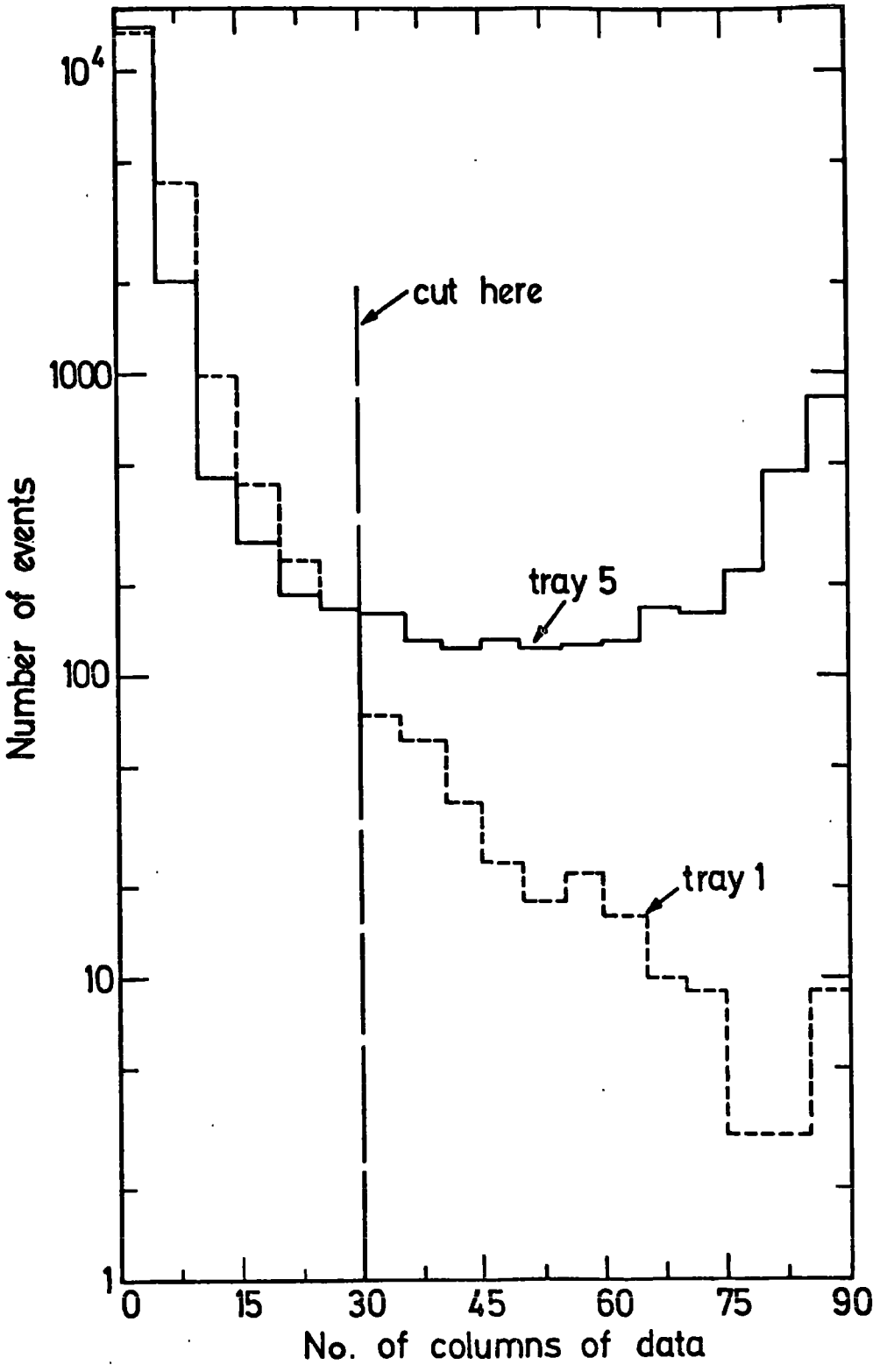

Figure 3·4. Distribution of number of columns of data per event in trays 1 and 5.

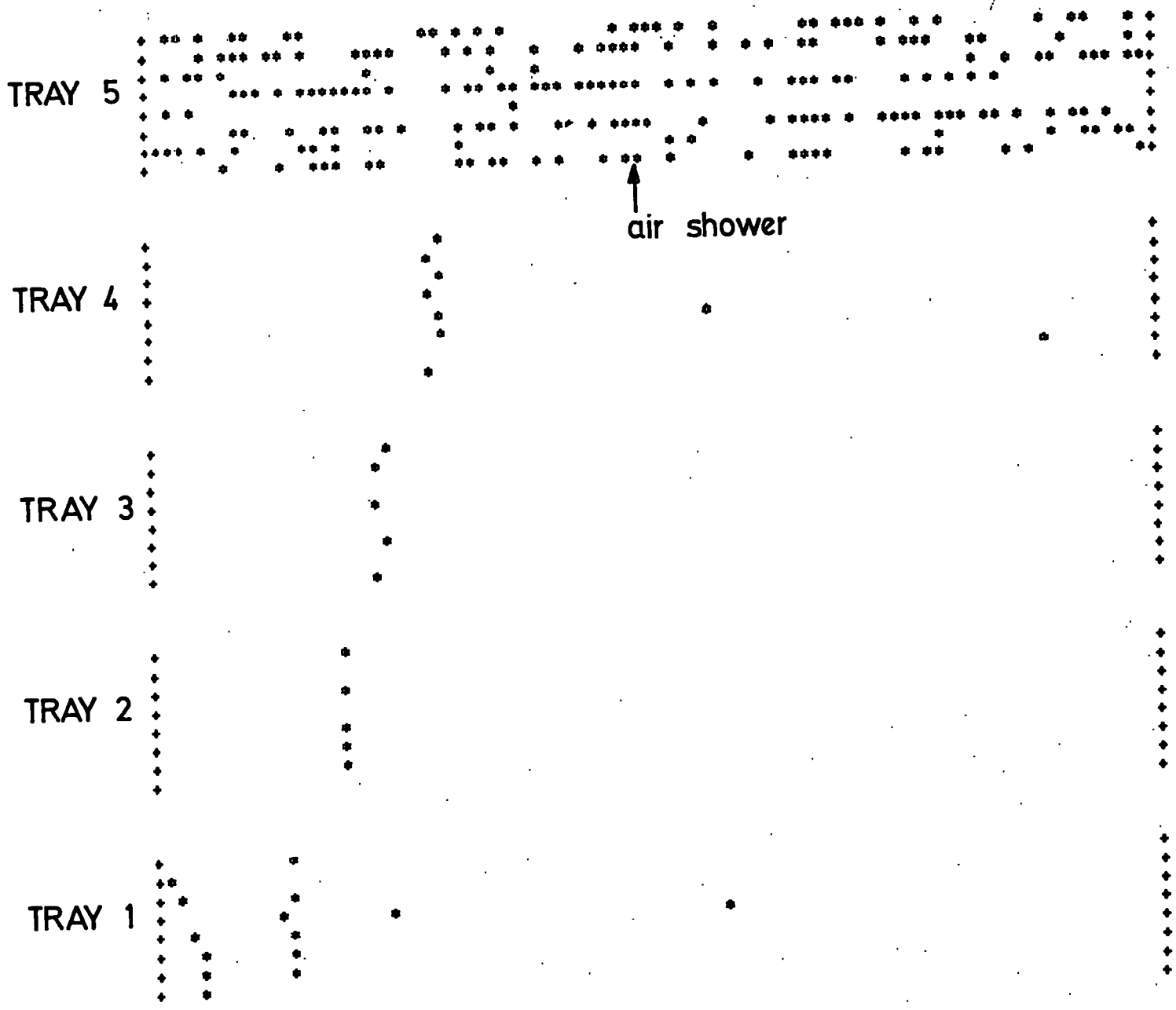

Figure 3.5.

A computer picture showing a muon accompanied by an air shower.

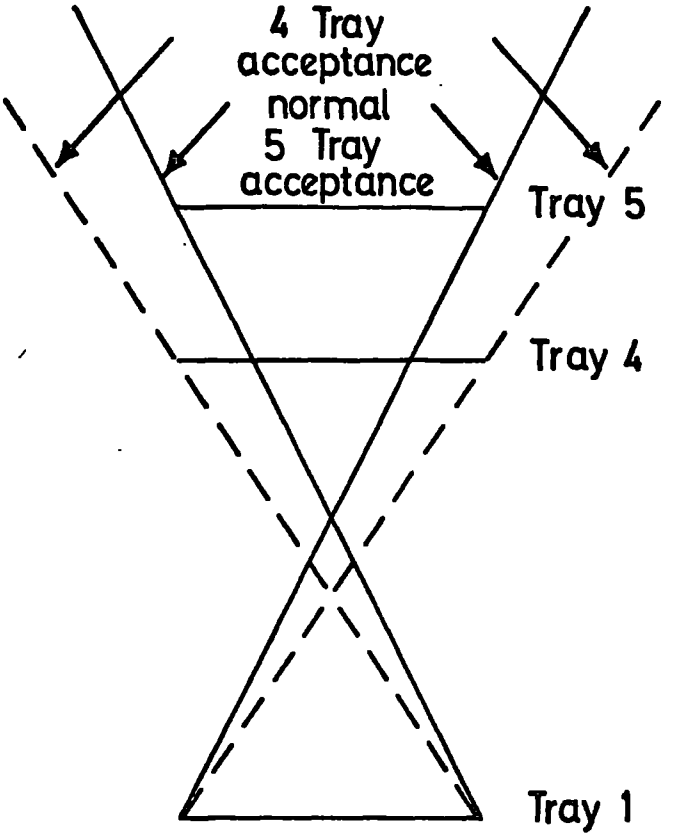

Figure 3·6. Schematic diagram showing how the acceptance for muons accompanied by an air shower triggering the top tray is increased.

the top tray accompanied by a shower in order that the spectrum can be measured.

3.5.4 EVENTS WITH LARGE STANDARD DEVIATION (Error Code 95)

The analysis programme has been thoroughly tested on the data obtained from the Mark I momentum selector. Each event was studied individually using its own computer 'picture'. Events which were possibly wrongly analysed were located and checked. It was found that all the wrongly analysed events in this sample of data, with an apparent momentum greater than 20 GeV/c, had a standard deviation for the fitted trajectory greater than 0.25×10^{-2}m. On this basis all particles with a computed momentum greater than 20 GeV/c and a standard deviation of the fitted trajectory greater than 0.25×10^{-2}m are failed by the analysis programme. For particles having a momentum of less than 20 GeV/c, the requirement is that the standard deviation of the fitted trajectory must not be greater than 0.1×10^{-1}m. The reason for the 'cut' being at a higher standard deviation for particles of lower momentum is that these particles are more likely to be scattered and hence the mean value of the standard deviation for the fitted trajectory is increased. Ideally the limitation on the value of the standard deviation would be a continuously varying function of momentum. However for the purposes of this experiment it is found to be sufficient to use the two different 'cuts' for particles with momenta above and below 20 GeV/c, to ensure that all events passing these tests are correctly analysed.

In order to check that the above 'cuts' are reasonable, the frequency distribution of the standard deviations of the fitted trajectories for actual events have been plotted and are shown in figure 3.7. As can be seen from the figure the distributions are dependent upon the momentum range considered. Obviously some

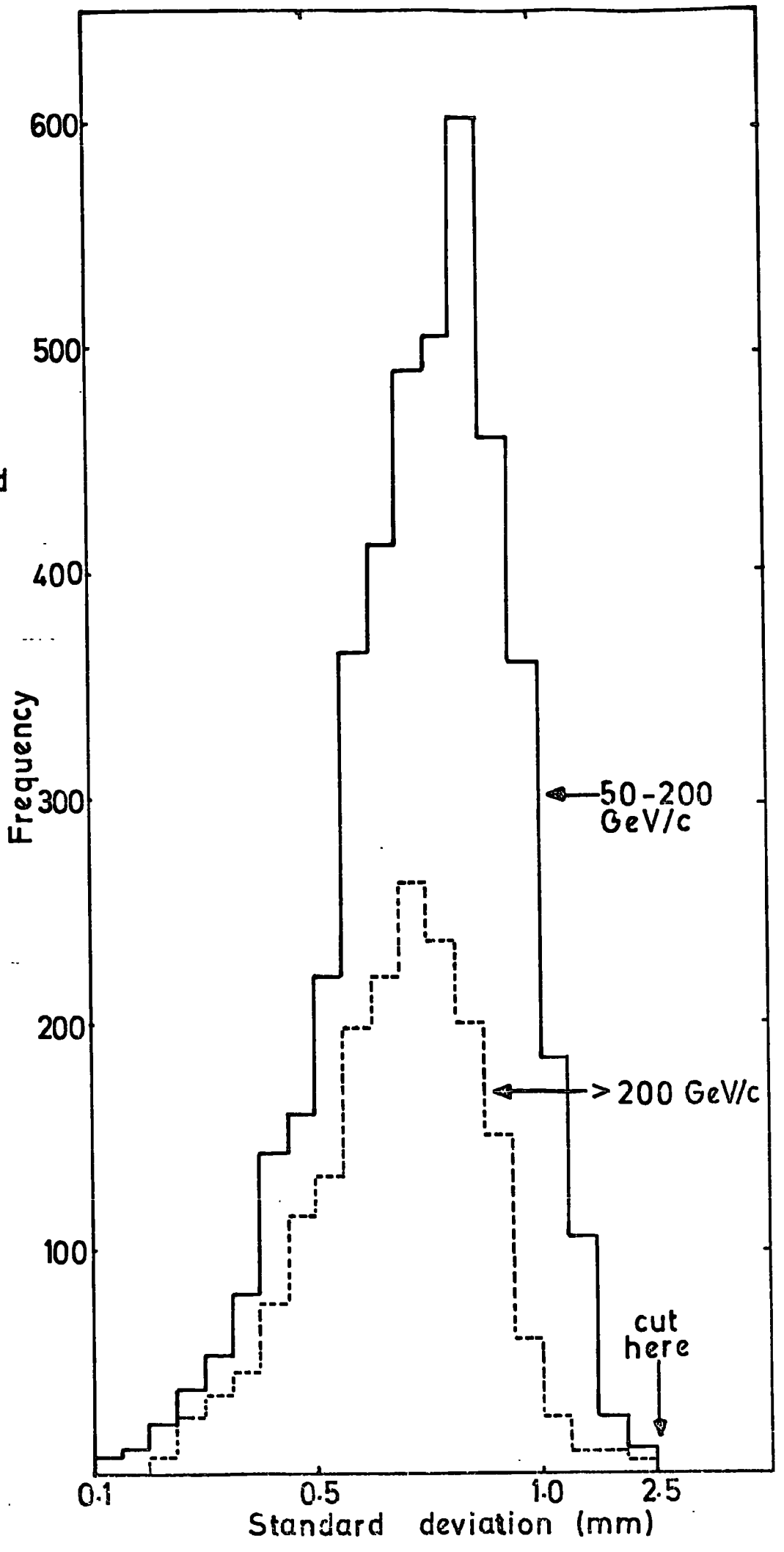

Figure 3.7
The distribution of the standard deviations of the fitted trajectories (for five tray fits only).

events that are rejected are in fact correctly analysed. These events are however reclaimed during the reanalysis stage, since all events failing these tests are studied individually before being reanalysed using the amended analysis programme.

A large standard deviation is usually indicative of a wrong track being considered in one of the trays where there are either two groups close together or two tracks which are confused into a single group. The reanalysis procedure for these events and those discussed in the following sections is described in section 3.6.

3.5.5 EVENTS WHICH FAIL THE ONE TUBE SPACING TEST (Error Code 95)

Events with no group within one tube spacing of the fitted trajectory in an unused tray are failed on the basis that there may be no track associated with the traversing particle in that tray. Figure 3.8 shows a computer picture of such an event. The tray in question in this case is tray 5. It can be seen that for this particular event the tracks in tray 5 are not associated with the tracks in the other four trays which are due to a single particle, which does not actually pass through tray 5. It is likely that the particle passed out of the back plane of the spectrograph.

3.5.6 EVENTS WITH TOO MANY UNUSABLE TRAYS (Error Code 94)

These events mainly correspond to the real trajectories of particles, but due to a combination of bursts in the instrument and the inefficient tubes there are three or more trays of the spectrograph which cannot be used. These events are checked visually before being placed in the 'fail' category, therefore this fail category incorporates real events for which no momentum can be calculated.

3.5.7 EVENTS WITH TOO MANY SUCCESSFUL COMBINATIONS OF GROUPS (Error Code 93)

Events which contain more than ten successfully fitted tracks

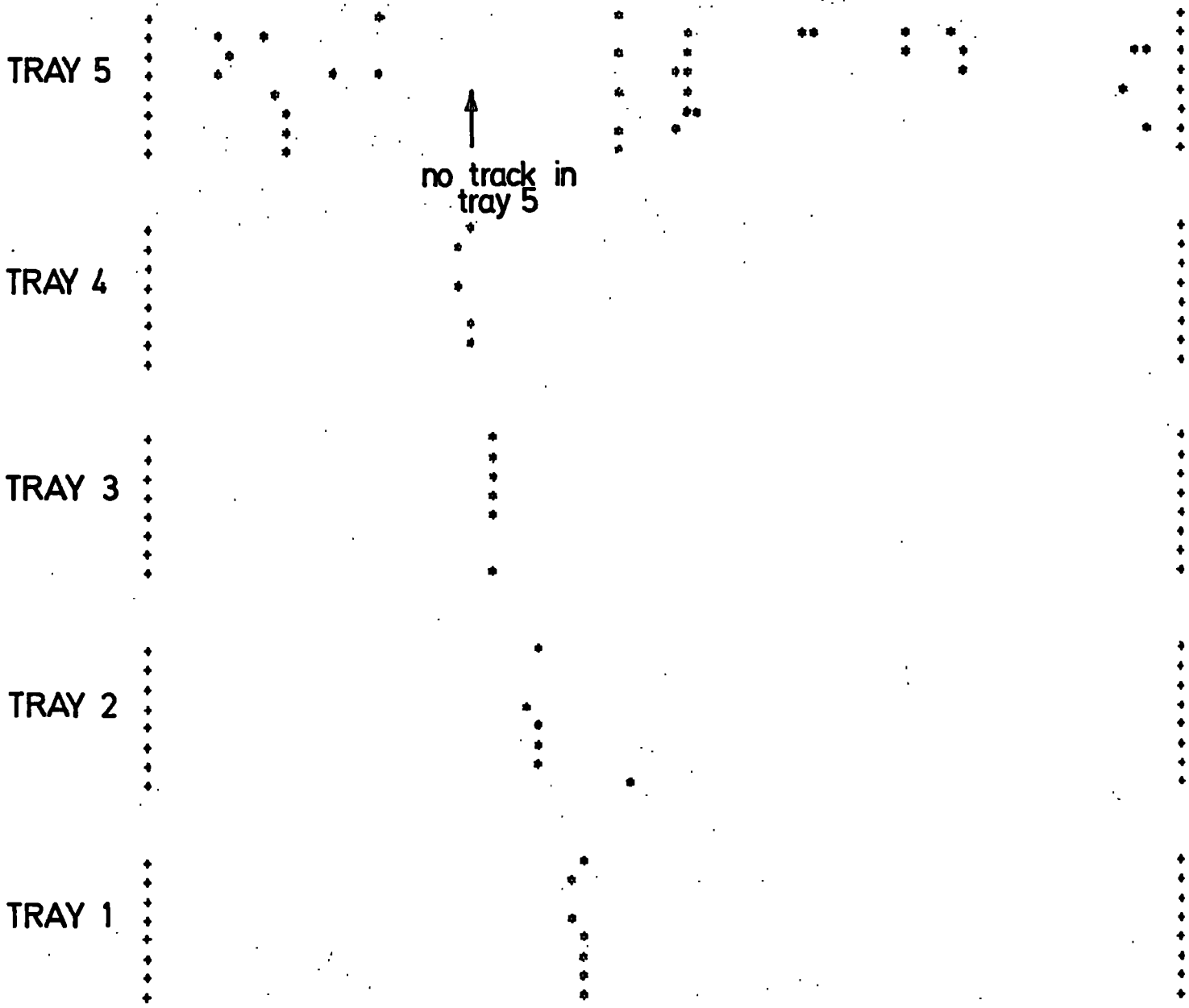

Figure 3·8.
A computer picture of an event with no track associated with traversing particle in tray 5.

distributed amongst the five trays are failed mainly because of the difficulty in deciding which of the tracks in the various trays are associated with each other. Figure 3.9 shows a computer picture of such an event. These events are analysed manually if it is considered that there are muons passing through the complete spectrograph. This error usually only occurs during the reanalysis of the events which fail on the first analysis attempt because there are too many possible group combinations.

3.5.8 POSSIBLE MULTIPLE MUON EVENTS (Error Code 96)

As mentioned previously the programme searches for trajectories of two muons if there are more than one successful group combination. However it is possible that there are three or more muons traversing the spectrograph, in which case there may be successful group combinations remaining after those group combinations using the groups associated with the first two muons are removed. These events are 'flagged' with error code 96, since it is possible that there may be more than two muons traversing the spectrograph. There are only a small number of these events and they are all studied individually, so that the correct trajectories (if any) can be identified. Events of this type are only found during the reanalysis of those events which fail the first analysis due to there being more than twenty-five possible group combinations.

3.6 THE REANALYSIS OF THE FAILED EVENTS

The first stage of the reanalysis procedure is to obtain a computer picture of each event to be reanalysed. The next stage is to plot out an accurate picture of any confused or complicated event. The accurate pictures are obtained by plotting the discharged tubes on a special diagram of the spectrograph. The flash-tube trays are drawn oversize but their respective centres are the correct relative distances apart. Figure 3.10 shows such a plot

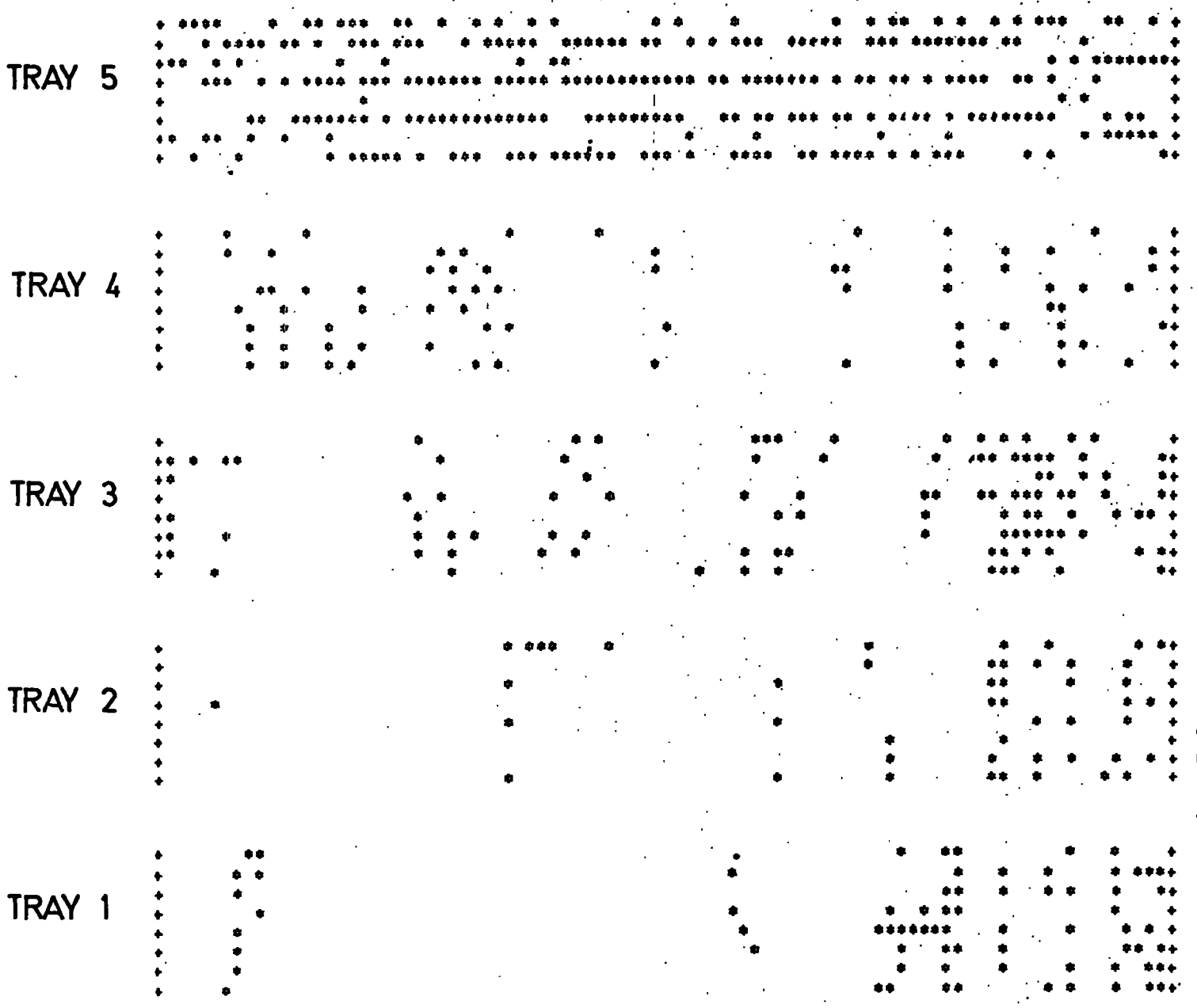

Figure 3.9.
A computer picture of an event with several muon tracks in each tray.

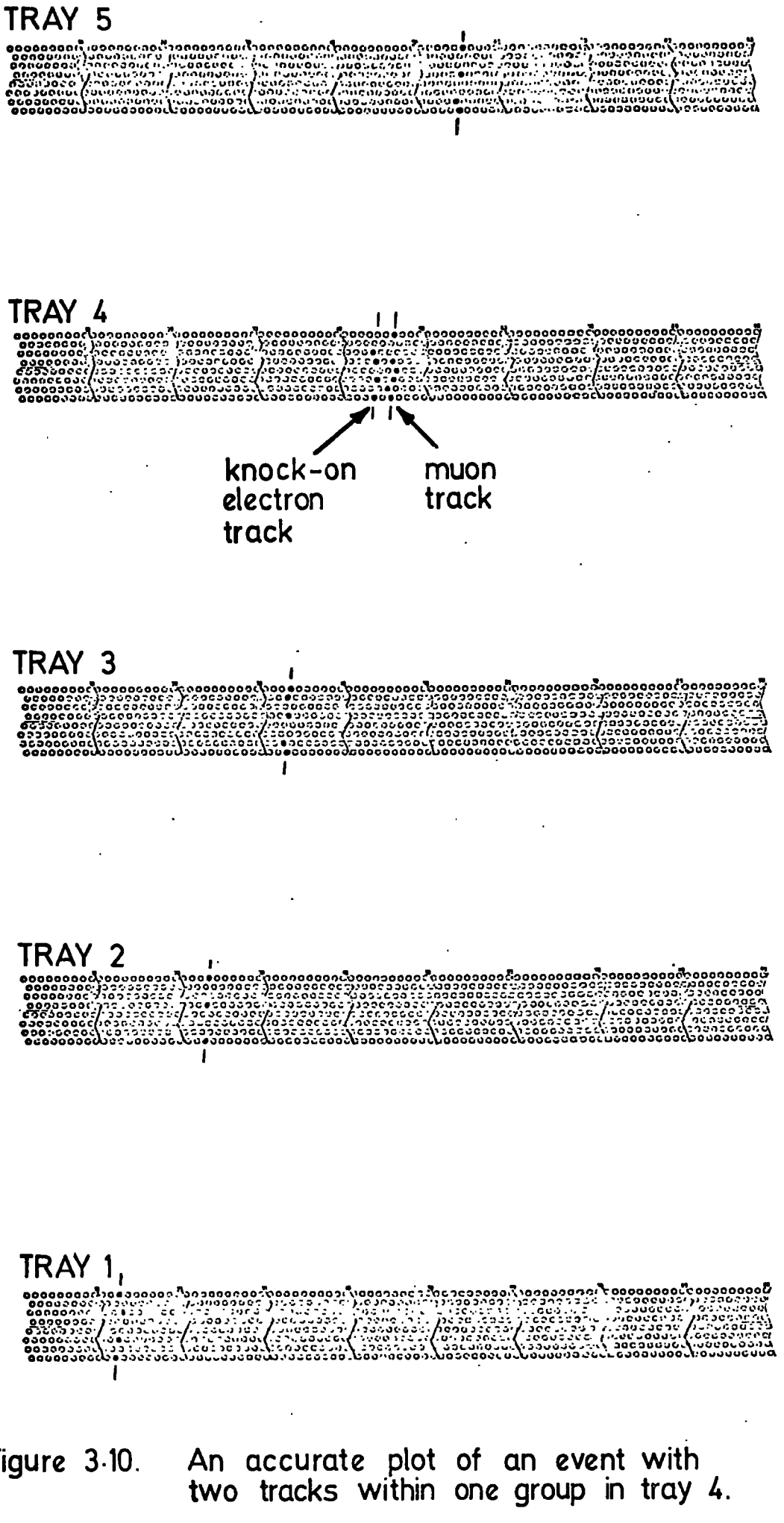

Figure 3·10. An accurate plot of an event with two tracks within one group in tray 4.

for an event with a confused group in tray 4.

The events all have to be placed into one of the following five categories on reanalysis:

a) FAILED

b) OMIT A TRAY } RECLAIMED

c) SCATTERED }

d) LOW MOMENTUM ($\leq$ 50 GeV/c) } REJECTED

e) OUTSIDE ACCEPTANCE }

Since the experiment was only concerned in measuring the muon momentum spectrum above approximately 300 GeV/c, a limit of approximately 50 GeV/c is placed on any event by the use of the computer momentum selector before it is reanalysed. Any event which does not pass the momentum selector test is omitted from the reanalysis stage, and only those events with momentum greater than 50 GeV/c are regarded as high momentum events requiring further investigation. If all the low momentum events were studied in detail the process would be very time consuming and since these events are usually due to spurious triggers of the momentum selector it is considered that it is reasonable to reject them. The lowest momentum accepted by the momentum selector is calculated to be approximately 90 GeV/c, therefore ideally there should be no events with a momentum lower than 90 GeV/c.

The events in the failed category include those for which no momentum can ever be calculated. These are added to those in the failed category as described earlier (section 3.5.6). A correction has subsequently to be made to the data for these events if an absolute spectrum is to be measured.

Those events which can be reclaimed by omitting a tray are labelled as such and are usually the result of the wrong track being used in a tray. This is checked by splitting the offending

group in the tray into two tracks or analysing two tracks close together individually and comparing the estimated momentum using each of the two tracks with that obtained by omitting the data from the tray. If the original answer obtained by the programme is consistent with using one of the tracks in the offending tray and that of omitting the tray consistent with the other track in that tray, then this event is placed in the 'omit a tray' category and is reclaimed by analysing the event omitting the offending tray.

Other muons are scattered when traversing the spectrograph and the extrapolated trajectory in trays 1 and 5 does not always pass within one tube spacing of the track in that tray as required in the initial analysis of the event. These events are reanalysed using 4cm instead of one tube spacing as the distance between the fitted trajectory and the nearest group in the tray and are reclaimed in this way. The reason for not using a 4cm test in the initial analysis is that for some events non-associated particle tracks are found within 4cm of the actual track, which in some cases would lead to the wrong answers being obtained. It is, therefore, easier to use a one tube spacing test and reclaim those events which are scattered.

By plotting out some of the failed events on the scale plots it can be seen clearly that in some of these events the penetrating particle of interest missed one of the flash-tube trays and also the top triggering scintillation counter. Figure 3.11 shows such an event, where the track in tray 5 is due to an accompanying particle at a large zenith angle. These events are all rejected as being outside the acceptance of the spectrograph.

Table 3.5 shows the error codes associated with the reclaimed events. These error codes occur in place of the tray fit code

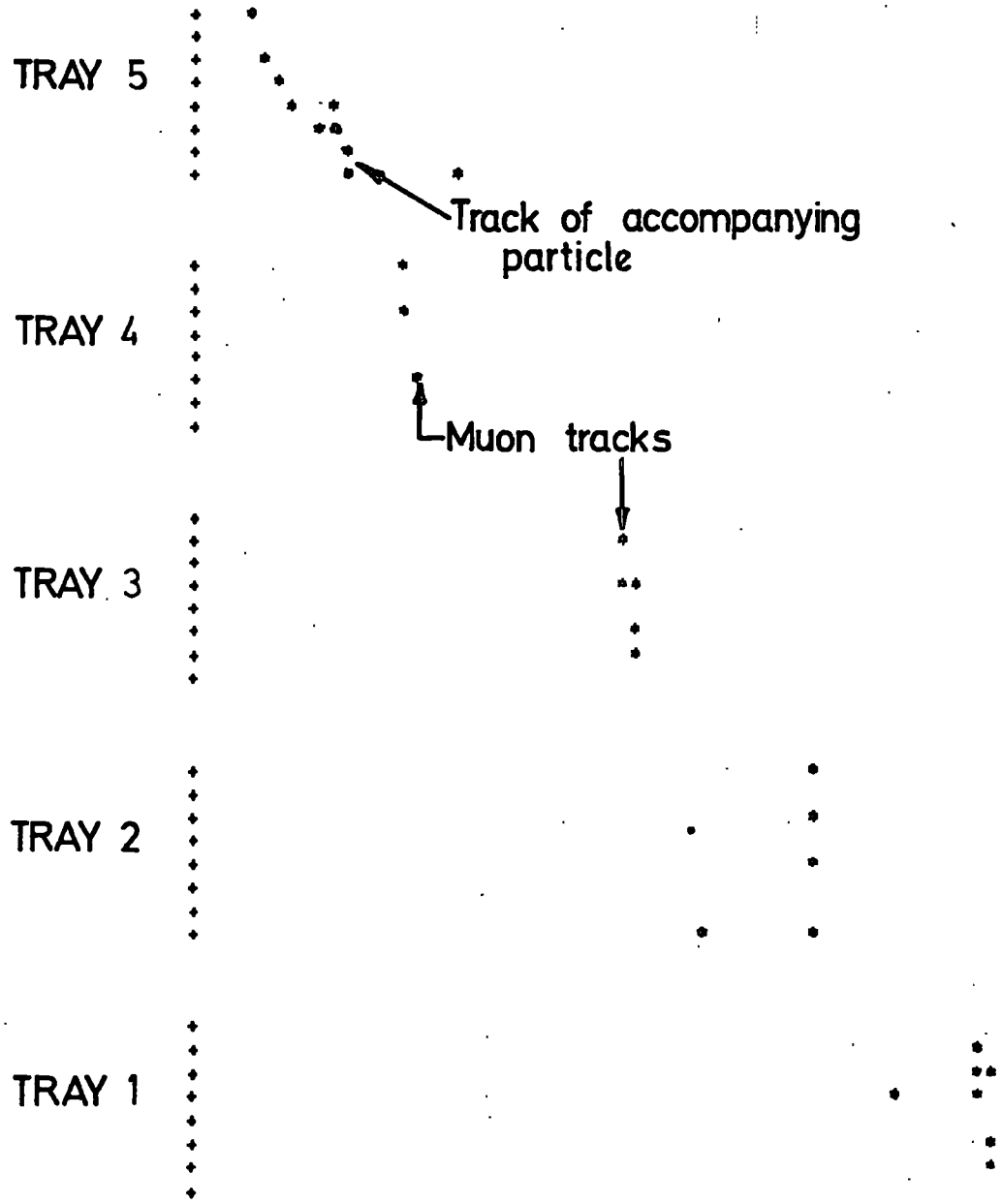

Figure 3.11.
A computer picture of an event which contains a muon which does not pass through tray 5.

for the tray concerned.

TABLE 3.5

TRAY FIT ERROR CODES FOR RECLAIMED EVENTS

ERROR CODE	ERROR
12	Only one tube on or near the track (Mark I data only)
13	Tray omitted in reanalysis
14	Track not used in fitting trajectory
15	Burst lies on fitted trajectory

3.7 THE CHECKING OF SOME SUCCESSFULLY ANALYSED EVENTS

After the analysis has been completed, it is found necessary to check the answers obtained for some of the successfully analysed events. The events involved all have momenta greater than 200 GeV/c with the standard deviation of the fitted trajectory greater than 0.1×10^{-2} m. These events are reanalysed in the same way as the failed events, the computer 'picture' of these events being studied and any events with suspect groups being reanalysed. The majority of events in this category are found to be correctly analysed. However, the wrongly analysed events are found to have standard deviations greater than 0.15×10^{-2} m. Thus it is considered that all wrongly analysed events are found if the limit is set at 0.1×10^{-2} m. It is also found that the events with momenta between 200 GeV/c and 250 GeV/c in this category are all correctly analysed. Thus it is also considered that a limit on the momentum of 200 GeV/c is sufficiently low to exclude any wrongly analysed events.

3.8 CONCLUSION

In this chapter every event for which a momentum can be calculated has been analysed using as many trays as possible.

The next chapter considers all the corrections which have to be applied to the data in order to derive the absolute momentum spectrum. This includes corrections for unanalysed events, showers and acceptance effects.

CHAPTER 4

INSTRUMENTAL BIASES

4.1 INTRODUCTION

For a large spectrograph such as MARS there are many instrumental effects which may cause biases in the results of experiments performed using the instrument. Some of the most important pieces of information required are the exact spatial coordinates of the detecting elements. The detectors must be aligned such that all the detectors are parallel to each other. The method used to align the measuring trays in MARS is unique, and has been briefly described by Ayre et al. (1975b). However a more detailed study has been made of the results and this subsequent analysis is described below.

Other instrumental effects, such as the overall acceptance and the efficiencies of the various detectors in the spectrograph are also discussed.

4.2 THE ALIGNMENT OF THE MEASURING TRAYS

4.2.1 THE ANALYSIS OF ZERO FIELD DATA

The spectrograph was initially operated in the zero magnetic field condition for approximately three months resulting in the collection of data for more than 30000 particles traversing the iron blocks. These data have been used check the alignment of the measuring trays.

The data are analysed in the same manner as that used for the magnetic field data, except that the final coordinates of the tracks used in each tray are recorded and a straight line rather than a parabola is used as the fitted curve. This can be seen to be reasonable, by considering the trajectory of a particle traversing a material in which there is no magnetic field which,

neglecting any scattering, would be a straight line.

For each set of coordinates thus obtained, the horizontal displacements of the tracks in trays 2, 3 and 4 from the straight line joining trays 1 and 5 are computed. Figure 4.1 shows schematically how these displacements are defined. Theoretically the distribution of displacements for each tray should be a normal distribution with a mean value corresponding to the error in the measured coordinate of that tray. Multiple Coulomb scattering of the particle in the iron blocks causes the distributions to be of greater width. This effect is discussed in more detail in section 4.8.

4.2.2 THE ESTIMATION OF THE SPATIAL COORDINATES OF THE MEASURING TRAYS

Two different sets of zero magnetic field data have been collected and analysed. Approximately 20000 events have been collected using the Mark I momentum selector to preselect the straighter, less scattered trajectories and approximately 13000 events without using any momentum selector (subsequently referred to as 'all events' data). The frequency distributions of the displacements of the tracks in the middle trays with respect to the line joining the tracks in the outer two trays are shown for both sets of data in figures 4.2 a), b), c) and 4.3 a), b) and c).

As can be seen from the figures, the frequency distributions obtained from the momentum selector data are asymmetric and this is more marked for larger values of the displacement. This is mainly due to spurious triggers caused by the zero bit (section 2.5) which selects trajectories with positive displacements in the middle trays and therefore the positive side of the distribution is enhanced as shown in figure 4.2. Therefore the mean displacement obtained will also be biased in the positive direction and hence it is necessary to locate the peak or mode of these distributions.

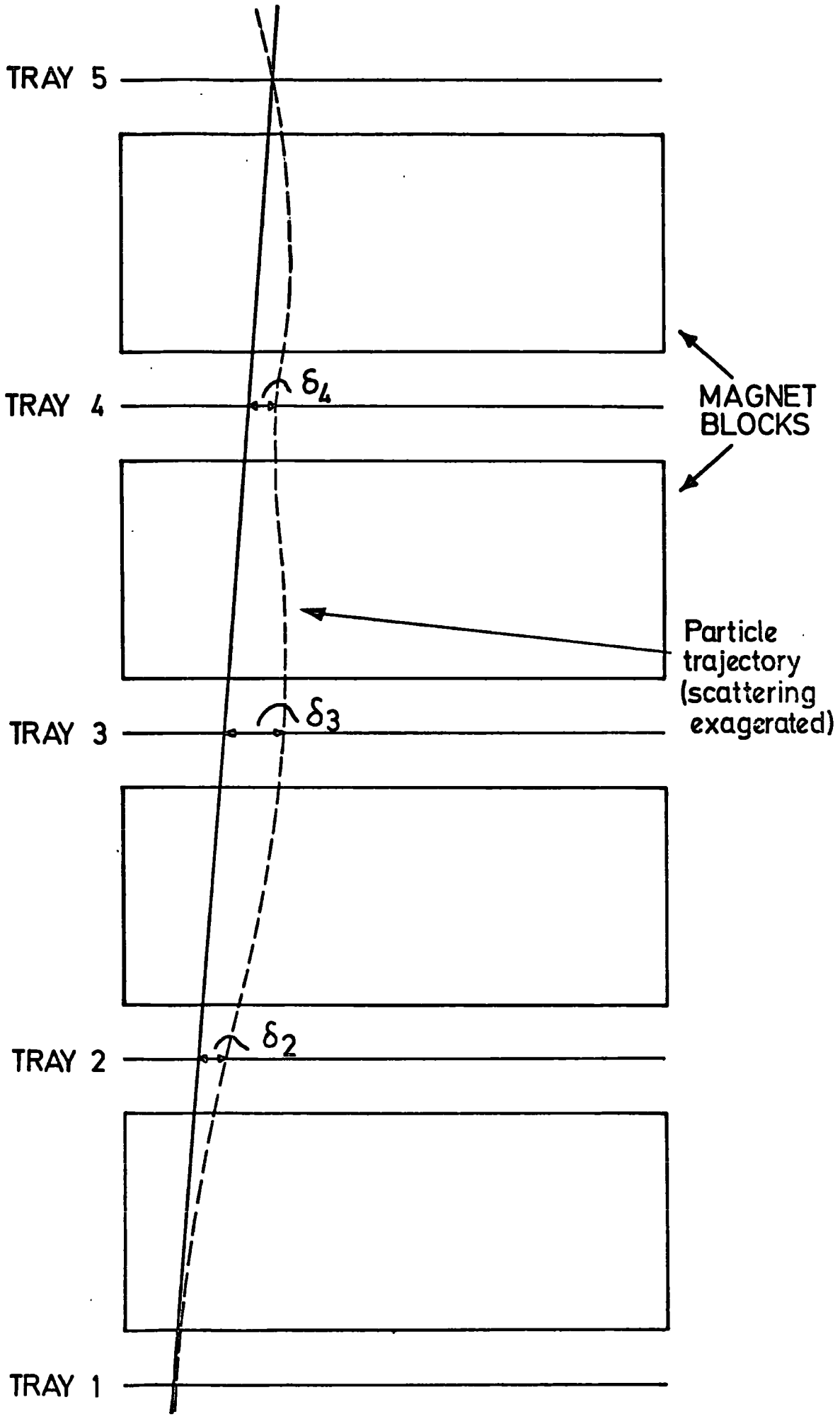

Figure 4.1. Diagram showing how the deflections in trays 2, 3 and 4 are obtained with respect to trays 1 and 5.

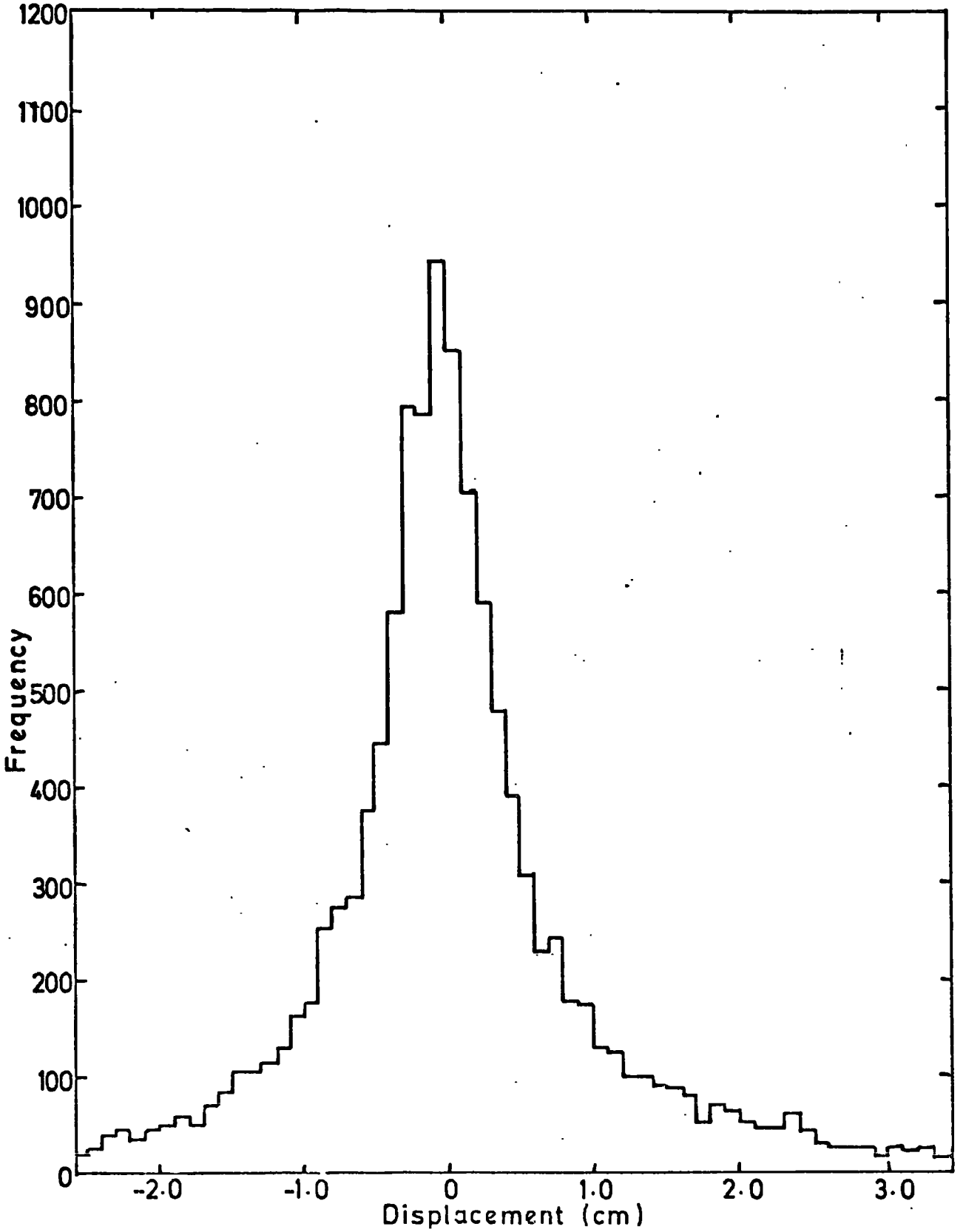

Figure 4.2(a) The displacement histogram for tray 2 for the momentum selector data.

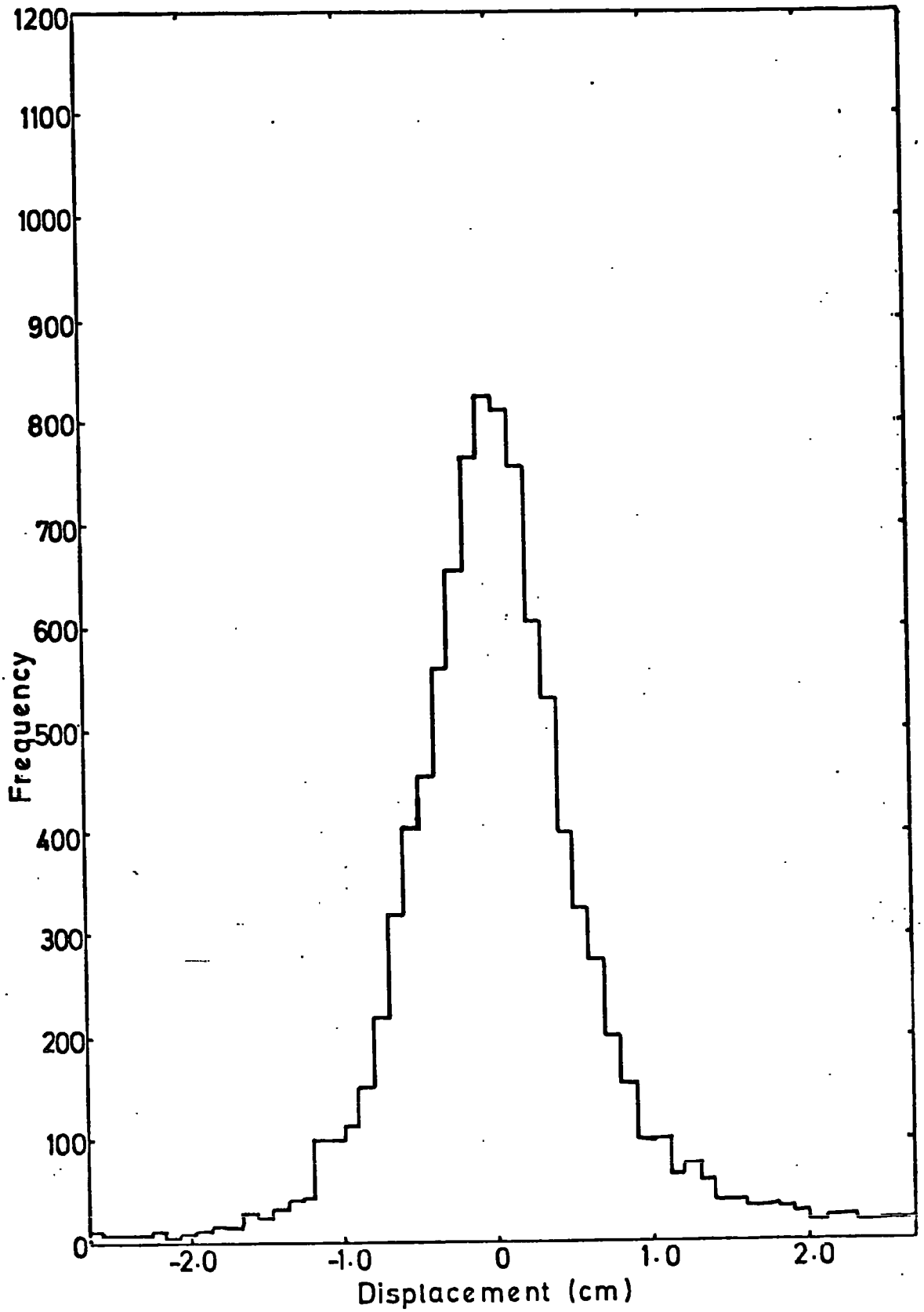

Figure 4.2(b) The displacement histogram for tray 3 for the momentum selector data.

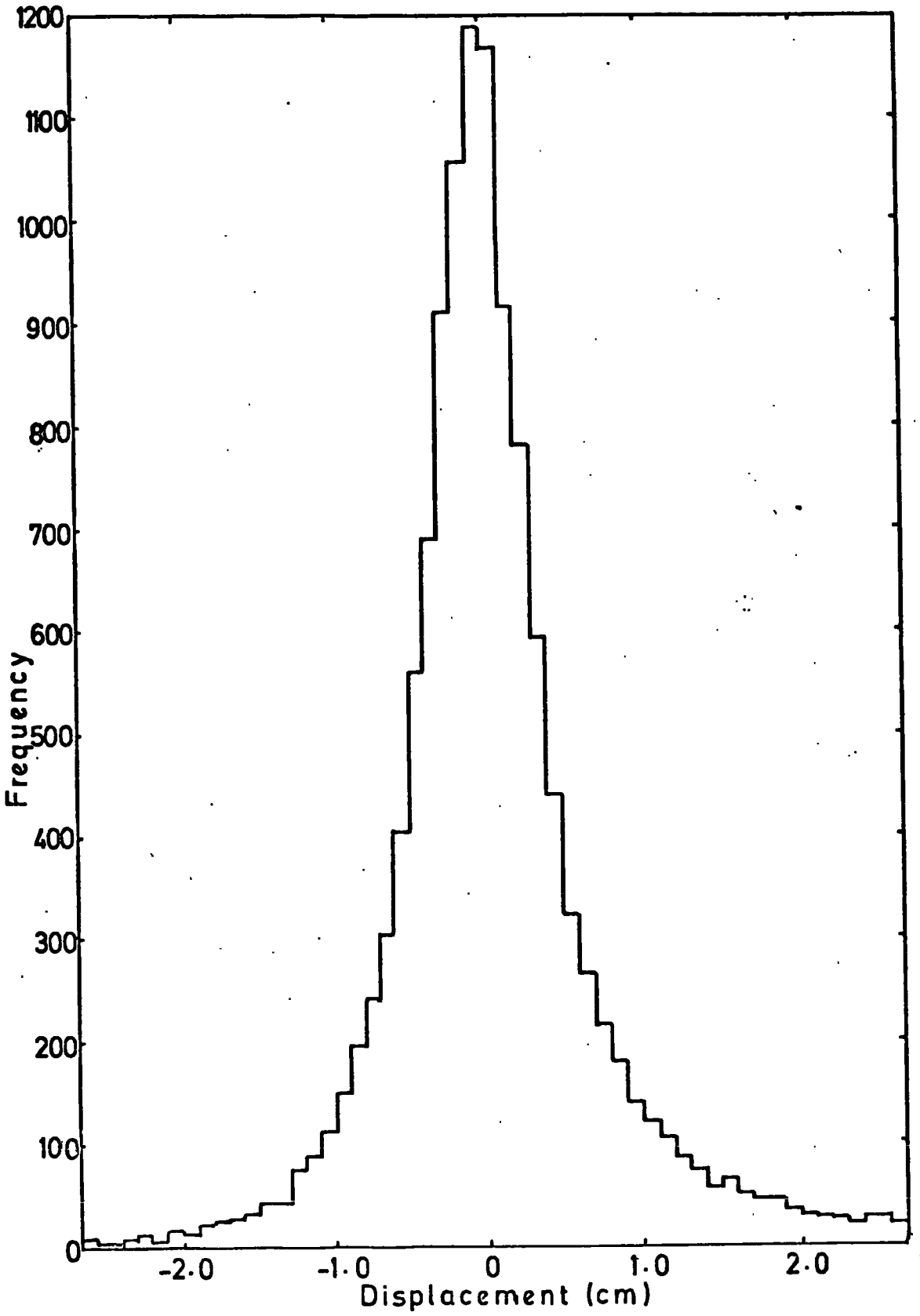

Figure 4.2(c) The displacement histogram for tray 4 for the momentum selector data.

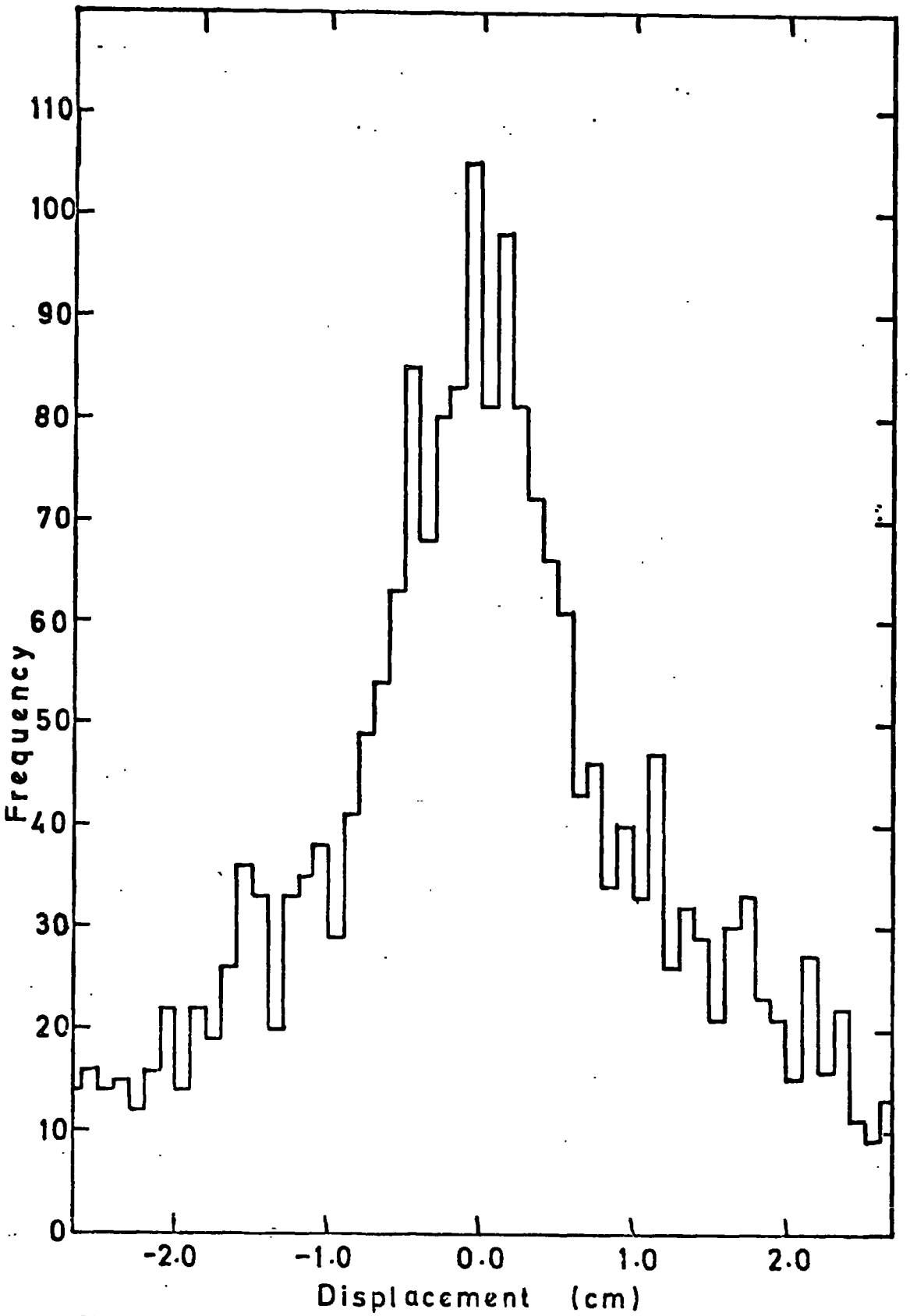

Figure 4.3 (a) Histogram of displacements for tray 2 (all events data)

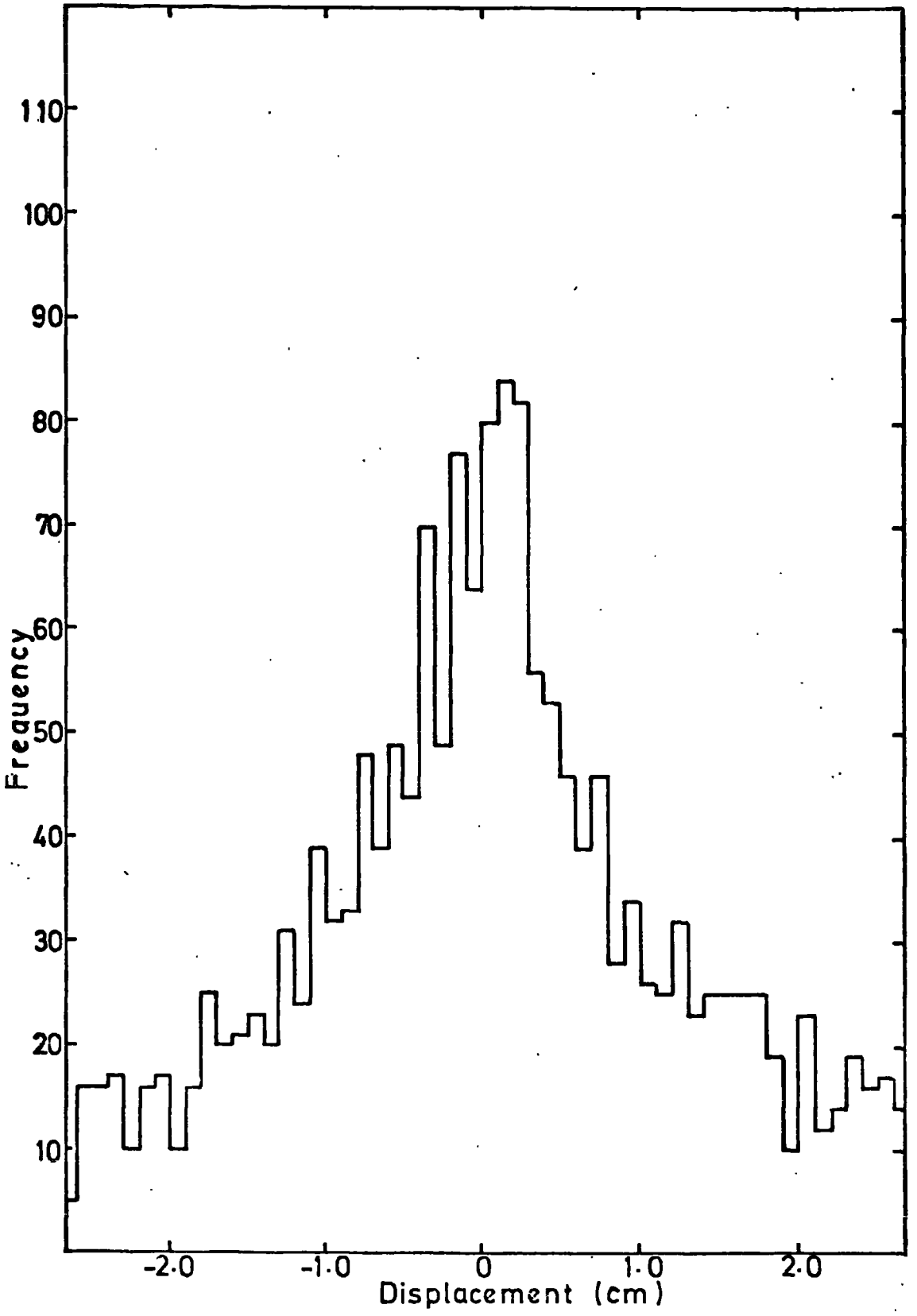

Figure 4·3(b) Histogram of displacements for tray 3 (all events data).

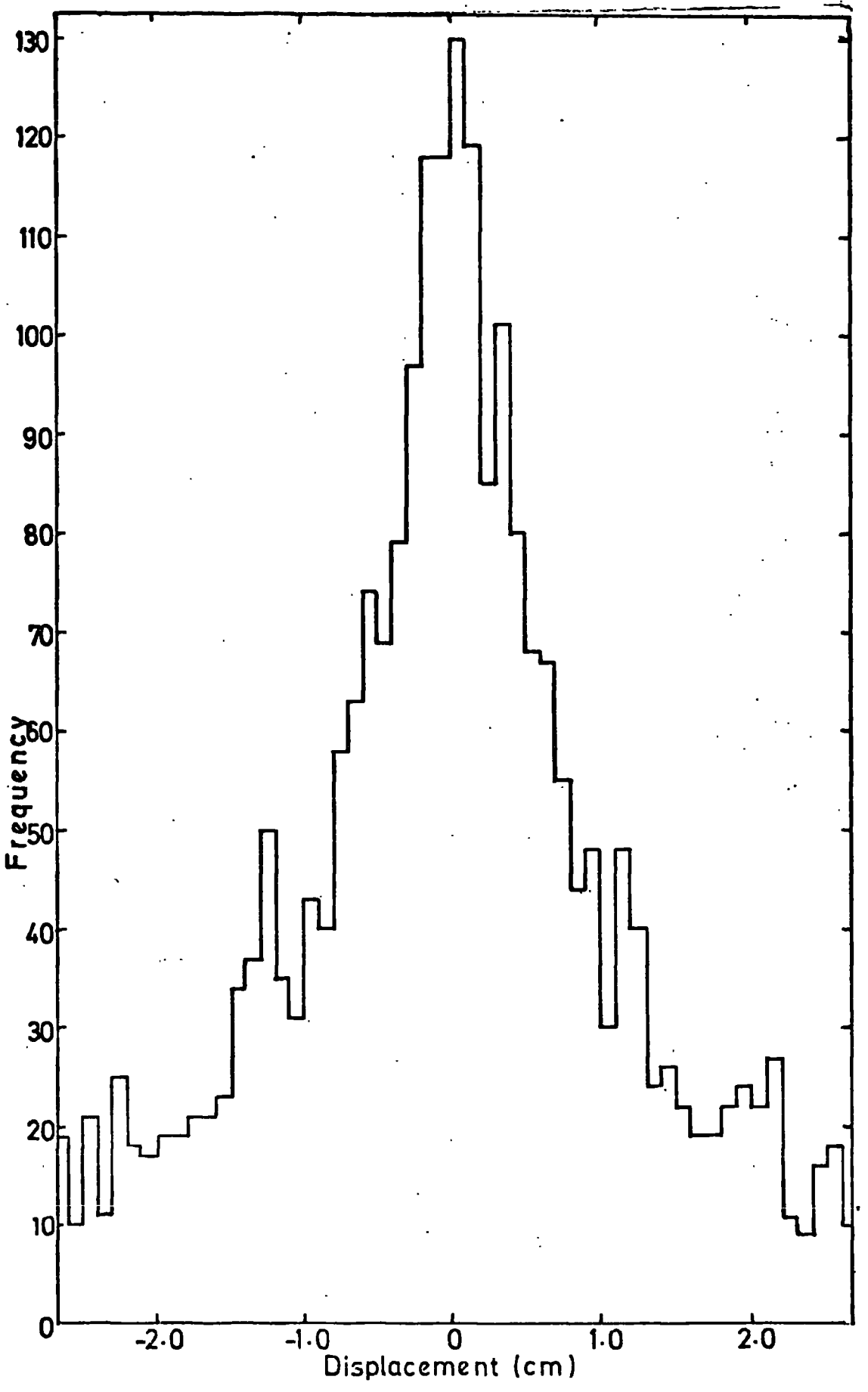

Figure 4.3 (c) Histogram of displacements for tray 4 (all events data).

The distributions of the all events data are much broader, and it appears from figure 4.2 that these may also be slightly asymmetric. The same method is used to find the mode of both sets of distributions, so that the modes of the distributions can be compared. The modes are located by the method of auto-convolution which is best illustrated by considering the example in figure 4.4. The distribution (figure 4.4a)) and the distribution reflected about the y axis (figure 4.4b)) are moved across each other. At each position where the 'bins' exactly overlap (figure 4.4c)) the sum of the products of each pair of y values is computed. The new distribution so formed (figure 4.4d)) has its mode at a value displaced from zero by twice the value of the mode of the original distribution. The curve is also smoother with a better defined peak. It is considered that this method locates the mode to within 0.2mm. The values obtained from the measurements of the modes of the all events run and the two separate 'high momentum' runs are shown in table 4.1. The high momenta data were divided up into two separate halves, containing approximately the same amount of data in each.

TABLE 4.1

THE PEAKS OF THE DISPLACEMENT DISTRIBUTION

(The position taken as zero is arbitrary.)

	TRAY 2	TRAY 3	TRAY 4
ALL EVENTS	- 1.49 mm	+2.12 mm	- 4.12 mm
HP (1)	- 1.31 mm	+2.25 mm	- 4.22 mm
HP (2)	- 1.43 mm	+2.31 mm	- 4.34 mm
FINAL VALUE	- 1.37 mm	+2.19 mm	- 4.28 mm

ALL ERRORS $\pm$ 0.20 mm

The displacement distributions from the momentum selector data

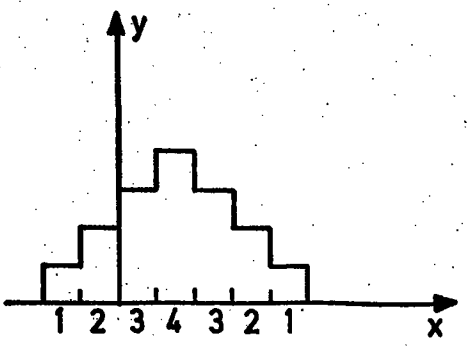

(a) ORIGINAL DISTRIBUTION.

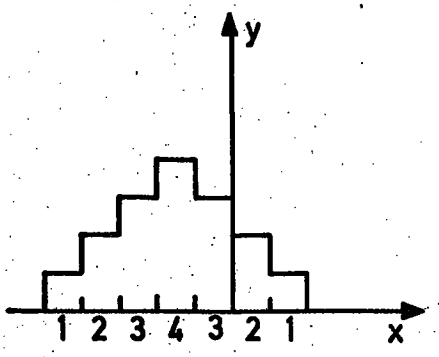

(b) DISTRIBUTION REVERSED.

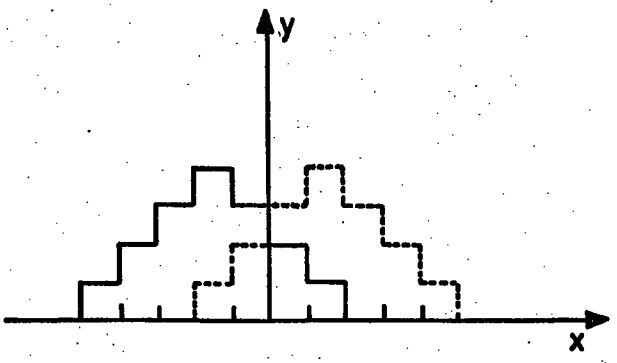

(c) THE TWO DISTRIBUTIONS WITH THEIR y AXES OVERLAPPING.

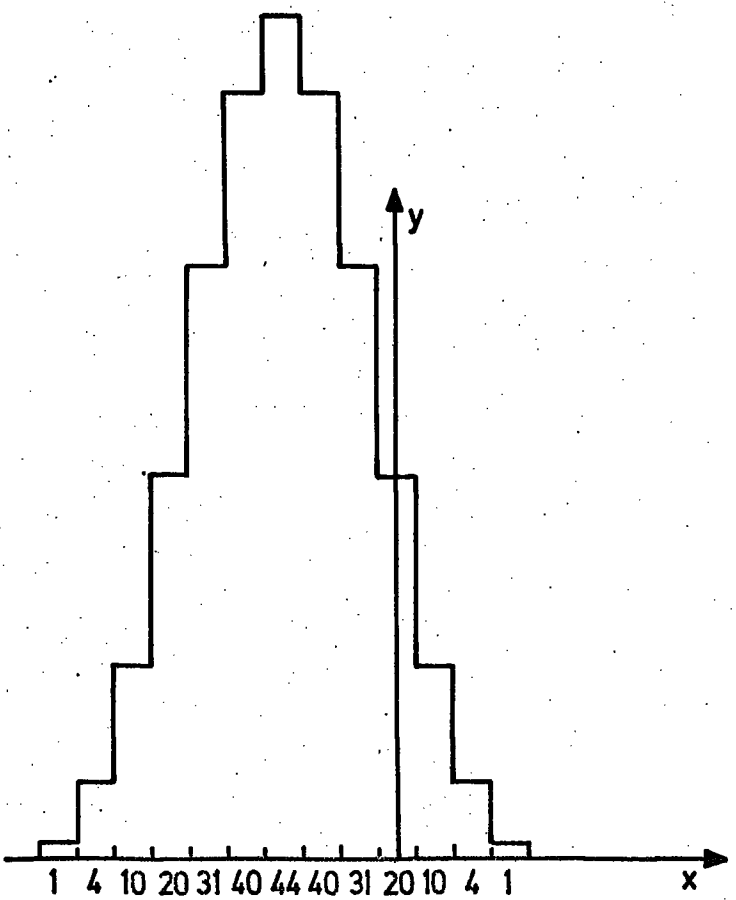

(d) AUTO CONVOLUTION CURVE OBTAINED FOR THE ABOVE DISTRIBUTION.

Figure 4.4. Illustration of auto convolution method used for the peaks of distributions.

are narrower due to the preselection of the straighter tracks. It is concluded that the modes of these distributions are the best ones to use for the final estimation of the coordinates of the middle three trays. The final coordinates used are shown in table 4.1. Figure 4.5 shows the auto-convolution curve obtained for tray 4 using the data obtained using the momentum selector. The modes of these distributions are obtained by fitting parabolas to these distributions and locating the maxima of the fitted parabolas.

4.2.3 THE ALIGNMENT OF THE MEASURING TRAYS

In order to check the relative skewness of the trays it is necessary to look at particles traversing the spectrograph in the four separate categories BB, BF, FB and FF as defined in figure 4.6. These events are selected using the information from the Geiger trays located at the ends of the top and bottom measuring trays. Using the method of Ayre et al. (1975b), if any tray is skew with respect to any others then the means of the BB, BF, FB, FF and total distributions will not all be the same. For example if tray 3 is skew with respect to trays 1 and 5 then the means of the FF and BB distributions for tray 3 will be symmetrically placed about the means of the other two distributions for that tray. Similarly if tray 5 is skew with respect to trays 1 and 3, then the FB and BF distributions and the BB and FF distributions for tray 3 will appear to split and hence have their means one on each side of the mean of the total distribution. For the purposes of these measurements the rate of particles traversing the spectrograph in any of these categories is small and there are approximately only 500 events included in each histogram. A typical histogram is shown in figure 4.7. For the purposes of these measurements the separate distributions are taken as being similar in shape to the overall distributions

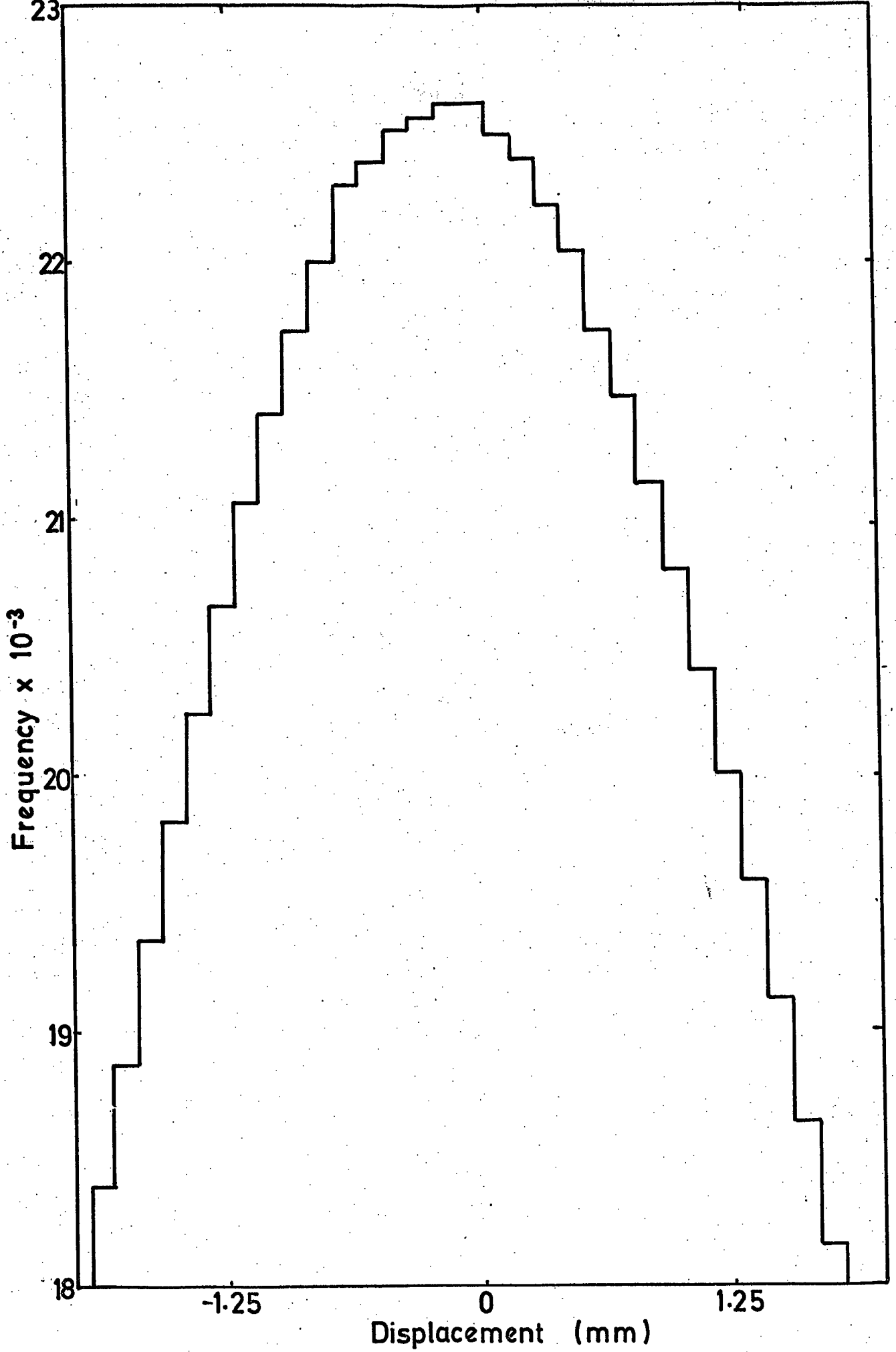

Figure 4.5 The auto-convolution histogram for tray4 (momentum selector data).

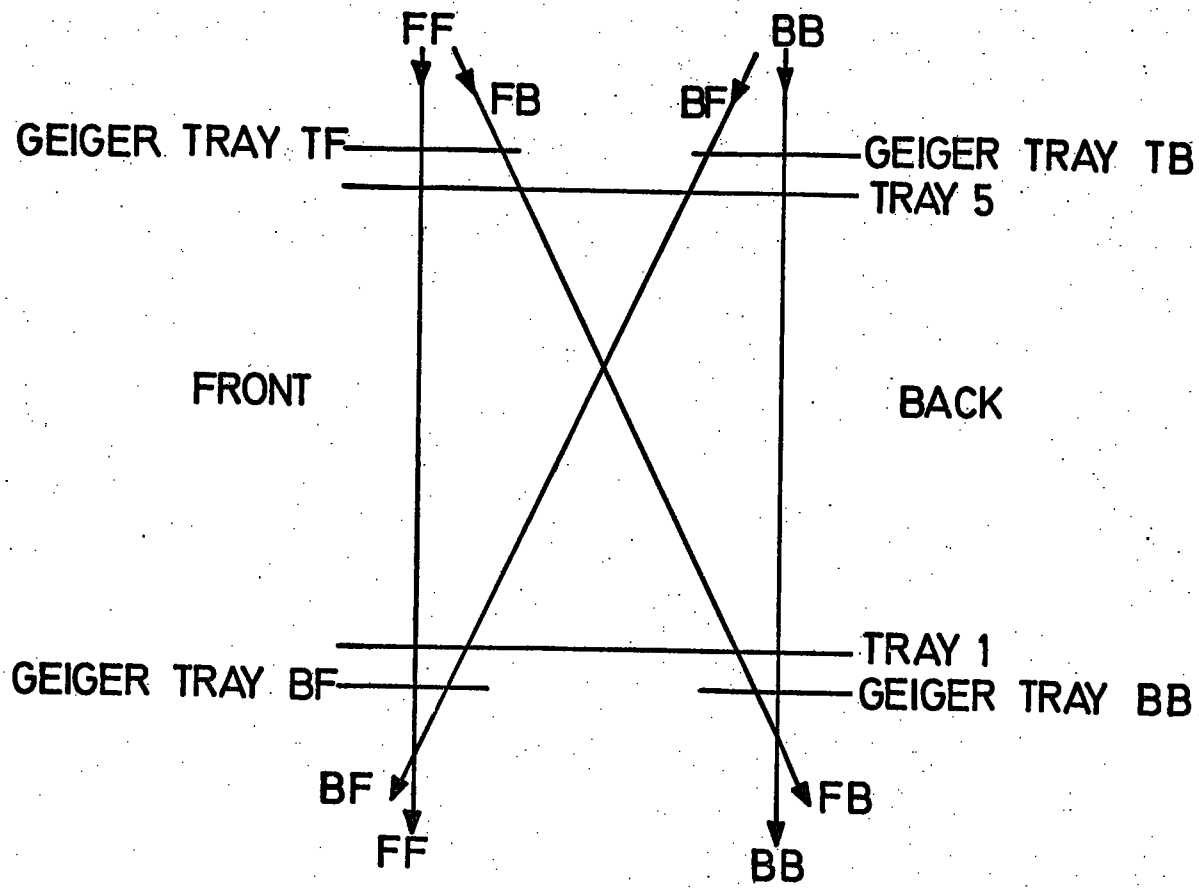

Figure 4.6. Schematic diagram showing the positions of the measuring trays and geiger trays with respect to the 4 different scattering distributions BB, BF, FB, FF.

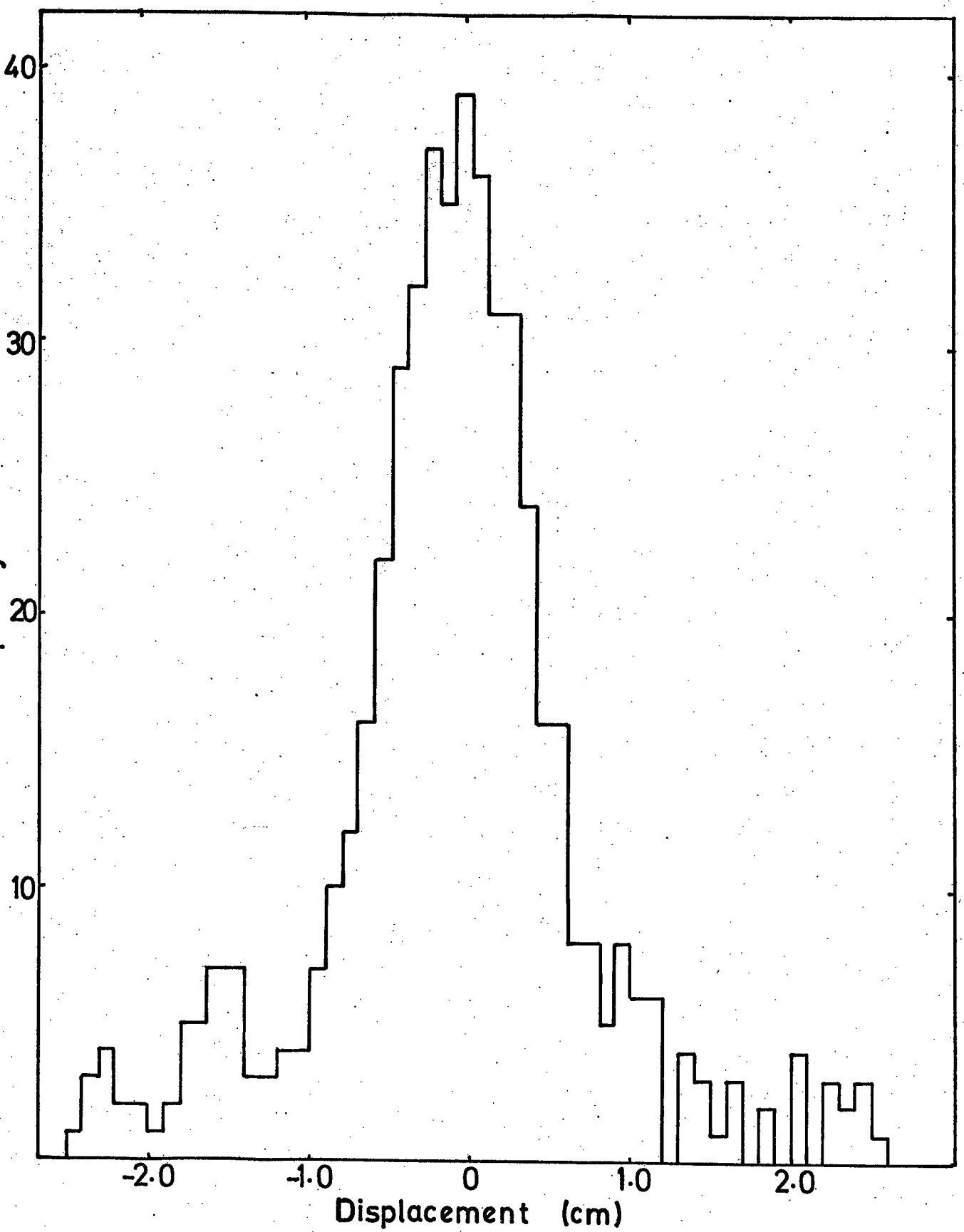

Figure 4.7 The displacement histogram for particles traversing the spectrograph in the BB mode for tray 2.

(figure 4.3) and therefore the means are considered as being in the same position relative to the mode for each distribution. (To locate the modes would require much more data.) If any skewness is present then the means of some of the distributions would be seen to split. Figure 4.8 shows the means of the distributions for each tray and each category together with the error on the mean. The large mean value of the BB distribution for tray 2 is not consistent with the other three measurements on tray 2 and is considered to be a large statistical fluctuation of the measurement.

From these data it is concluded that the skewness of the trays is less than 10^{-2} degrees (ie ± 0.2 mm over 133 cm).

4.3 INACCURACIES OF THE COMPUTER PROGRAMME

During the analysis procedure two approximations are used. The coordinate of the track to which the final parabola is fitted is only accurate to the width of the channel for which particles can traverse the measuring tray setting off the same flash tubes and requiring the same option of fit to be used. This is known as the track location accuracy. A Monte-Carlo simulation of particles traversing a tray with the same angular distribution as that for a measuring tray in MARS has been performed. The computer programme has been used to assign a coordinate for each track and this has been compared with the actual track. The distribution of these discrepancies is shown in figure 4.9, assuming the flash-tubes to be 100% efficient. The mean and standard deviation of the distribution are 0.007 mm and 0.304 mm respectively. If, however, the tube inefficiencies are considered, using the layer efficiencies for each layer in each tray (table 3.3) and the simulation repeated, the new means and standard deviations obtained are shown in table 4.2.

The other inaccuracy associated with the computer programme is in the computed value of the momentum. Equation 3.2, used to

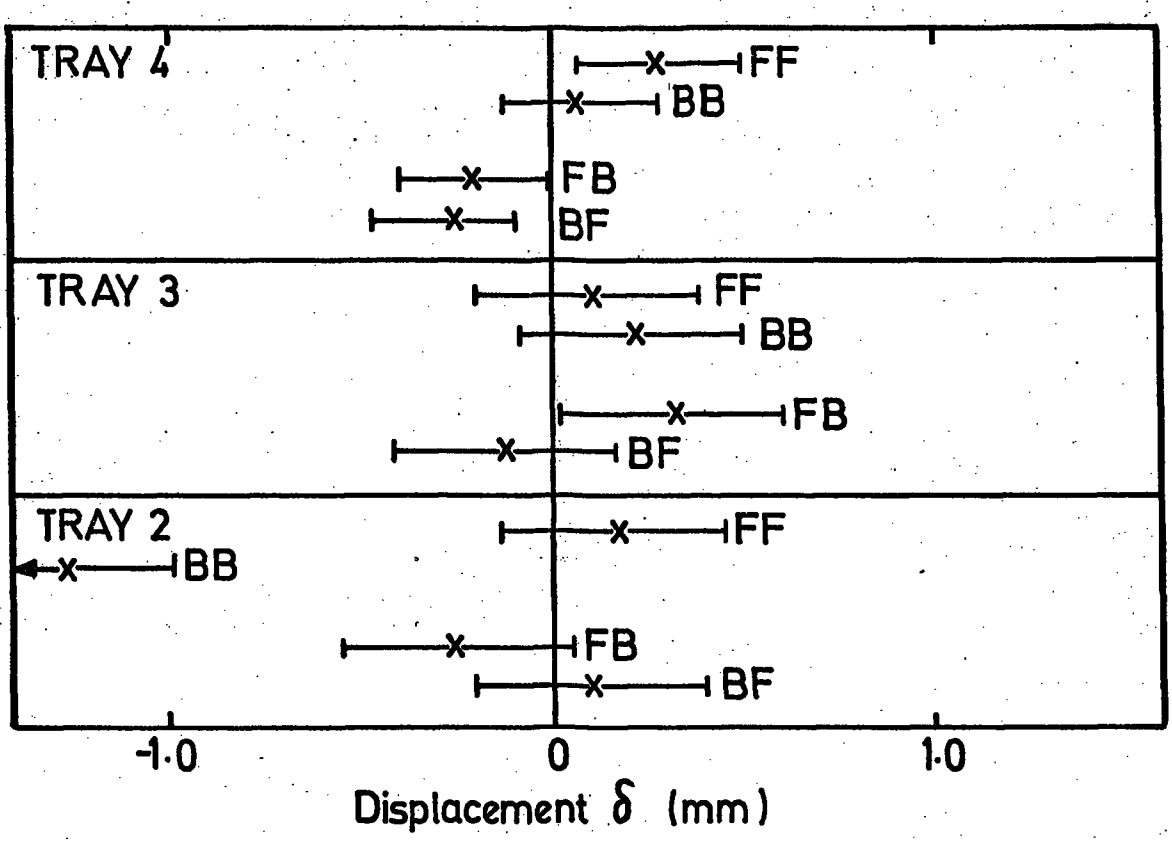

Figure 4·8. The mean values of δ_i obtained for each tray.

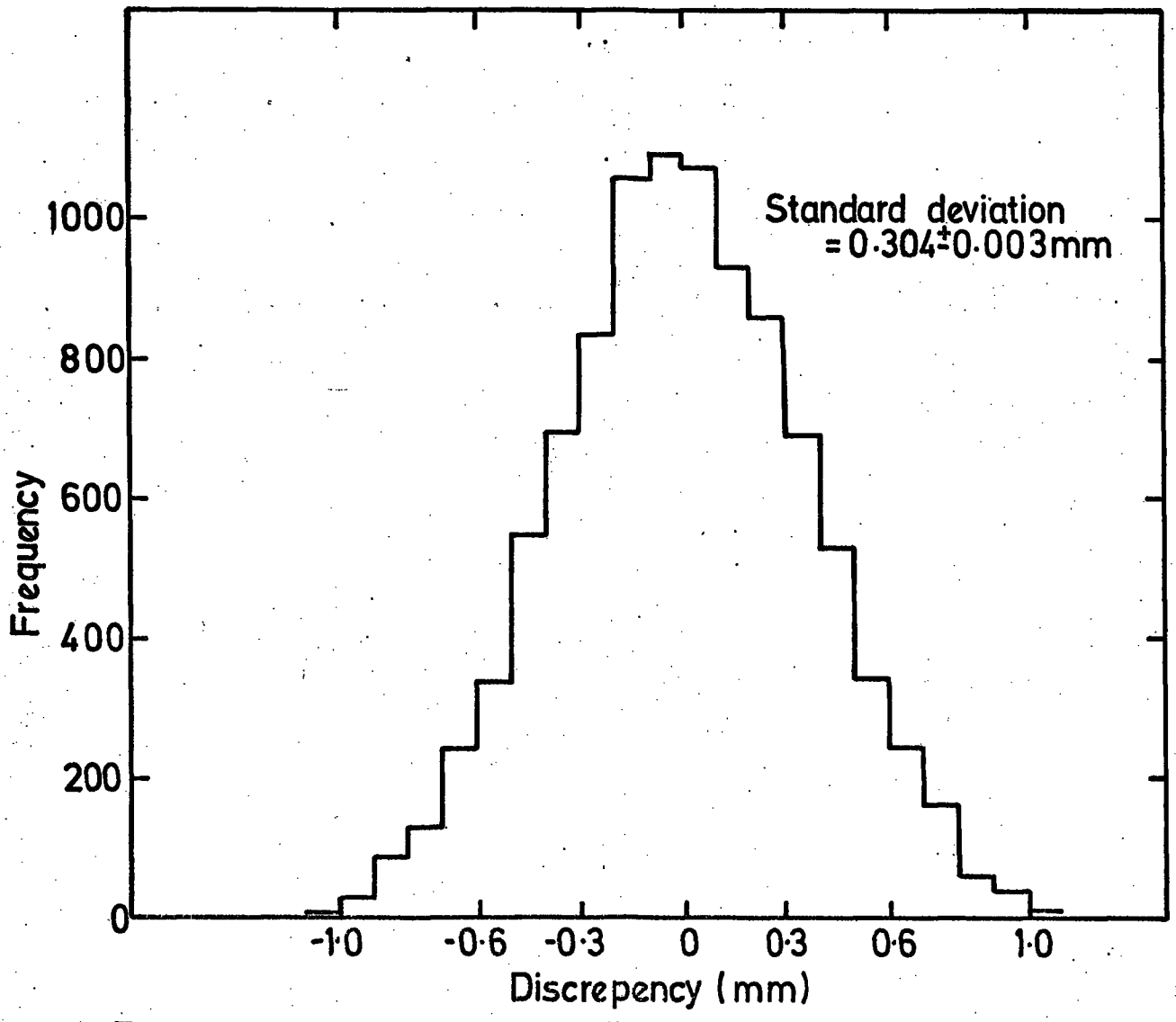

Figure 4·9. The frequency distribution of the discrepancies between the true and computed trajectories in a tray.

TABLE 4.2

THE MEANS AND STANDARD DEVIATIONS OF THE TRACK LOCATION ACCURACY DISTRIBUTIONS FOR EACH TRAY

	STANDARD DEVIATION	MEAN
ALL TRAYS (100% efficient flash-tubes)	0.304 mm	0.003 mm
1	0.538 mm	0.005 mm
2	0.559 mm	0.006 mm
3	0.658 mm	0.007 mm
4	0.556 mm	0.006 mm
5	0.592 mm	0.006 mm

calculate the momentum from the coefficient of the fitted parabola, is only true for a muon with an energy of 1000 GeV, incident in the vertical direction and losing no energy traversing the magnet. The corrections for these effects have been calculated by other workers (Wells, 1972) and tables 4.3 a) and b) summarise the corrections which must be added to the computed momentum.

For the purposes of this experiment the variation with zenith angle is considered small and a mean correction has been calculated for each momentum and tray combination used. It is calculated that the maximum error for any computed momentum due to the use of a mean correction is approximately $\pm$ 1%.

4.4 THE MAXIMUM DETECTABLE MOMENTUM

The maximum detectable momentum (m.d.m.) is defined to be that momentum for which the uncertainty in the momentum is equal to the momentum. Any measurements made for momenta above the m.d.m. must be regarded as suspect due to the large uncertainty involved. Its value depends on the accuracy to which the trajectory can be

TABLE 4.3 a)

THE CORRECTIONS TO BE ADDED TO THE COMPUTED MOMENTA

MOMENTUM (GeV/c)	ZENITH ANGLE (°)	TRAY COMBINATION							
		12345	1234	1235	1245	1345	2345	123	124
50	-6	5.5	6.0	5.5	6.3	5.0	3.6	11.0	7.6
	0	4.3	4.7	4.3	5.1	3.9	2.5	9.8	6.4
	+6	4.7	5.0	4.7	5.5	4.3	3.0	9.9	6.6
	MEAN	4.8	5.2	5.0	5.0	4.4	3.0	10.3	6.9
100	-6	6.4	6.2	6.2	8.0	5.7	3.8	15.8	9.4
	0	4.4	4.1	4.2	6.1	3.7	1.9	13.8	7.3
	+6	5.6	5.3	5.3	7.2	4.9	3.2	14.7	8.4
	MEAN	5.5	5.2	5.2	7.1	4.8	3.0	14.8	8.4
200	-6	8.0	6.6	7.4	11.4	6.8	4.1	25.2	12.7
	0	4.4	2.9	3.7	7.9	3.2	0.5	31.7	9.0
	+6	7.2	5.6	6.6	10.6	6.1	3.5	24.2	11.7
	MEAN	6.5	5.0	5.9	10.0	5.4	2.7	27.0	11.1
500	-6	13.0	7.7	11.1	21.6	10.2	5.1	53.5	22.7
	0	4.5	-1.0	2.5	13.3	1.7	-3.4	45.5	14.2
	+6	12.2	6.7	10.3	20.9	9.5	4.5	52.5	21.7
	MEAN	9.9	4.5	8.0	18.6	7.5	2.1	50.5	19.5
1000	-6	21.2	9.4	17.1	38.6	15.9	6.7	101.0	39.2
	0	4.5	-7.6	0.4	22.2	-0.8	-10.1	85.1	22.7
	+6	20.4	8.3	16.3	27.8	15.2	6.1	99.5	38.2
	MEAN	15.4	3.4	11.3	29.9	10.1	0.9	95.2	33.7
5000	-6	86.5	22.3	65.2	173.0	60.8	19.1	476.0	171.0
	0	4.4	-60.9	-17.2	93.1	-21.6	-64.0	401.0	89.9
	+6	85.7	21.3	64.4	173.0	60.1	18.5	476.0	170.0
	MEAN	58.9	-5.8	37.5	146.3	33.1	-8.8	451.0	143.6

TABLE 4.3 b)

THE CORRECTIONS TO BE ADDED TO THE COMPUTED MOMENTA

MOMENTUM (GeV/c)	ZENITH ANGLE (°)	TRAY COMBINATION							
		134	234	125	135	235	145	245	345
50	-6	4.5	0.4	7.0	4.9	2.4	5.5	4.7	6.4
	0	3.2	-0.9	5.8	3.7	1.3	4.4	3.6	5.4
	+6	3.5	-0.5	6.1	4.1	1.7	4.8	4.2	6.0
	MEAN	3.7	-0.3	6.3	4.2	1.8	4.9	4.2	5.9
100	-6	3.4	-4.3	8.7	5.1	0.9	7.2	6.4	10.6
	0	1.2	-6.5	6.7	3.1	-1.1	5.3	4.6	8.9
	+6	2.4	-5.1	7.8	4.3	0.2	6.6	5.9	10.1
	MEAN	2.3	-5.3	7.7	4.2	0.0	6.4	5.6	9.9
200	-6	1.0	-13.7	12.1	5.5	-2.3	10.7	9.9	18.9
	0	-2.8	-17.7	8.5	1.9	-6.0	7.2	6.5	15.7
	+6	0.1	-14.5	11.2	4.7	-2.9	10.0	9.5	18.5
	MEAN	0.6	-15.3	10.6	4.0	-3.7	9.3	8.6	17.7
500	-6	-6.0	-41.8	22.2	6.6	-11.7	21.0	20.4	43.9
	0	-14.9	-51.3	13.8	-2.0	-20.5	12.7	12.2	36.1
	+6	-6.9	-42.7	21.3	5.8	-12.4	20.4	20.0	43.5
	MEAN	-9.3	-45.2	19.1	3.5	-14.8	18.0	17.5	41.2
1000	-6	-17.8	-88.9	38.9	8.4	-27.5	38.2	37.9	85.5
	0	-35.2	-107.0	22.4	-8.5	-44.9	21.9	21.6	70.1
	+6	-18.7	-89.8	38.0	7.6	-28.1	37.6	37.4	85.2
	MEAN	-23.9	-95.2	33.1	2.5	-33.5	32.6	32.3	80.3
5000	-6	-112.0	-466.0	172.0	22.4	-154.0	176.0	177.0	418.0
	0	-198.0	-557.0	91.5	-60.8	-240.0	95.0	96.8	342.0
	+6	-113.0	-467.0	171.0	21.6	-155.0	175.0	177.0	418.0
	MEAN	-141.0	-496.7	144.8	-5.6	-183.0	148.7	150.3	392.7

located at each measuring level. In MARS this corresponds to the track location accuracy and the uncertainty in the position of the measuring trays. It is calculated, using the method of Allkofer et al., (1971c), where

$$\text{m.d.m.} = \frac{0.03\ B\ H}{21\ \Delta a} \qquad 4.1$$

where B is the magnetic field in kgauss, H the length of the magnet and Δa is the uncertainty in the value of a, in m, which is defined from the parabola fit as

$$a = \frac{\Sigma x^3 (N\Sigma xy - \Sigma x \Sigma y) - \Sigma x^2 (\Sigma xy \Sigma x - \Sigma x \Sigma x^2) - \Sigma x^2 y (N\Sigma x^2 - (\Sigma x)^2)}{\Sigma x^4 ((\Sigma x)^2 - N\Sigma x^2) + \Sigma x^3 (N\Sigma x^3 - \Sigma x \Sigma x^2) - \Sigma x^2 (\Sigma x^3 \Sigma x - (\Sigma x^2)^2)} \qquad 4.2$$

and

$$\Delta a = \left(\sum_{i=1}^{N} \left(\frac{\delta a}{\delta y_i} \right)^2 \Delta y_i^2 \right)^{\frac{1}{2}} \qquad 4.3$$

which can be written as $\Delta a = \sum_{n=1}^{N} F_n(x) \Delta y_n$

where $F_n(x)$ is a constant of the apparatus.

For the actual case of MARS the track location accuracies at each level differ and so the calculation of the m.d.m. is tedious using the above formulae. However the trajectories of infinite momentum particles were simulated through the spectrograph and the position of the particles at each level selected from the relevant track location accuracy distribution for the particular level. The momentum is then calculated using a parabola fit as previously described. The mean and standard deviation of the distribution of inverse momentum is then calculated. The mean should approach zero and the standard deviation should be the inverse of the m.d.m. Table 4.4 shows the values of the m.d.m. using a) the formula, b) the simulation with the theoretical track location accuracies and c) the simulation using the actual measured track location accuracies. As can be seen from the table the m.d.m.

TABLE 4.4

THE MAXIMUM DETECTABLE MOMENTUM FOR THE SEPARATE TRAY COMBINATIONS

TRAY COMBINATION	MAXIMUM DETECTABLE MOMENTUM (GeV/c)		
	THEORETICAL VALUES USING FORMULA	VALUES USING Δy_i = constant = 0.304	VALUES USING INDIVIDUAL TRACK LOCATION ACCURACIES
12345	5427	5300	2950
1234	3075	2810	1480
1235	5162	4850	2640
1245	4392	4200	2560
1345	5094	5090	2790
2345	2749	3040	1750
145	3329	3510	2140
135	4705	4840	2380
125	3543	3140	1840
134	2472	2130	1110
124	2481	2250	1260
235	2110	2570	1310
245	2276	2480	1490
123	1210	1240	696
234	1111	1210	626
345	1346	1140	640

is reduced to approximately 3000 GeV/c for five tray fits for the actual data, which is only approximately half the design value.

4.5 OVERALL ACCEPTANCE

The acceptance of MARS is defined by the three scintillation counters. When the magnetic field is operating, muons with low momentum can be deflected out of the magnet and as a result the acceptance for these particles is low. For muons of infinite momentum the acceptance of the blue side of the spectrograph is 408 ± 2 cm^2 sterad. The acceptance of the spectrograph has been calculated as a function of momentum and is shown in figure 4.10. For the purposes of this experiment the acceptance is taken as constant at 408 ± 2 cm^2 sterad and this limiting value is reached to within 1% for all particles with momenta above 100 GeV/c.

The acceptance of MARS is not constant with incident angle. The maximum incident angles for which infinite momentum particles can traverse the magnet are $\pm 6.8^\circ$ in the plane perpendicular to the magnetic field and $\pm 15.5^\circ$ in the parallel plane. The angular acceptance has been calculated by simulating the traversal of particles with a given momentum through the spectrograph and the results for particles with momenta of 500 GeV/c and 50 GeV/c are shown in figure 4.11. The ideal angular acceptance is a triangle whose vertices lie at 0° and $\pm 6.8^\circ$ as shown by the third line in figure 4.11.

4.6 THE EFFICIENCY OF THE MOMENTUM SELECTOR

In order to measure the momentum spectrum, the efficiency of the Mark I and Mark II momentum selectors must be calculated as a function of momentum. A Monte-Carlo simulation of the passage of particles of a given momentum and incident angle through the magnet has been made using a computer. At each momentum selector tray level, the exact tray position and angle of the particle

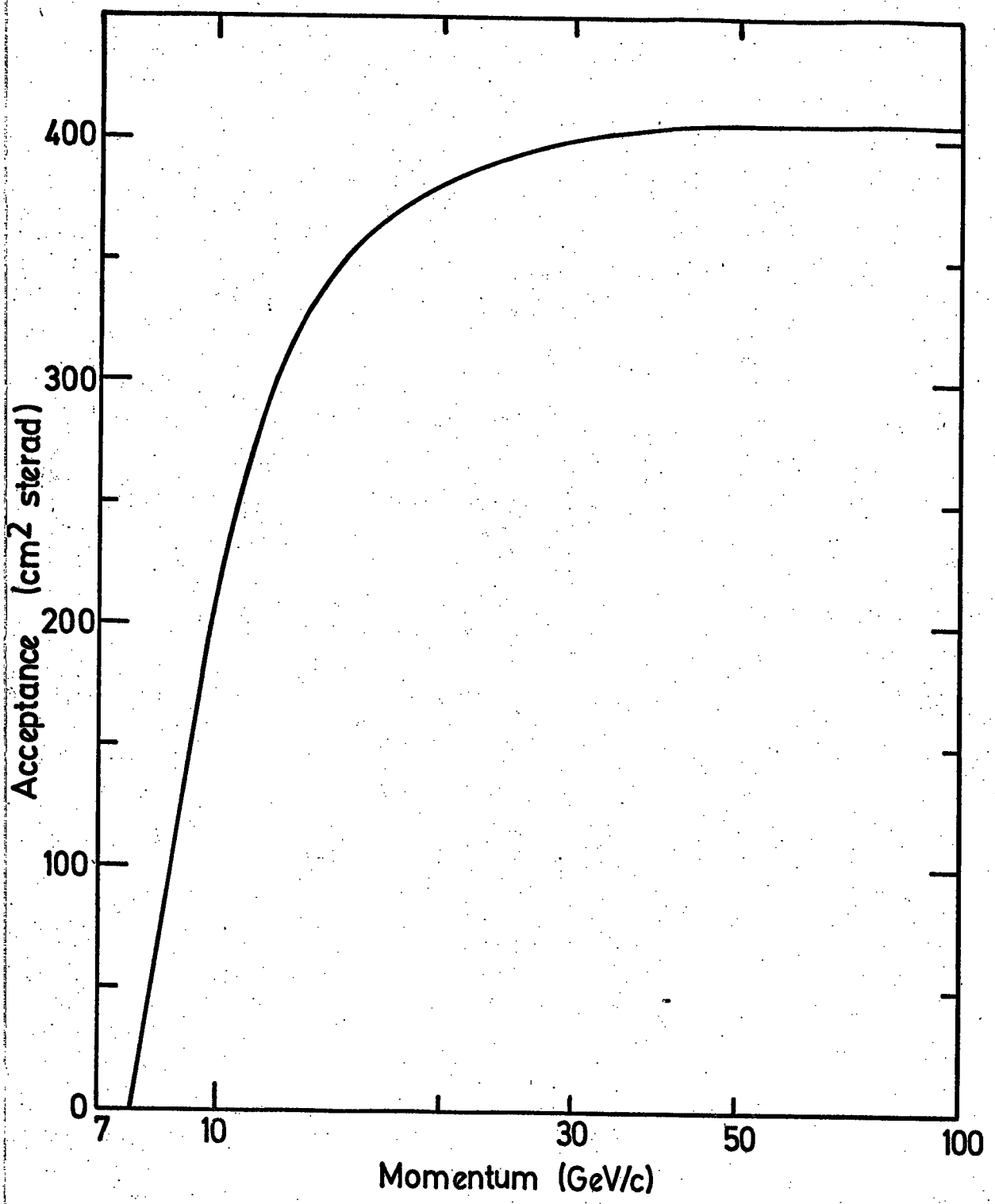

Figure 4.10. The acceptance function for the blue side of MARS.

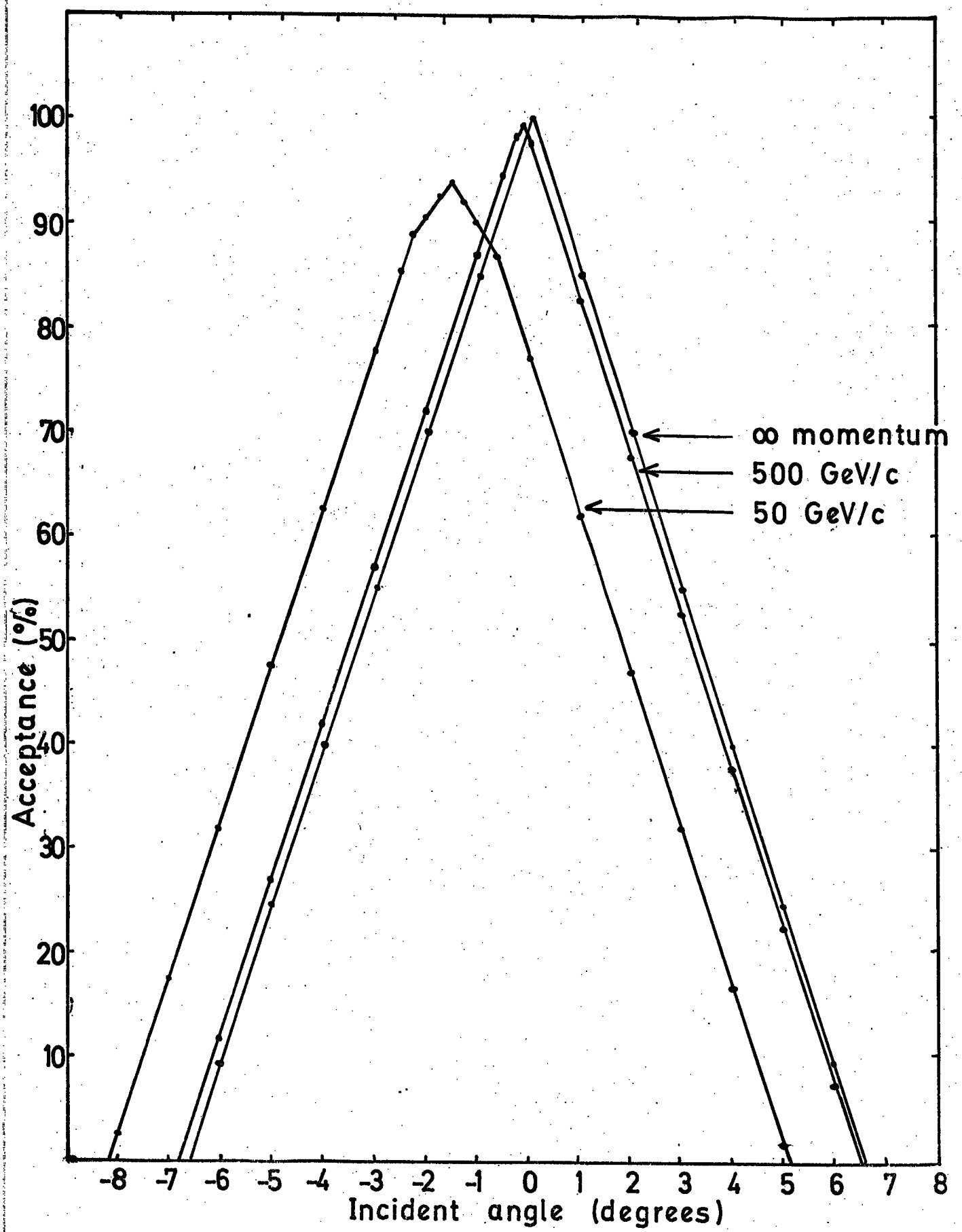

Figure 4.11 The angular acceptance of MARS.

trajectory is calculated, from which the flash-tubes which would have discharged are located and hence the cell triggered at each level is found. For each incident zenith angle and momentum the deflection at each level is the same for every incident position in the top tray. Since the tube and cell patterns repeat after every 2 cm for the Mark I momentum selector and after every 6 cm for the Mark II momentum selector, the efficiency can be calculated to the nearest per cent by calculating the tubes discharged and cells triggered for one hundred equally spaced incident positions over 2 cm in the top tray for the Mark I data and three hundred equally spaced incident positions over 6 cm in the top tray for the Mark II data.

The calculated efficiencies of the Mark I momentum selector are shown in figure 4.12 for incident angles of 3^{o} and 0^{o} and the efficiencies for the Mark II data are shown in figure 4.13 for incident angles of 0^{o} and 5^{o}. It should be noted that the efficiency of each momentum selector will be different for positive and negative particles for the same incident zenith angle. However, the efficiency for positive particles in a positive field is the same as that for negative particles in a negative field. The sharp peaks seen in figures 4.12 and 4.13 are caused by the edges of cells, where a small change in the position of the particle causes a different cell to be triggered which does not fit the selection criteria. The small inefficiencies for particles with momenta above 600 GeV/c are due to particles for which the wrong cell has been allocated in one level. This is more likely to occur at larger zenith angles, as can be seen from figure 4.14, which shows the probability of the wrong cell being allocated as a function of incident zenith angle. The effect of the wrong

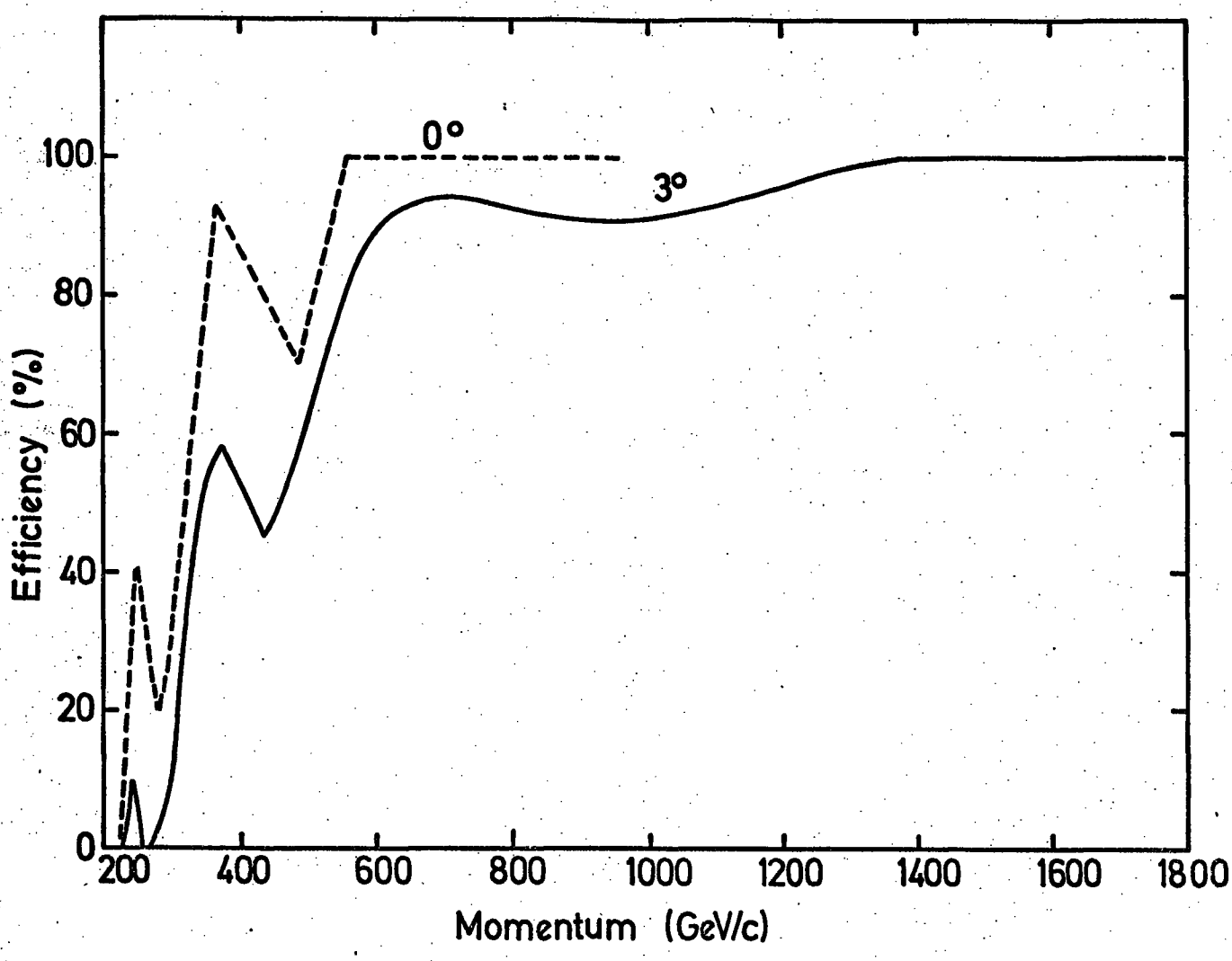

Figure 4.12. Efficiency of Mark I momentum selector for incident angles of 0° and 3° for negative particles in positive field.

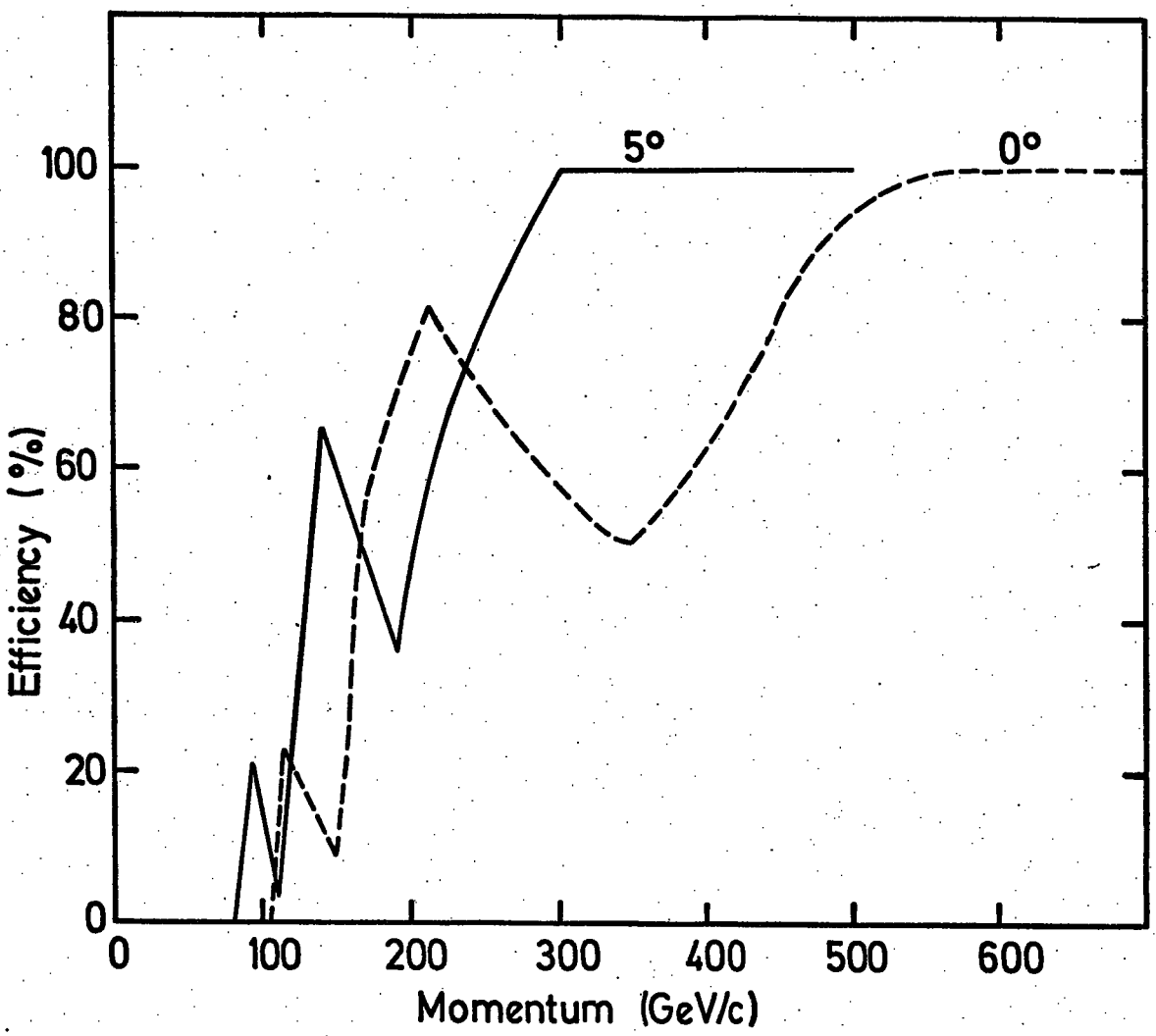

Figure 4.13. Efficiency of MARK II momentum selector at 0° and 5° to the vertical for positive momenta in a positive field.

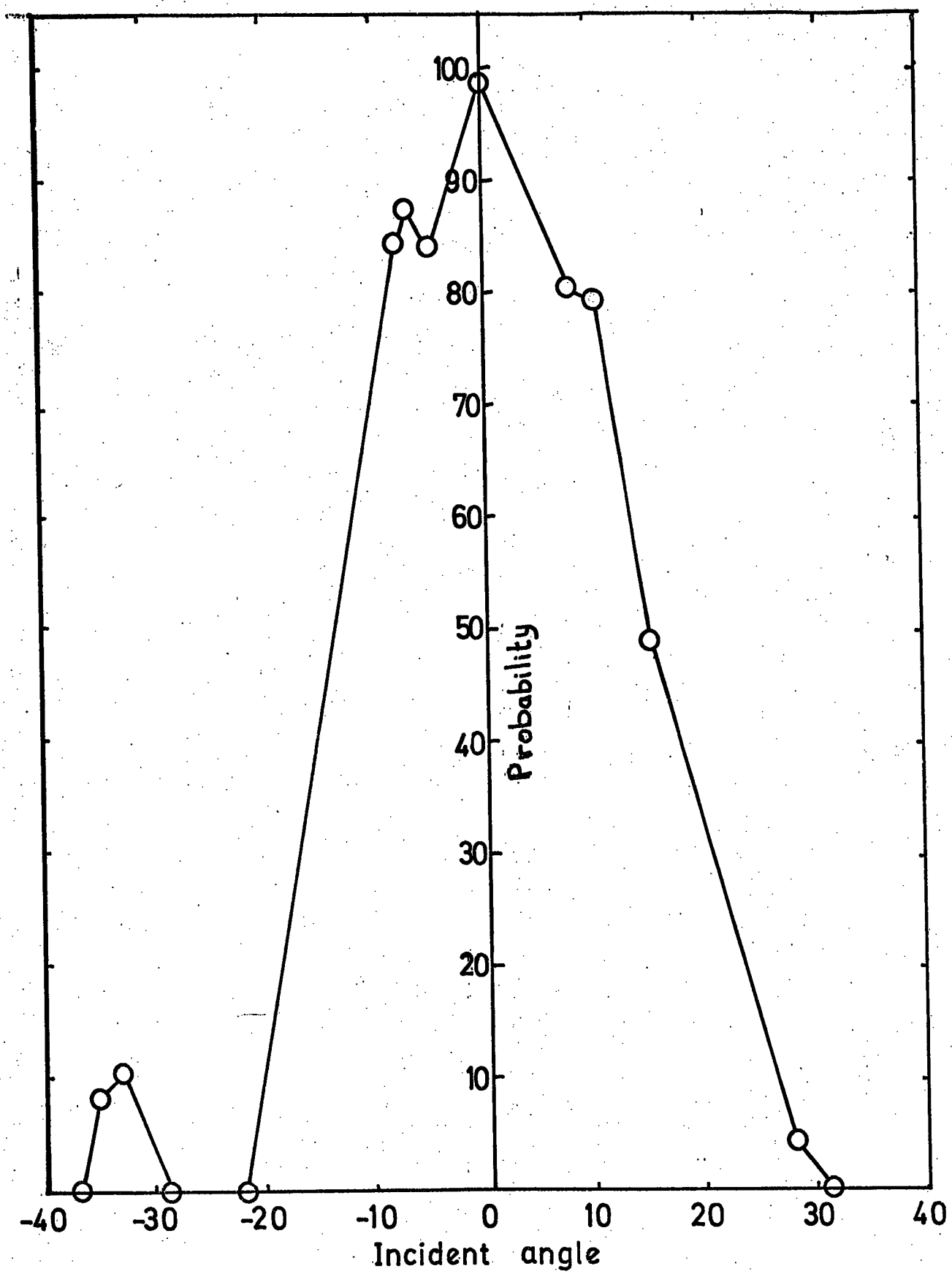

Figure 4.14 The probability of the correct cell being allocated by the momentum selector as a function of incident angle.

celling is considerably worsened by the fact that the three momentum selector trays are not equally spaced. Therefore particles of an infinite momentum appear to have a finite deflection which means that if such a particle is wrongly celled at any level, then it may not be accepted as a high momentum event by the momentum selectors.

The efficiencies calculated above are only true for unaccompanied particles where a single cell is triggered at each level. A correction must be made to the final efficiency to take account of accompanying particles, showers and spurious zero bit triggers from the Mark I momentum selector and the spurious triggers of the Mark II instrument due to electronic faults. Before any corrections can be applied to the calculated efficiencies the overall efficiency must be calculated for each momentum.

4.6.1 THE OVERALL EFFICIENCY OF THE MOMENTUM SELECTORS

To calculate the overall efficiency, the individual efficiencies at each incident zenith angle are combined taking into account the angular acceptance of MARS (section 4.4). The angular acceptance used is that shown in figure 4.11 and these curves are assumed to be exactly triangular. The efficiency is calculated for angles between $+ 6.5^{o}$ and $- 6.5^{o}$. The overall efficiency is taken as the ratio of the area underneath the 'angular acceptance times efficiency' curve to the area underneath the angular acceptance curve. A typical pair of curves are shown in figure 4.15. As can be seen from the figure, the efficiency of the Mark II momentum selector varies slowly with angle and if measurements are made for intervals of 0.5^{o} in incident angle these accurately represent the shape of the curve and the overall efficiency is known to greater accuracy than each individual efficiency (ie 1%). For the Mark I momentum selector the variation of efficiency with angle is more rapid. Hence to get a reasonable

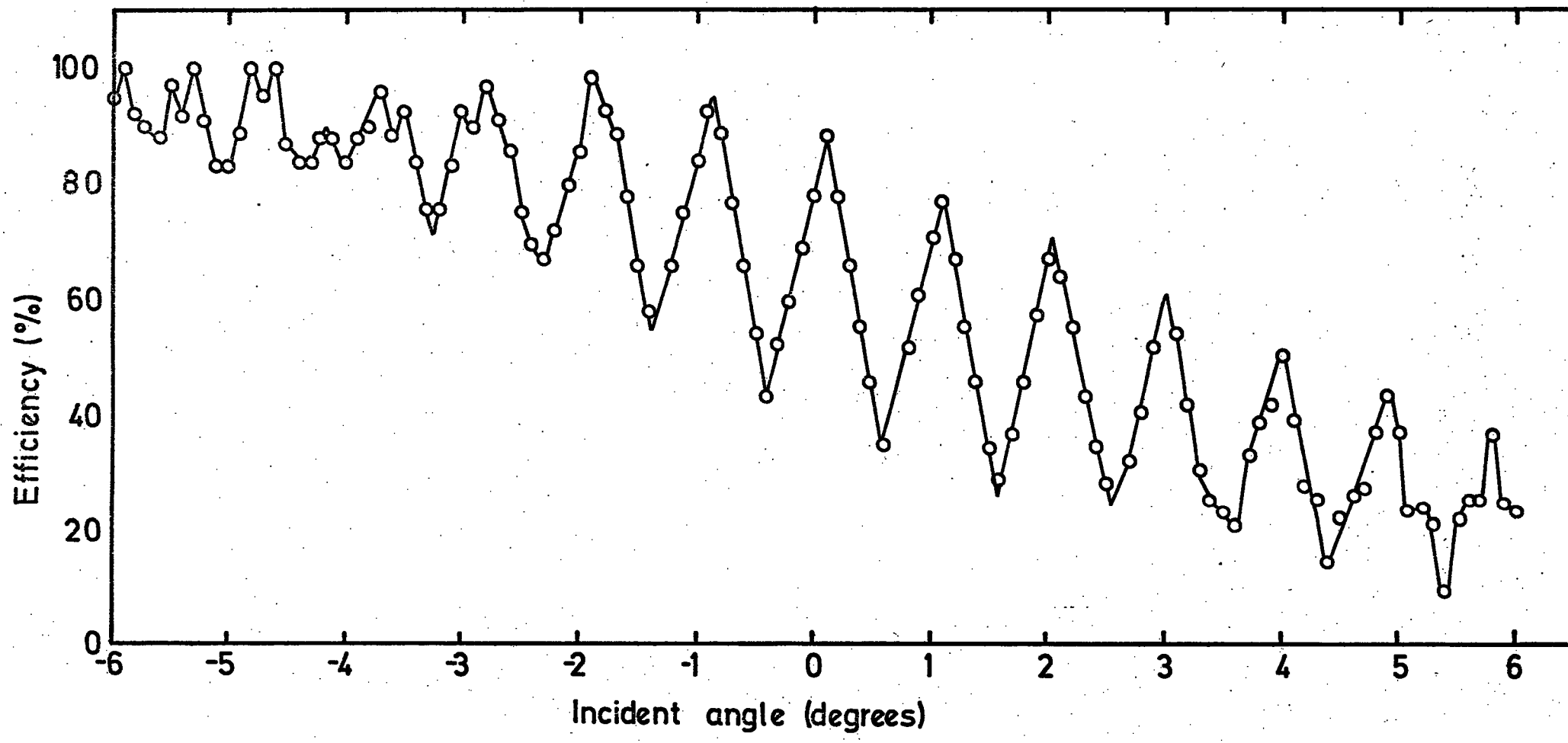

Figure 4·15a. The variation of the efficiency of the Mark I momentum selector with incident angle for particles with momentum +350 GeV/c.

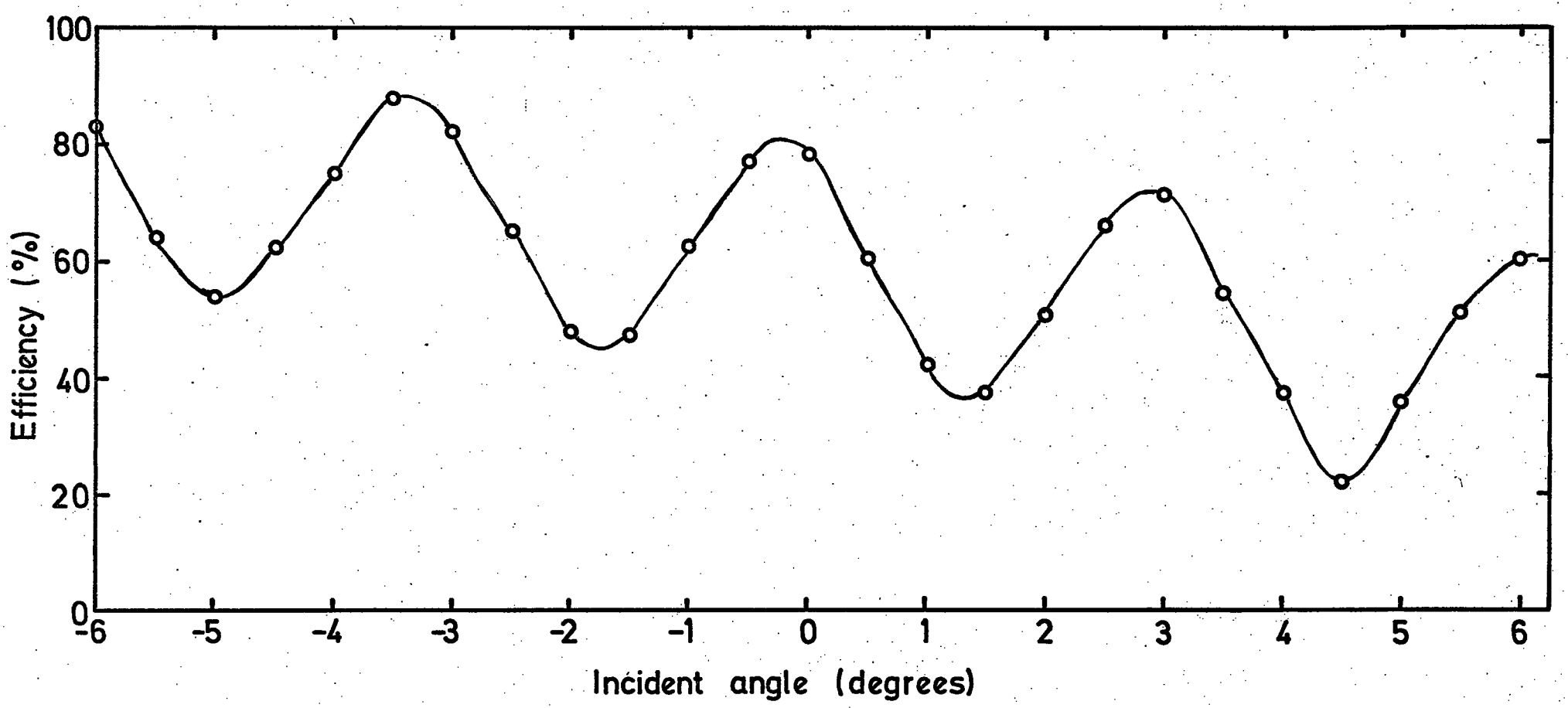

Figure 4·15b. The variation of the efficiency of the Mark II momentum selector with incident angle for particles with momentum+200 GeV/c.

value of overall efficiency, measurements are made at 0.1^{o} intervals of incident angle. With this interval the overall efficiency is again known to better than each of the individual efficiencies (ie 1%).

4.6.2 THE EFFECT OF THE SPURIOUS ZERO BIT TRIGGERS ON THE EFFICIENCY OF THE MARK I MOMENTUM SELECTOR

As discussed in chapter 2, the checking zero bit associated with the Mark I momentum selector causes spurious high momentum events to be recorded. The rate of the spurious triggers which would not normally trigger the momentum selector has been calculated using a similar method to that used for calculating the efficiency of the momentum selector. Table 4.5 shows this spurious trigger rate as a function of momentum. The values in table 4.5 must be added directly to the values of the efficiency calculated in the previous section.

TABLE 4.5

THE RATE OF 'ZERO BIT' TRIGGERS FOR THE MARK I MOMENTUM SELECTOR

MOMENTUM (GeV/c)	RATE OF EXTRA TRIGGERS (%) DUE TO '0' BIT
200	3.0%
250	2.2%
300	1.6%
400	0.8%
500	0.5%
700	0.2%
1000	0.1%

4.6.3 THE EFFECT OF BURSTS AND KNOCK-ON ELECTRONS ON THE EFFICIENCY OF THE MOMENTUM SELECTORS

If a muon is accompanied by a burst or a single knock-on electron from a magnet block, then these accompanying particles

may trigger extra momentum selector cells. These may in turn cause a high momentum event to be indicated due to there being a straight line combination between the extra cell and the cells in the other two momentum selector trays. The probability of a burst or two or more knock-on electrons has been calculated by other workers and the results of Said (1966) are shown in figure 4.16.

To estimate the probability of a burst triggering an extra cell in the momentum selector, the measuring tray data were used from trays 2 and 4. These measuring trays are located in the same positions relative to the magnet blocks as the momentum selector trays in the bottom two levels. It is necessary to consider trays in the same relative positions, to ensure that any bursts will have developed to the same extent in both types of detector. The momentum selector tube pattern is superimposed on to the actual measuring tray flash-tube data. Any momentum selector tray flash-tube whose circumference encircles the centre of a discharged measuring tray flash-tube is also said to have been discharged. These data are then converted to cells corresponding to the discharged flash-tube pattern.

The results of this analysis shows that 11% of all the events would have two or more cells triggered and 4% would have more than two cells triggered in any one level. It is assumed that if more than two cells are triggered at any one level then the Mark I momentum selector is also triggered. This is reasonable since the minimum deflection for such a particle will be at least one cell less than its actual deflection and for particles with momenta above 100 GeV/c, this is probably enough to trigger the Mark I momentum selector. For the events with two cells triggered, the cell to the left will be triggered 50% of the time as will the cell to the right. One will decrease the minimum deflection, the other will leave

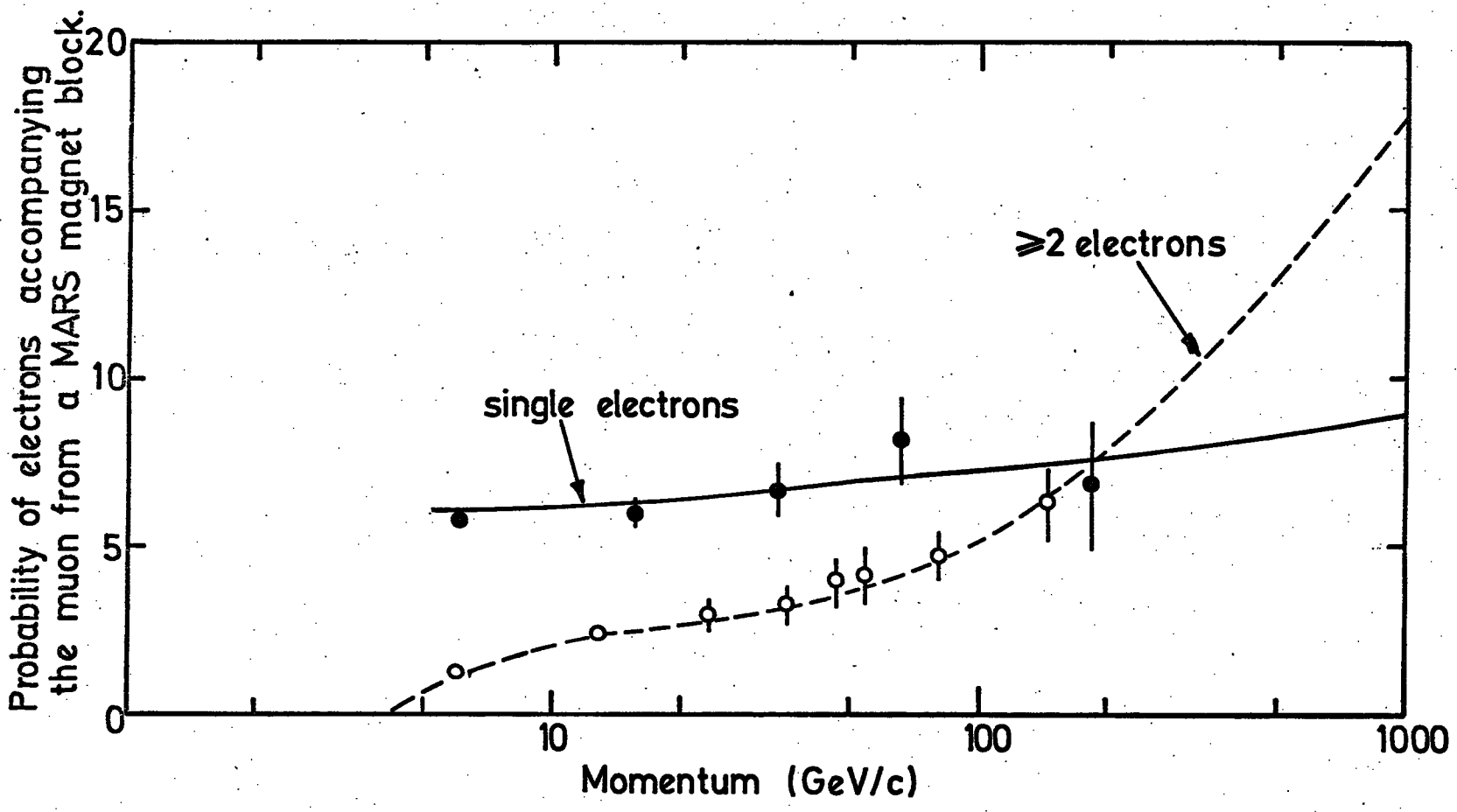

Figure 4.16. Probability of electrons accompanying the muon from a magnet block.

the minimum deflection unchanged. Hence it is assumed that only 50% of these events cause the Mark I momentum selector to be triggered. The percentages of events which have more than one cell triggered in any one level and trigger the momentum selector are shown in table 4.6 as a function of momentum. A correction must be made to the overall efficiency of each momentum selector to take account of this effect. The corrections for the Mark II momentum selector are calculated in a similar way, except that in this case the probability of triggering the next Mark II momentum selector cell is much smaller due to the much larger cell width.

TABLE 4.6

THE PERCENTAGES OF EVENTS TRIGGERING THE MOMENTUM SELECTORS DUE TO BURSTS AND KNOCK-ONS

MOMENTUM (GeV/c)	PERCENTAGE OF EXTRA EVENTS DUE TO BURSTS	
	MARK I	MARK II
100	9.5	3.9
150	10.0	2.6
200	8.5	1.9
300	4.4	1.2
500	1.5	0.6
700	0.8	0.4
1000	0.2	0.3

4.6.4 THE EFFECT OF THE HIGH RATE DATA ON THE EFFICIENCY OF THE MARK II MOMENTUM SELECTOR

During the operation of the Mark II momentum selector, the fraction of high momentum events being recorded was too high due to spurious events being accepted (approximately 2%).

This was the consequence of electronic faults developing in the momentum selector. As a consequence of the faults only a two fold coincidence was required between two particular cells in any two levels to register an event as being of high momentum. The normal fraction of high momentum events is 0.015 when the momentum selector is working with no faults, and the average fraction is 0.018. Therefore the extra events correspond to 0.3% of the total number of muon traversals and this 0.3% should not be accepted as high momentum events. Therefore the efficiencies must be amended to correct for this effect.

4.6.5 THE FINAL CORRECTED MOMENTUM SELECTOR EFFICIENCIES

The overall efficiencies after corrections for all the effects discussed in the previous sections are shown in figure 4.17 for the Mark I momentum selector and figure 4.18 for the Mark II momentum selector. For comparison purposes the overall corrected efficiencies for both momentum selectors are shown in table 4.7.

TABLE 4.7

THE FINAL CORRECTED EFFICIENCIES OF THE TWO MOMENTUM SELECTORS

MOMENTUM (GeV/c)	EFFICIENCY OF THE MARK I MOMENTUM SELECTOR (%)	EFFICIENCY OF THE MARK II MOMENTUM SELECTOR (%)
100	13.5	9.0
150	15.0	40.5
200	20.0	61.0
300	55.0	80.5
500	89.5	92.0
700	96.2	95.0
1000	99.0	97.0
5000	100.0	97.5

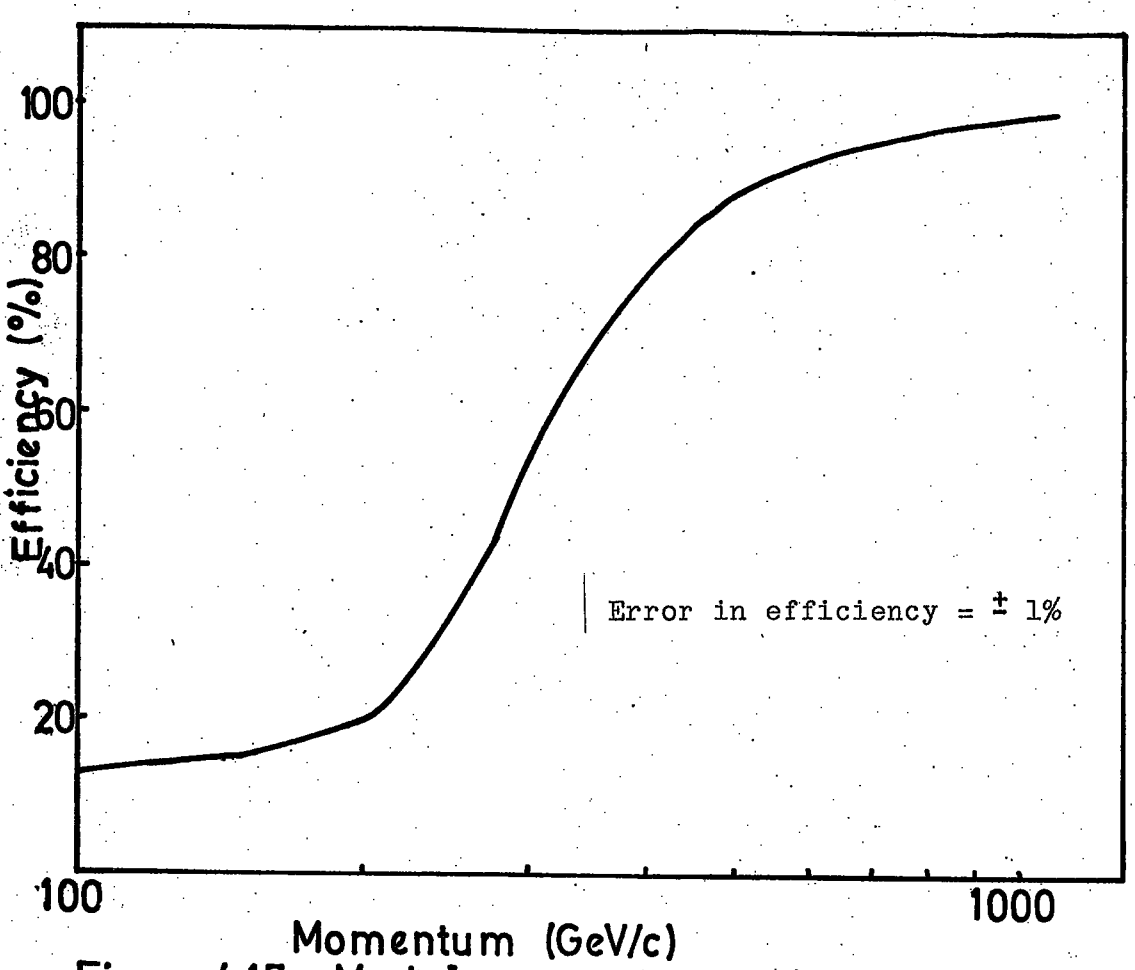

Figure 4.17 Mark I momentum selector acceptance.

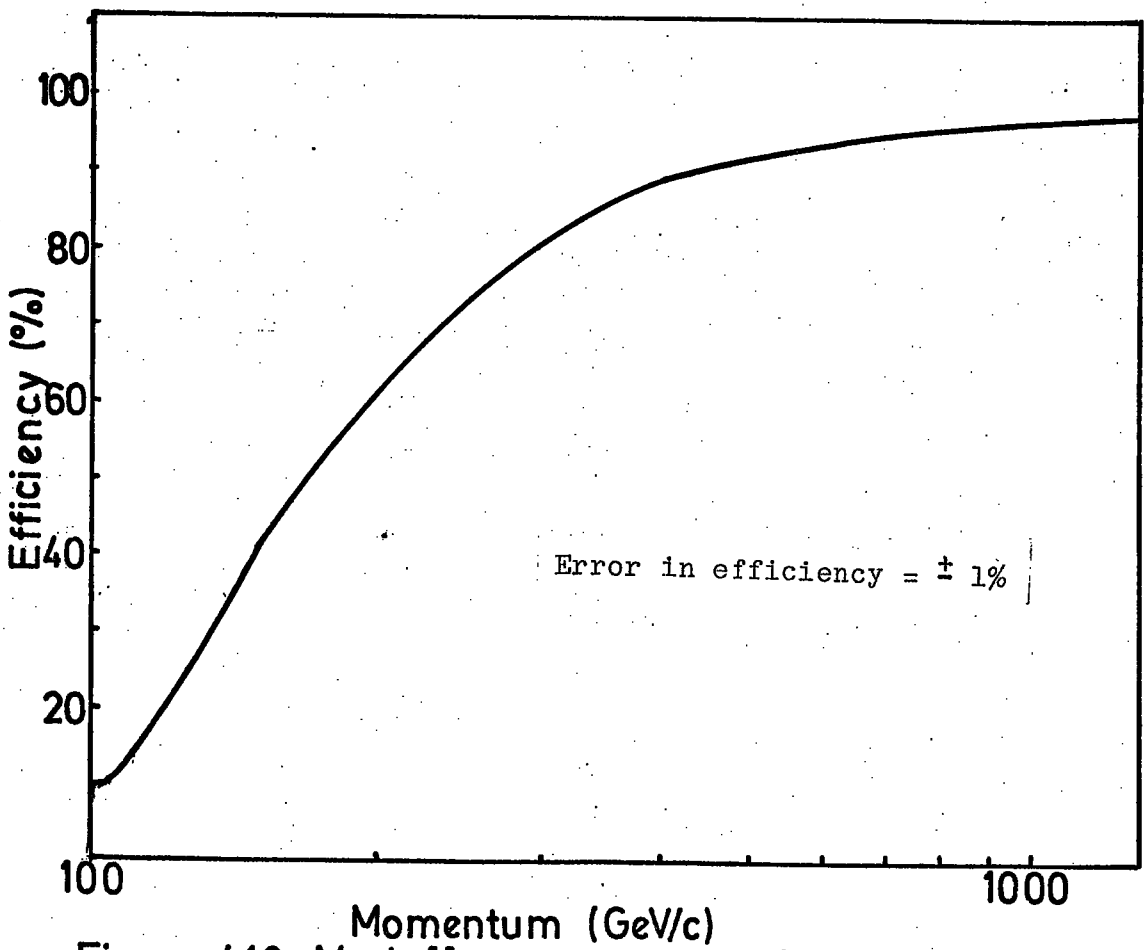

Figure 4.18 Mark II momentum selector acceptance.

4.6.6 THE MOMENTUM SELECTOR TRAY EFFICIENCIES

Apart from the momentum selector efficiency itself, each individual tray has its own efficiency. The theoretical probability of no cells being triggered by particles traversing MARS has been calculated for each tray by Whalley (1974). Both the spectrum and the angular distribution of particles at each level have been considered. Using these data and the average measured inefficiency of the apparatus over the duration of the experiment the inefficiency of the trays in levels 1,3 and 5 are $0.0\pm0.5\%$, $2.0\pm0.5\%$ and $7.5\pm0.5\%$ respectively. Combined together this leads to an overall inefficiency of $8.2 \pm 0.7\%$.

4.7 THE EFFICIENCY OF THE SCINTILLATION COUNTERS

In order that an absolute spectrum can be measured it is necessary to know the efficiency of the triggering detectors which in the case of MARS are the three scintillation counters. The efficiency of each scintillation counter has been measured while the counters remained in situ in the magnet. A small scintillation counter is placed immediately above or below the counter whose efficiency is to be measured. Two sets of coincidence rates are measured, firstly the four-fold coincidence rate between the smaller counter and the three main scintillation counters and secondly the three-fold coincidence rate between the smaller counter and the two main scintillation counters whose efficiency is not being measured. This procedure is repeated for several positions of the smaller counter with respect to the scintillation counter whose efficiency is being measured and each of the three main scintillation counters is treated similarly. The average efficiency of each counter is calculated from the means of the two separate three-fold and four-fold coincidence rates.

The average efficiency of each of the scintillation counters is $99.1 \pm 0.4\%$, $96.8\pm 0.3\%$ and $92.7 \pm 0.3\%$ for the counters in levels

1, 3 and 5 respectively. This results in an overall efficiency of 88.9 ± 0.6% for the triggering rate of the spectrograph. The overall live-time of the spectrograph must therefore be decreased by the above percentage in order that the effective live-time of the experiment is determined.

4.8 MULTIPLE COULOMB SCATTERING Multiple Coulomb scattering of the trajectory of a particle in the iron blocks has the effect of enhancing the high momentum end of the spectrum.
This is due to more low energy particles being scattered such that they appear to be of a higher momentum than high energy particles being scattered such that their trajectories resemble those of low energy particles. The main reasons for this are that there are relatively more lower energy particles and lower energy particles undergo more scattering.

The theory of multiple scattering has been given by Rossi and Greisen (1942) and the r.m.s. displacement $\langle y \rangle$ for a muon with momentum p (in GeV/c) traversing a medium of thickness t (in radiation lengths) is

$$\langle y \rangle = \frac{1}{6} \times \frac{21}{p\beta} t^{3/2} \qquad 4.4$$

Similarly the r.m.s. projected angular scatter $\langle \theta_s \rangle$ is given by

$$\langle \theta_s \rangle = \frac{21}{\sqrt{2}p\beta}\sqrt{t} \qquad 4.5$$

From equation 2.2 the magnetic angular deflection θ_m in MARS is Bet/Pβ where B is the magnetic field flux density. Therefore the ratio of

$$\frac{\langle \theta_s \rangle}{\theta_m} = \frac{21}{\sqrt{2}e\sqrt{t}B} \qquad 4.6$$

This ratio is a constant for a given thickness of material and when the values of thickness and radiation lengths for MARS are used, the ratios are 0.12, 0.14 and 0.17 for particles traversing

four, three and two magnet blocks respectively.

In order to investigate the effect of scattering on events where different tray combinations are used to calculate the momentum, a Monte-Carlo simulation of particles traversing the magnet blocks has been made using the theory of Rossi and Greisen. The trajectories of 1000 particles for each of several different incident momenta were simulated, and the momentum calculated using the same method as the analysis programme (ie using equation 3.2). A histogram showing the frequency distribution of the calculated momentum for particles with incident momenta of 1000 GeV/c is shown in figure 4.19 and this distribution is asymmetric. However, the frequency distribution of the inverse momentum for the same particles is symmetric and is shown in figure 4.20. Both the distributions in the figures are for five tray fits, that is for particles traversing four magnet blocks. The ratio of the standard deviation of the inverse momentum distribution to the inverse momentum is 0.118 for the distribution in figure 4.20. The ratio has been calculated for several tray combinations and for several different momenta. These are shown in table 4.8, for particles traversing four magnet blocks and in table 4.9 for particles traversing two and three magnet blocks. As can be seen from the tables the mean values for each tray combination depend on how many magnet blocks lie between the two extreme trays in the combination. The values in the tables are in agreement with those predicted by the theory. However it appears that scattering has a larger effect on three tray fits spanning four magnet blocks than four or five tray fits spanning four magnet blocks. Similarly the scattering also has more effect for the three tray fits than for four tray fits spanning three magnet blocks.

In order to estimate the effect of scattering on the muon spectrum

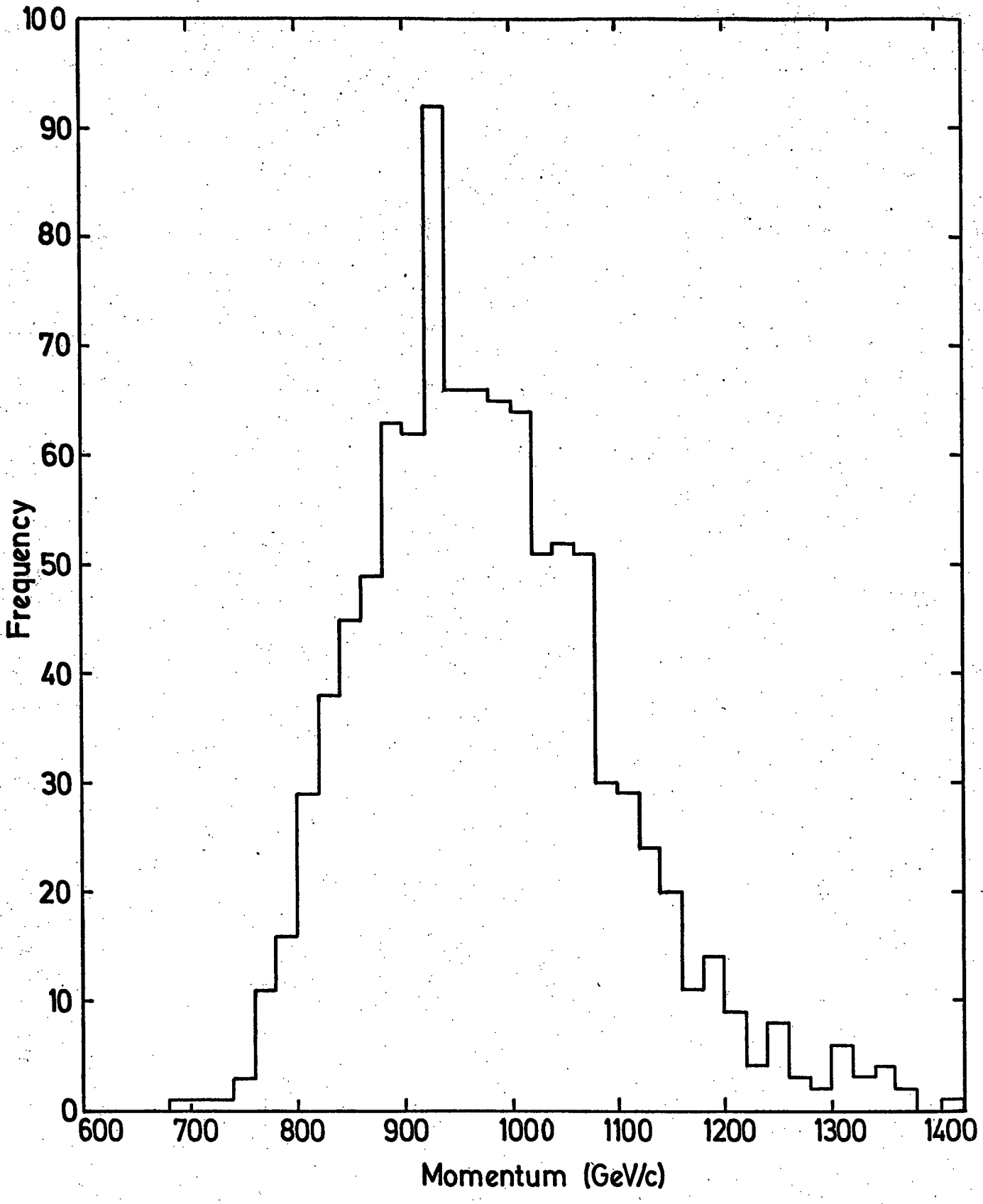

Figure 4.19. Histogram of the calculated momentum after multiple scattering through 4 magnet blocks for 1000 particles with incident momentum of 1000 GeV/c (5 tray fits).

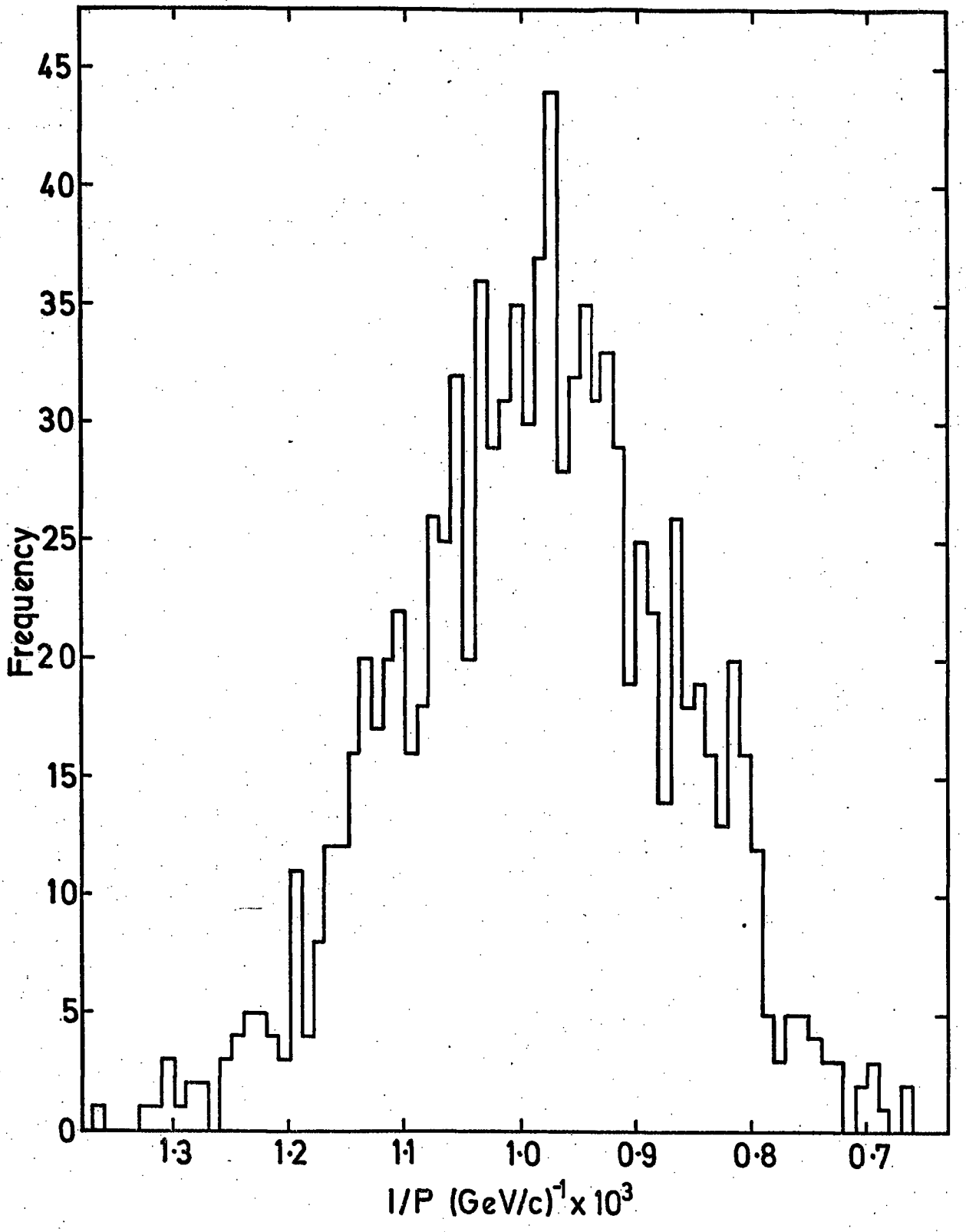

Figure 4·20. Histogram of I/P after multiple colomb scattering through 4 magnet blocks for 1000 particles with incident momentum of 1000 GeV/c.

TABLE 4.8

VALUES OF $p\sigma\left(\frac{1}{p}\right)$ FOR TRAY COMBINATIONS TRAVERSING FOUR MAGNET BLOCKS

MOMENTUM (GeV/c)	NUMBER OF PARTICLES	TRAY COMBINATION 12345	1245	1235	135	125	145
1000	1000	11.8	11.7	11.9	12.1	12.5	12.3
700	400	11.8	11.6	11.8	12.0	12.3	12.4
500	1000	11.4	11.0	11.2	11.3	11.7	11.8
300	1000	11.1	11.0	11.1	11.3	11.4	12.0
200	400	11.5	11.4	11.6	11.7	12.3	12.2
100	1000	11.4	11.5	11.8	11.9	12.1	12.4
MEAN		11.5	11.4	11.5	11.7	12.1	12.2

TABLE 4.9

VALUES OF $p\sigma\left(\frac{1}{p}\right)$ FOR TRAY COMBINATIONS TRAVERSING TWO OR THREE MAGNET BLOCKS

MOMENTUM (GeV/c)	NUMBER OF PARTICLES	TRAY COMBINATION 1234	124	123	245
1000	1000	13.5	14.5	16.8	14.0
700	400	13.4	14.3	17.4	14.1
500	1000	12.9	13.9	16.9	13.8
300	1000	12.3	13.2	16.3	14.1
200	400	13.4	14.5	17.8	14.2
100	1000	13.3	14.1	17.0	14.4
MEAN		13.1	14.1	17.0	14.1

Note: The values of $p\sigma\left(\frac{1}{p}\right)$ in the above tables have been multiplied by 100.

it is necessary to start with a trial momentum spectrum. Since the deflection of a particle traversing MARS is inversely proportional to the momentum, the ratio of the standard deviation of the inverse momentum distribution to the inverse momentum is the same as the ratio of the standard deviation of the deflection distribution to the deflection for a given momentum ($\sigma_\Delta = \sigma_{1/p}$). It is, therefore, easier to work in terms of a deflection spectrum $N(\Delta)$. The scattered deflection spectrum $N'(\Delta')$ is calculated from the relationship

$$N'(\Delta') = \frac{1}{\sqrt{2\pi}} \int_{-\infty}^{\infty} \frac{1}{\sigma_\Delta} N(\Delta) \exp\left\{\frac{-(\Delta - \Delta')^2}{2\sigma_\Delta^2}\right\} d\Delta \quad 4.7$$

The ratio of the scattered spectrum to the unscattered spectrum at given momenta is shown in table 4.10 for various values of σ_Δ, the scattering constant. The trial spectrum used in each case is discussed and derived in the next chapter. However for completeness it will be stated here as

$$N(E_\mu)\, dE_\mu = A\, P_\mu\, E_\mu^{-\gamma} \left[\frac{0.76^{\gamma-1} \times 90}{E_\mu + 90} + \frac{67.5 \times 0.52^{\gamma-1}}{E_\mu + 450}\right] \quad 4.8$$

where E_μ is muon energy, (GeV), P_μ, the survival probability of the muon at sea level, γ the slope of the production spectrum and A a constant. The variation of the effect of the scattering on the spectrum for different values of γ is small and is independent of the slope of the spectrum for $2.4 < \gamma < 2.8$. Therefore corrections are applied to each of the spectra obtained for each tray combination according to the scattering constant for that particular tray combination. It should be noted that the effect of scattering is the same for tray combinations with the same number of magnet blocks between their respective trays (ie for tray combinations 1, 2 and 4 and 2, 3 and 5, similarly for tray combinations 1, 2, 3 and 4 and 2, 3, 4 and 5).

TABLE 4.10

THE EFFECT OF SCATTERING ON THE SPECTRUM

MOMENTUM (p) (GeV/c)	σ_p/P 0.115	0.120	0.131	0.141	0.170
			$N'(\Delta')/N(\Delta)$		
100	1.035	1.038	1.046	1.054	1.083
200	1.045	1.048	1.059	1.069	1.107
300	1.048	1.053	1.065	1.076	1.118
500	1.052	1.058	1.071	1.084	1.131
700	1.056	1.062	1.075	1.088	1.139
1000	1.058	1.064	1.078	1.092	1.145
2000	1.062	1.068	1.083	1.098	1.154
3000	1.062	1.069	1.084	1.099	1.157
5000	1.064	1.070	1.086	1.101	1.161

4.9 THE ACCEPTANCE OF THE INSTRUMENT FOR EXTENSIVE AIR SHOWERS

As discussed in section 3.5.3, events with more than thirty columns of data in the top measuring tray are reanalysed as a separate group. The momentum selector efficiency is different for this type of event. This can be seen by considering an event with more than thirty columns of data in the top measuring tray which will in general have more than fifty cells triggered in the momentum selector. This means that nearly all particles for which the extrapolated line joining the cells in the bottom two trays passes through the top tray will be accepted by the momentum selector as a high momentum event. Therefore any event with a particle traversing the bottom four trays and with the extrapolated trajectory in the end plane of the spectrograph passing through tray 5 is accepted as a high momentum event. When reanalysed any event whose extrapolated trajectory does not pass through tray 5 is

rejected. However events with particles which do not pass through tray 5 in the side plane are accepted and it is therefore necessary to modify the acceptance for these events. This modified acceptance can be estimated by considering the apparent increase in length dy of the top tray such that all particles traversing the bottom four trays would also pass through the top tray. If the dimensions of the top tray are x cm by y cm, then the increased area of the top tray, A', is given by

$$A' = x\,(y + dy) \qquad 4.9$$

Therefore the acceptance, which is proportional to the increase in area of the top tray is $(1 + dy/y)\ A_c$ where A_c is the original acceptance. Substituting the values for y and dy, the new acceptance is 649 $cm^2 sr$. This calculation is only true for particles of infinite momentum, but it is considered adequate for particles whose momentum is greater than 100 GeV/c (when the asymptotic limit for the acceptance appears to be reached). Thus the actual spectrum must be decreased to take into account the increased acceptance for these particles.

CHAPTER 5

THE MOMENTUM SPECTRUM

5.1 INTRODUCTION

In the preceding chapter an attempt has been made to calculate the momentum of as many particles which traverse the magnet as possible. A correction must be made to the momentum of each particle to account for the error in the computed momentum by adding the appropriate corrections which have been discussed in chapter 4 (table 4.3). It is convenient to divide the spectrum into three, four and five tray fits, and further into each of the individual tray combinations. These two sets of spectra are shown in tables 5.1 and 5.2 respectively. The final momentum spectrum is derived from these data. The Mark II data are discussed in detail and the Mark I data, consisting of fewer events, is discussed more briefly at the end of the chapter.

TABLE 5.1

THE MARK II DATA DIVIDED INTO THE NUMBER OF TRAYS USED

	MOMENTUM RANGE (GeV/c)										
TRAYS USED	100-120	120-150	150-175	175-200	200-300	300-500	500-700	700-1000	1000-1500	1500-2000	2000-3000
3	67	98	53	50	127	90	34	13	12	5	4
4	354	499	330	261	619	358	93	58	25	9	7
5	596	1026	756	575	1092	591	140	63	29	8	5
TOTAL	1017	1623	1139	886	1838	1039	267	134	66	22	16

5.2 THE MOMENTUM SPECTRUM

5.2.1 INTRODUCTION

Due to the m.d.m. effects the data obtained from some three

tray fits above 500 GeV/c and some four tray fits above 700 GeV/c is suspect. It is therefore necessary to use only five tray fits above 700 GeV/c and four and five tray fits from 500 to 700 GeV/c in the final spectrum. In the next section, an estimation is made of the numbers of three and four tray fits expected for momenta above 500 GeV/c. An estimation is also made of the number of events with more than two unusable trays for all momenta.

5.2.2 THE PROBABILITY OF LOSING ONE OR MORE TRAYS

There are several reasons why certain trays are unusable in a particular event, each reason being separately labelled by the computer. The main reasons are as follows:

1) Knock-on electrons causing a group of flash-tubes to be confused,
2) A flash-tube inefficiency,
3) No data in a column (electronics fault),
4) A burst of particles from a magnet block accompanying a muon (essentially eleven or more tubes in a group or more than five columns of data in that group).

The probability of a knock-on electron being detected in a tray has been calculated by Said (1966) and is found to be sensibly independent of momentum. Thus the first three types of tray failure are momentum independent, (the second and third being properties of the flash-tube trays) and the fourth type (bursts) is momentum dependent.

Theoretical curves to predict the probability of a burst accompanying a muon from an iron block have been produced by several workers. The curves of Hansen (1975) and Said (1966) are shown in figure 5.1. The difference in absolute value for each set of data is due to the different minimum electron energy required for detection by each worker (7 MeV/c and 3 MeV/c respectively).

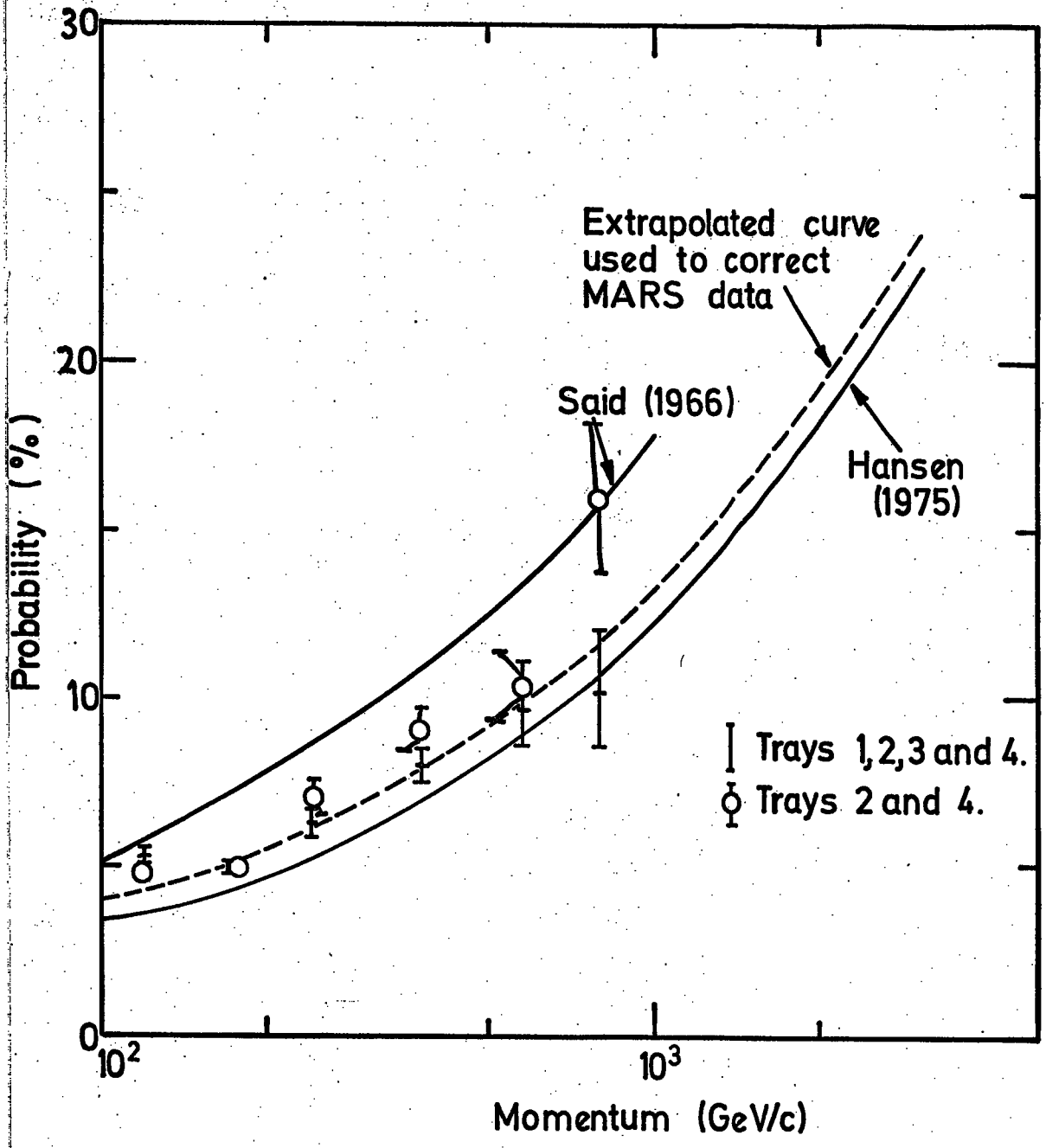

Figure 5.1. The probability of a burst accompanying a muon from a magnet block.

The probability of losing a tray due to a burst in MARS can be obtained by studying the computer analysis. The probability of a muon being accompanied by a burst can be calculated for various trays from the analysed data. It is advantageous to look at tray 5 separately since this tray is situated above all the magnet blocks, and to look at trays 2 and 4 together since these are the only trays which are situated directly beneath a magnet block. The probabilities of a tray being unusable for every other reason can also be obtained from the analysed data. These probabilities are shown in table 5.3 and are plotted on figure 5.1 so that comparisons may be made with the theoretical predictions of Hansen and Said.

TABLE 5.3

THE PROBABILITIES OF A TRAY BEING UNUSABLE IN THE ANALYSIS OF AN EVENT

TRAY		MOMENTUM RANGE						
		100-150	150-200	200-300	300-500	500-700	700-1000	>1000
		PROBABILITIES (%)						
5	BURST	1.6±0.2	1.3±0.2	1.6±0.2	1.2±0.4	3.4±1.1	2.3±1.0	7.4±3.0
2 4	BURST	4.8±0.3	4.9±0.3	7.0±0.4	9.0±0.9	10.4±1.5	16.0±1.7	9.2±2.5
1 2 3 4	BURST	5.4±0.2	5.0±0.1	6.4±0.2	8.0±0.9	9.8±1.0	10.4±1.4	11.4±1.5
5	OTHER	2.9±0.3	3.1±0.3	2.8±0.3	3.3±0.6	3.0±1.0	3.1±1.5	10.3±3.5
2 4	OTHER	1.9±0.2	1.9±0.2	2.4±0.2	2.0±0.4	2.8±0.8	2.7±1.3	2.6±1.3
1 2 3 4	OTHER	4.5±0.2	3.9±0.2	4.4±0.2	4.0±0.6	4.0±0.6	3.9±1.0	5.7±1.2

As can be seen from the data of table 5.3 and figure 5.1 the probability of a burst accompanying a muon in MARS is slightly

TABLE 5.2

THE DATA DIVIDED INTO TRAY COMBINATIONS

TRAY COMBS.	MOMENTUM RANGE 100-120	120-150	150-175	175-200	200-300	300-500	500-700	700-1000	1000-1500	1500-2000	>2000
123	6	3	3	1	2	1	0	0	2	1	0
124	6	9	3	4	12	2	3	0	2	1	2
134	2	2	2	4	4	2	3	1	0	0	0
234	4	7	4	4	10	3	2	1	3	0	3
1234	42	46	32	26	59	36	8	5	5	1	2
125	3	10	7	5	17	14	2	3	1	0	2
135	7	9	3	2	11	10	5	1	0	0	0
235	4	15	4	10	16	17	4	2	1	0	3
1235	59	87	51	66	141	95	20	22	3	0	3
145	7	10	3	7	16	12	3	2	0	0	1
245	20	23	15	12	25	18	5	2	1	0	1
1245	127	169	101	62	185	92	23	6	6	2	4
345	8	10	9	1	14	11	7	1	2	3	2
1345	32	70	39	41	110	53	21	16	4	2	4
2345	94	127	107	66	124	82	21	9	7	4	10
12345	596	1026	756	575	1092	591	140	63	29	8	15

higher than the probability as calculated by Hansen (1975) but the probability varies similarly with momentum.

Also the slight rise at low momenta is due to the preferential selection of bursts in tray 3 by the momentum selector. Therefore it is reasonable to extrapolate the curve obtained from the data for trays 1, 2, 3 and 4 parallel to the curve of Hansen. This is shown as a dotted line in figure 5.1.

It can also be seen from the data that the probability of losing tray 5 due to a burst is constant (1.5 ± 0.2%) and the probability due to any other effect is also constant (3.0 ± 0.3%), for $P_\mu <$ 1000 GeV/c. The probability of losing trays 1, 2, 3 or 4 due to all other reasons except bursts is also constant (4.0 ± 0.2%), $P_\mu <$ 1000 GeV/c.

It can be shown using probability theory that the probability of having a five tray fit, P_5, is defined as

$$P_5 = (1 - P)^4 (1 - P_{TOP}) \qquad 5.1$$

where P is the total probability of losing any of the first four trays and P_{TOP} is the probability of losing tray 5 for any reason at all. Similarly the probabilities of an event being a four tray fit (P_4) and a three tray fit (P_3) are defined as

$$P_4 = 4P (1 - P)^3 (1 - P_{TOP}) + P_{TOP}(1 - P)^4 \qquad 5.2$$

$$\text{and } P_3 = 6P^2 (1 - P)^2 (1 - P_{TOP}) + 4P_{TOP}P (1 - P)^3 \qquad 5.3$$

Similarly the probabilities of it being impossible to analyse the event, P_0, P_1 and P_2 are

$$P_0 = P^4 \times P_{TOP} \qquad 5.4$$

$$P_1 = P^4 (1 - P_{TOP}) + 4P^3 P_{TOP}(1 - P)$$

$$P_2 = 4P^3 (1 - P) (1 - P_{TOP}) + 6P_{TOP} P^2 (1 - P)^2 \qquad 5.4$$

These quantities have been calculated at the median momenta of each energy range in table 5.1, using the extrapolated curve in figure 5.1 and the constant probabilities, and are shown in table 5.4.

TABLE 5.4

THE THEORETICAL PROBABILITIES OF AN EVENT LOSING A GIVEN NUMBER OF TRAYS

MOMENTUM	P_{TOP}	P	P_5	P_4	P_3	$P_0 + P_1 + P_2$
100-120	4.5±0.4	8.0±0.5	68.4±0.7	27.0±1.6	4.2±0.5	0.4±0.1
120-150	4.5±0.4	8.5±0.5	66.9±0.7	28.0±1.6	4.6±0.6	0.4±0.1
150-175	4.5±0.4	9.0±0.5	65.5±0.7	29.0±1.6	5.1±0.6	0.4±0.1
175-200	4.5±0.4	9.5±0.5	64.1±0.7	29.9±1.5	5.5±0.6	0.5±0.1
200-300	4.5±0.4	10.0±0.5	62.7±0.7	30.7±1.5	5.9±0.6	0.7±0.1
300-500	4.5±0.4	11.8±0.5	57.8±0.7	33.3±1.4	7.7±0.6	1.2±0.2
500-700	4.5±0.4	14.0±0.5	52.2±0.6	36.4±1.3	9.9±0.7	1.5±0.2
700-1000	4.5±0.4	16.2±0.5	47.1±0.6	38.6±1.2	12.0±0.7	2.3±0.2
1000-1500	4.5±0.4	18.9±0.5	41.3±0.5	40.3±1.1	15.1±0.8	3.3±0.3
1500-2000	4.5±0.4	21.7±0.5	35.8±0.5	41.4±1.0	18.4±0.8	4.4±0.3
2000-3000	4.5±0.4	24.1±0.5	31.7±0.4	41.7±0.9	21.0±0.9	5.6±0.4

To check the above assumptions, the ratio of the expected to the actual numbers of five, four and three tray fits is shown in table 5.5.

All the ratios in the table for 200 GeV/c to 500 GeV/c are close to 1.00, therefore it is concluded that the method is acceptable for the higher momentum ranges.

TABLE 5.5

RATIO OF EXPECTED TO ACTUAL NUMBERS OF FIVE, FOUR AND THREE TRAY FITS

MOMENTUM RANGE	EXPECTED NUMBER OF n TRAY FITS / ACTUAL NUMBER OF n TRAY FITS 3/3	4/4	5/5
100-120	0.64 ± 0.25	0.78 ± 0.17	1.16 ± 0.11
120-150	0.76 ± 0.23	0.91 ± 0.16	1.06 ± 0.11
150-175	0.92 ± 0.24	1.00 ± 0.16	0.99 ± 0.11
175-200	1.02 ± 0.24	1.01 ± 0.16	0.99 ± 0.11
200-300	0.85 ± 0.20	0.91 ± 0.16	1.05 ± 0.11
300-500	0.88 ± 0.22	0.97 ± 0.16	1.02 ± 0.12
500-700	0.78 ± 0.24	1.05 ± 0.17	1.00 ± 0.14
700-1000	1.23 ± 0.32	0.89 ± 0.17	1.00 ± 0.17

5.2.3 CORRECTIONS FOR MULTIPLE COULOMB SCATTERING

The spectrum given in the previous section incorporates the scattering of the muon in the magnet blocks. To estimate the effect of this scattering on the incident muon spectrum, the average scattering for each momentum range is calculated from the data obtained in the previous chapter. A theoretical fit to the sea-level momentum spectrum (see section 5.6) is converted to a deflection spectrum and scattered. (It is necessary to convert to a deflection spectrum since the scattering is only symmetric in deflection and not in momentum.) The ratio of the scattered to the unscattered spectra for each momentum is then calculated. The average scattering and ratio of the scattered to unscattered spectrum is shown in table 5.6.

TABLE 5.6

THE RATIO OF SCATTERED TO UNSCATTERED SPECTRUM AS A FUNCTION OF MOMENTUM

MOMENTUM RANGE (GeV/c)	AVERAGE SCATTERING (%)	$\frac{N_{SCATTERED}}{N_{UNSCATTERED}}$
100-120	11.9	1.039
120-150	11.9	1.042
150-175	11.9	1.045
175-200	11.8	1.046
200-300	11.8	1.049
300-500	11.8	1.053
500-700	11.7	1.057
700-1000	11.5	1.059

5.3 SHOWERS

The analysed data for the showers, divided into individual tray combinations and into three and four tray fits is shown in table 5.8. These data were collected over 4120443 seconds and as mentioned previously the acceptance is 689 $cm^2 sr$. The intensity of muons in showers has been calculated up to 500 GeV/c using all the data and up to 1000 GeV/c using only the four tray fits, the number of three tray fits and the number of events expected to fail being estimated using the equations 5.2, 5.3 and 5.4 with $P_{TOP} = 1.0$. The spectrum for the showers is shown in table 5.9.

As can be seen from the data in table 5.9 the muons in showers contribute very little to the overall spectrum especially at lower momenta being 1.13×10^{-1}% of the total rate at 110 GeV/c and 7.1×10^{-1}% at 1000 GeV/c.

5.4 ERRORS IN THE MEASURED SPECTRA

There are two types of error involved in the measurement of

TABLE 5.8

THE SHOWER DATA FOR THE MARK II DATA IN THE FORM OF THE NUMBER OF TRAYS USED AND THE TRAY COMBINATION USED

TRAY COMB	MOMENTUM RANGE GeV/c								
	100-120	120-150	150-175	175-200	200-300	300-500	500-700	700-1000	>1000
123	1	0	2	1	2	2	1	1	1
124	0	1	1	1	6	1	1	1	3
134	1	3	1	0	2	0	1	0	0
234	1	2	1	0	3	3	2	2	2
1234	13	7	4	7	11	17	5	1	6
3 tray fits	3	6	5	2	13	6	5	4	6
4 tray fits	13	7	4	7	11	17	5	1	6
ALL DATA	16	13	9	9	24	23	10	5	12

TABLE 5.9

THE SPECTRUM OF MUONS IN SHOWERS FOR THE MARK II DATA

MOMENTUM RANGE	N	N(P) SHOWER $cm^{-2}st^{-1}sec^{-1}(GeV/c)^{-1}$	INTENSITY OVERALL $cm^{-2}st^{-1}sec^{-1}(GeV/c)^{-1}$	SHOWER INTENSITY / OVERALL INTENSITY
100-120	16	2.9×10^{-10}	2.6×10^{-7}	1.13×10^{-3}
120-150	13	1.6×10^{-10}	1.2×10^{-7}	1.3×10^{-3}
150-175	9	1.3×10^{-10}	6.5×10^{-8}	2.0×10^{-3}
175-200	9	1.3×10^{-10}	4.1×10^{-8}	3.2×10^{-3}
200-300	24	8.4×10^{-11}	1.7×10^{-8}	4.9×10^{-3}
300-500	23	4.3×10^{-11}	4.0×10^{-9}	1.1×10^{-2}
500-700	10	1.6×10^{-11}	9.3×10^{-10}	1.7×10^{-2}
700-1000	5	2.3×10^{-12}	3.3×10^{-10}	7.0×10^{-3}

the absolute momentum spectrum. Firstly there are those which only affect the absolute height, that is the momentum independent errors, and secondly there are those which affect the shape of the spectrum, that is those dependent upon momentum.

The main sources of error are as follows:

1) Error in magnetic field ($\pm$ 1%)

2) Error in measured scintillation counter efficiency (0.6%)

3) Error in measured momentum selector tray efficiency (0.9%)

4) Error in overall acceptance ($\pm$ 0.5%)

5) Statistical errors in measured numbers of particles

6) Error in calculated momentum selector efficiency

7) Error in estimated number of 'lost' events.

The first four quantities are momentum independent, the last three being momentum dependent.

An error in the magnetic field of $\pm$ 1% leads to an error in the measured momentum of $\pm$ 1% for each particle. The spectrum can be approximated by the expression

$$N(P)\, dP = K\, P^{-\gamma}\, dP,$$

where N(P) is the differential intensity, K is a constant, P the momentum and γ the slope of the spectrum. Since the error in P is $\pm$ 1% the error in N(P) is (γ x 1)%. For the purposes of this work γ can be regarded as constant and equal to 3.5. This results in an estimated error of 3.5% in the measured intensity due to an uncertainty in the magnetic field of 1%. The remaining momentum independent errors are straightforward. These errors are all added together resulting in a total uncertainty of 3.8%.

The momentum dependent errors are all similarly combined by the relation

$$\varepsilon_{tot} = \sqrt{\sum_{i=1}^{n} \varepsilon_i^2}$$

where ε_{tot} is the total error, and ε_i the individual errors. The errors are shown in table 5.10 as a function of momentum together with their combined values. The momentum selector efficiency as a percentage has been calculated for each momentum, as has also the burst correction to the efficiency. This explains the larger errors at lower momentum since the efficiencies involved are much smaller at these lower momenta.

TABLE 5.10

THE ERRORS ON THE MEASURED INTENSITIES

MOMENTUM RANGE	MOMENTUM SELECTOR EFFICIENCY	ERRORS (%) LOST EVENTS	STATISTICAL ERRORS	TOTAL ERROR
100-120	10.7	0.05	3.1	11.6
120-150	4.6	0.05	2.5	6.1
150-175	2.7	0.05	3.0	5.1
175-200	2.1	0.1	3.4	5.1
200-300	1.5	0.1	2.3	2.7
300-500	1.1	0.2	3.1	3.3
500-700	1.0	0.3	6.5	6.6
700-1000	1.0	0.4	9.1	9.2
1000-1500	1.0	0.6	18.5	18.5
1500-2000	1.0	0.8	37.5	37.5
2000-3000	1.0	1.0	60.0	60.0

5.5 THE OVERALL MOMENTUM SPECTRUM FOR THE MARK II DATA

The total live-time for the collection of the Mark II data is 1144 hours, 34 minutes, 3 seconds, which is 4120443 seconds. Using this time, the overall inefficiency, overall acceptance, momentum selector efficiency and scattering correction, the differential momentum spectrum has been calculated from the

relationship

$$N(P) = \frac{N}{T \times Acc} \times \frac{100}{E} \times \frac{1}{S} \times \frac{100}{M_E} \times \frac{1}{(P_2 - P_1)}$$

where N is the number of measured particles in the momentum range P_1 to P_2 GeV/c, E the overall efficiency (excluding the momentum selector efficiency), M_E the momentum selector efficiency and S the scattering correction. T is the total live-time and Acc the overall acceptance of the instrument. The differential spectrum is shown in figure 5.3, and the differential spectrum times the effective mean momentum cubed in figure 5.3. The effective mean momentum (P_m) is calculated from the expression of Hayman and Wolfendale (1963) which is given by

$$P_m = \frac{\int P^{-\gamma} dP}{P_1 - P_2}$$

where γ is the slope of the differential spectrum.

The data for the showers has also been added to these data. The spectrum is also shown in table 5.11. The errors shown on the figures and quoted in the table are only the momentum dependent errors. The errors not affecting the shape of the spectrum are omitted.

5.6 THE CHARGE RATIO FOR THE MARK II DATA

The ratio of the number of positive particles to the number of negative particles (charge ratio) has been calculated for the data collected by the spectrograph. Since the actual live-times for the different field directions are not the same a correction must be applied to the measured charge ratio to obtain the true charge ratio. For particles with momenta below 500 GeV/c the data for the three, four and five tray fits are added together, for the momentum range 500 GeV/c to 700 GeV/c only the data for the four

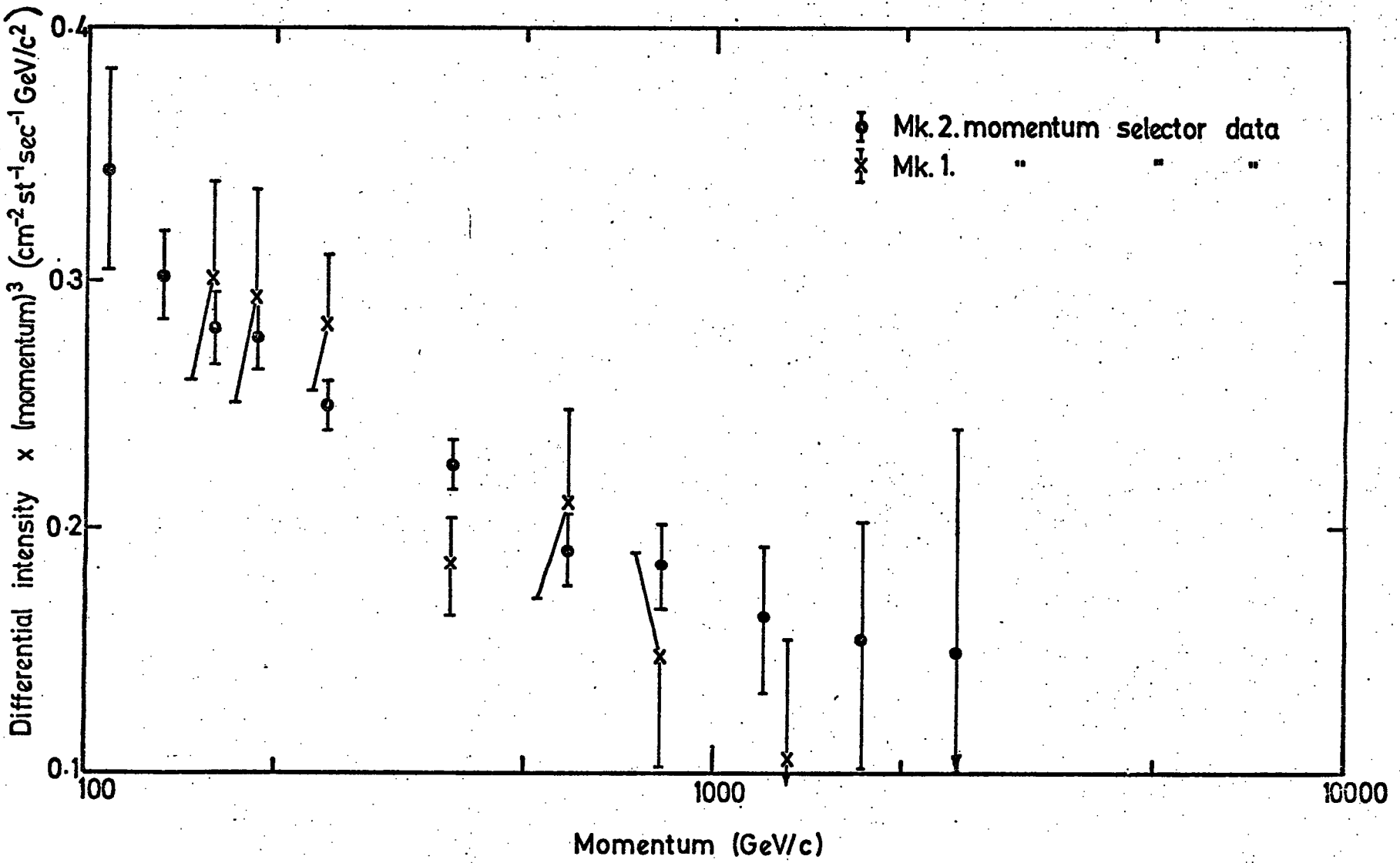

Figure 5.2. The muon momentum spectrum x (momentum)^3

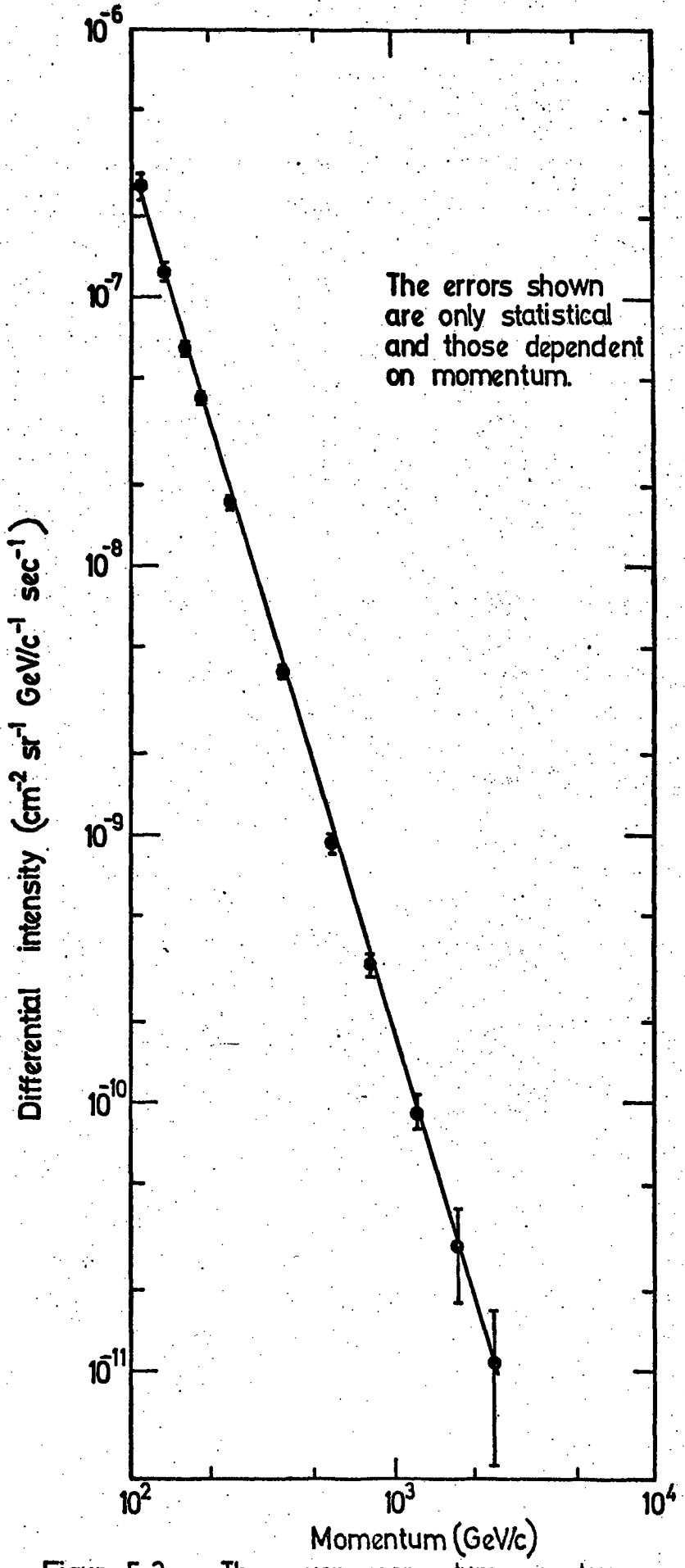

Figure 5.3. The muon momentum spectrum.

TABLE 5.11

THE MOMENTUM SPECTRUM FOR THE MARK II DATA

MOMENTUM RANGE	MEAN MOM. (GeV/c)	N	DIFFERENTIAL INTENSITY (including showers) (N(P)) $cm^{-2}sr^{-1}sec^{-1}(GeV/c)^{-1}$	ERROR (%)	N(P) P_m^3 $cm^{-2}sr^{-1}sec^{-1}(GeV/c)^2$
100-120	109.4	1017	2.60×10^{-7}	11.6	0.340
120-150	133.8	1623	1.25×10^{-7}	6.1	0.299
150-175	161.8	1139	6.56×10^{-8}	5.1	0.278
175-200	186.9	886	4.20×10^{-8}	5.1	0.274
200-300	242.7	1838	1.74×10^{-8}	2.7	0.249
300-500	381.4	1039	4.02×10^{-9}	3.3	0.223
500-700	587.5	233	9.31×10^{-10}	6.6	0.189
700-1000	829.9	121	3.26×10^{-10}	9.2	0.186
1000-1500	1211.9	29	9.01×10^{-11}	18.5	0.160
1500-2000	1722.8	8	2.94×10^{-11}	37.5	0.150
2000-3000	2423.9	5	1.04×10^{-11}	60.0	0.148

and five tray fits are used and above 700 GeV/c the data from only the five tray fits are used. This is to ensure that the data used for calculating the charge ratios are well below the respective m.d.m.s for the respective number of trays used. The formula used for calculating the charge ratio, C.R., is given by

$$C.R. = \frac{\frac{t^-}{t^+} N_\mu^{++} + N_\mu^{+-}}{\frac{t^-}{t^+} N_\mu^{-+} + N_\mu^{--}} = \frac{N_{\mu^+ c}}{N_{\mu^- c}} \qquad 5.6$$

where $N_{\mu^+ c}$ and $N_{\mu^- c}$ are the corrected numbers of positive and negative muons respectively and where N_μ^{++} and N_μ^{+-} are the numbers of positive particles measured in positive and negative fields respectively. N_μ^{--} and N_μ^{-+} are similarly defined for negative particles and t^+ and t^- are the total live-times in positive and negative fields respectively. Table 5.12 shows the numbers of particles measured in each field direction, together with the momentum range and charge ratio. The error in the charge ratio (δ C.R.) is calculated as follows:

$$\delta C.R. = C.R. \times \sqrt{\frac{1}{N_{\mu^+ c}} + \frac{1}{N_{\mu^- c}}} \qquad 5.7$$

The respective live-times for the positive and negative field directions are 2.26×10^6 seconds and 1.86×10^6 seconds for the Mark II data respectively. Thus the ratio of live-times for the two field directions is 0.82. The data are shown in table 5.12 as a function of momentum arranged in order of field direction, charge and number of trays used, together with the calculated charge ratios. Figure 5.4 shows the charge ratio as a function of momentum.

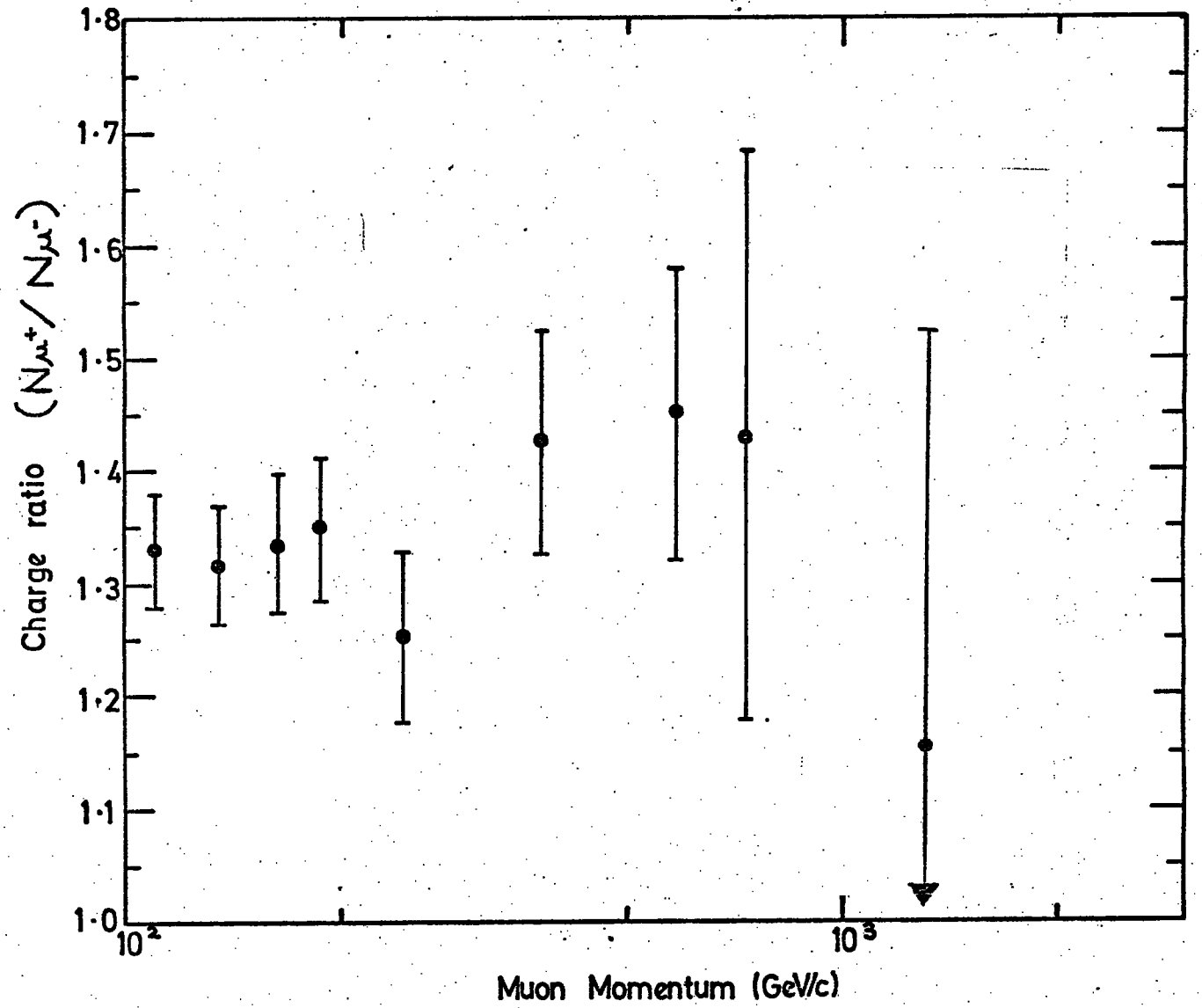

Figure 5.4. The charge ratio as measured using the Mark II momentum selector data.

TABLE 5.12

THE CHARGE RATIO (MARK II DATA)

FIELD	MUON CHARGE	TRAYS USED	MOMENTUM RANGE 100-120	120-150	150-175	175-200	200-300	300-500	500-700	700-1000	1000-2000
+	+	3	25	30	19	11	42	24	12	6	4
-	+	3	10	25	15	17	29	22	9	0	4
+	-	3	23	23	13	15	30	20	7	3	6
-	-	3	9	20	6	7	26	24	6	4	3
+	+	4	111	143	97	72	170	120	35	13	12
-	+	4	86	133	90	73	152	89	22	15	12
+	-	4	93	132	79	65	164	92	21	14	4
-	-	4	64	91	64	51	133	57	15	16	6
+	+	5	174	294	221	194	319	201	40	17	14
-	+	5	172	292	206	141	306	153	44	20	6
+	-	5	140	249	189	130	262	147	28	14	11
-	-	5	110	191	140	110	205	90	28	12	6
Charge ratio			1.33	1.32	1.34	1.35	1.25	1.43	1.53 +	1.43 *	1.16 *
δ Charge ratio			0.08	0.11	0.10	0.11	0.08	0.12	0.24	0.36	0.38

\+ Four and five tray fits * Five tray fits

5.7 THE DERIVATION OF THE PION PRODUCTION SPECTRUM

5.7.1 INTRODUCTION

Muons arriving at sea level are the decay products of pions and kaons produced in nuclear interactions or the decay products of nuclear active particles. It is possible to calculate the

expected muon spectrum which would result from given pion and kaon production spectra. In this section an attempt is made to estimate the slope of the production spectra and also the contribution to the sea level spectrum from kaons.

5.7.2 THEORY

Using the diffusion equation of pions in the atmosphere the muon production spectrum has been calculated by several workers (Smith and Duller (1959), Bull et al. (1965)). Most of these workers base their studies on that of Barrett et al. (1952). The production spectrum is then extrapolated to sea level. The process is repeated for kaons and the resulting two sea level spectra combined.

Several simplifying assumptions are made in the model. These simplifications are listed below, together with the final theoretical expression, the derivation of which is not considered here. The assumptions are as follows:

1) that the pion and kaon spectra follow a power law given by $AE^{-\gamma}$ where A is a constant, E the particle energy and γ the slope of the spectrum
2) that all particles travel in the vertical direction (ie with no transverse momentum)
3) that all muons are produced at the same depth in the atmosphere (ie 100 gcm^{-2})
4) that the atmosphere is isothermal (A further correction is made later for this assumption.)
5) that the relation between the muon and parent energies is constant
6) that the interaction lengths for protons and pions are the same (ie 120 gcm^{-2}).

As previously stated, the starting point for the model is the diffusion equation for pions which is

$$\frac{dN_\pi}{dy} = \frac{A_\pi E_\pi^{-\gamma}}{\lambda_p} \exp\left(\frac{-y}{\lambda_p}\right) - \frac{N_\pi}{\lambda_\pi} - \frac{m_\pi c^2 N_\pi}{\rho(y)\tau_\pi c E_\pi} \qquad 5.8$$

The terms on the right hand side represent the production of pions in nuclear interactions, the loss due to interaction and the loss due to decay into muons. The symbols have their usual meaning, λ_p being the proton absorption length, m_π the pion mass, τ_π the pion lifetime and $\rho(y)$ the atmospheric density at depth y.

The muon spectrum at sea level due to pion decay alone, calculated from the above formula and using all the assumptions stated earlier is given by

$$N_\mu(E_\mu)\, dE_\mu = A_\pi P_\mu (E_\mu + \Delta E_\mu)^{-\gamma} \frac{r_\pi^{\gamma-1} B_\pi}{(E_\mu + \Delta E_\mu + B_\pi)} \qquad 5.9$$

where E_μ is the muon energy, ΔE_μ the energy loss from production, P_μ the muon survival probability to sea level and r_π is the fraction of the pion energy taken by the muon. This is approximately equal to the ratio of the particle masses (ie 0.76). B_π is a constant energy depending on the rest mass and lifetime of the pion and is taken as 90 GeV.

Equation 5.9 must be modified to include the muons produced from decaying kaons and therefore becomes

$$N_\mu(E_\mu)dE_\mu = A\, P_\mu(E_\mu + \Delta E_\mu)^{-\gamma}\left[\frac{r_\pi^{\gamma-1} B_\pi}{(E_\mu + \Delta E_\mu) + B_\pi} + \frac{k\, r_k^{\gamma-1} B_k}{E_\mu + \Delta E_\mu + B_k}\right] \qquad 5.10$$

where k is the kaon to pion ratio at production and r_k and B_k are assigned the values 0.52 and 450 GeV/c respectively.

5.7.3 THE COMPARISON OF THE MEASURED AND THEORETICAL MUON SPECTRA

Using equation 5.10 the best fit to the spectrum obtained

in section 5.3 has been calculated as a function of k, γ and A which are the only unknown quantities in equation 5.10. The method used is a simple χ^2 test, the best fit being defined by the minimum value of χ^2 where χ^2 is given by

$$\chi^2 = \sum \frac{(I_o - I_e)^2}{\delta I_o} \qquad 5.11$$

where I_o, I_e and δI_o are the measured intensity, theoretical intensity and the error on the measured intensity respectively.

5.7.4 THE BEST K/π RATIO

With the χ^2 test used to determine the best fit to the data, the value of A is allowed to vary for particular values of the K/π ratio (k) and the slope of the production spectrum (γ) in equation 5.10. χ^2 is calculated for each set of values and the minimum value of χ^2 determined. It is found that several combinations of k and γ give χ^2 fits which are better than the 90% confidence level. This is mainly due to the large statistical errors in the high momentum region of the spectrum. A graph of the best value of the K/π ratio as a function of γ is shown in figure 5.5. As can be seen from the figure the value of γ required to give the best χ^2 fit to the data, increases as the K/π ratio increases. The minimum values of χ^2 obtained for each K/π ratio are shown in figure 5.6. As can be seen from the figure, no actual value of K/π can be deduced with any certainty. However, it is considered that the K/π ratio lies between 0.05 and 0.25.

In order to obtain a value for γ, a particular value of the K/π ratio must be taken. Several workers have predicted values for the ratio using the results obtained at the Interacting Storage Rings (CERN). The results of several of these workers (Hume, 1974, Adair, 1974, Erlykin et al., 1974, Morrison and Elbert, 1973)

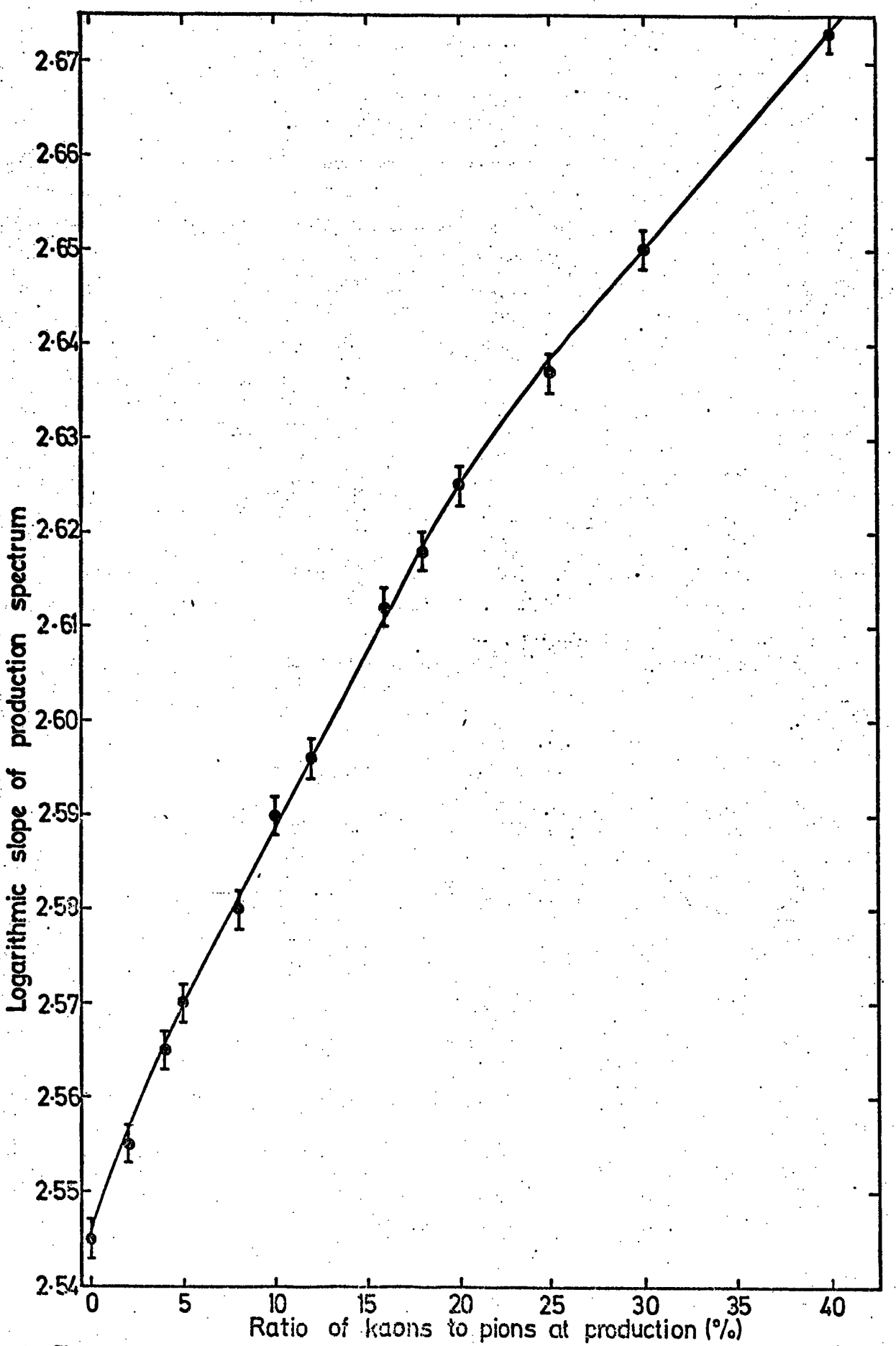

Figure 5.5. The values of the k/π ratio and slope of production spectrum for conditions of minimum χ^2.

are shown in table 5.13.

As can be seen from table 5.13, the values of the K/π ratio obtained by all these workers are similar and therefore the mean value of 0.106 is used in all the following calculations.

5.7.5 THE LOGARITHMIC SLOPE OF THE PRODUCTION SPECTRUM

Using the value of the K/π ratio obtained previously,(0.106), the values of χ^2 for various values of γ are calculated, and are shown in figure 5.7. As can be seen from this figure the best value of γ for the given K/π ratio is 2.592 ± 0.004. However it should be noted that a small change in the value of the K/π ratio would lead to a change in the value of γ as can be seen from figure 5.5. Using the values of K/π and γ as calculated a plot of minimum χ^2 against the scaling factor (A) is shown in figure 5.8. Thus the values of A, K/π and γ which give the best fit to the present data are 0.1456, 0.106 and 2.592 respectively.

TABLE 5.13

THE K/π RATIO OBTAINED BY OTHER WORKERS

WORKERS	K/π RATIO
Hume (1974)	0.102
Adair (1974)	0.099
Erlykin et al. (1974)	0.135
Morrison and Elbert (1973)	0.088
OVERALL MEAN	0.106

5.8 THE BEST ESTIMATE OF THE SPECTRUM

Using the values of K/π, γ and A obtained in the previous section, the theoretical spectrum has been calculated. This theoretical spectrum is compared with the measured spectrum by

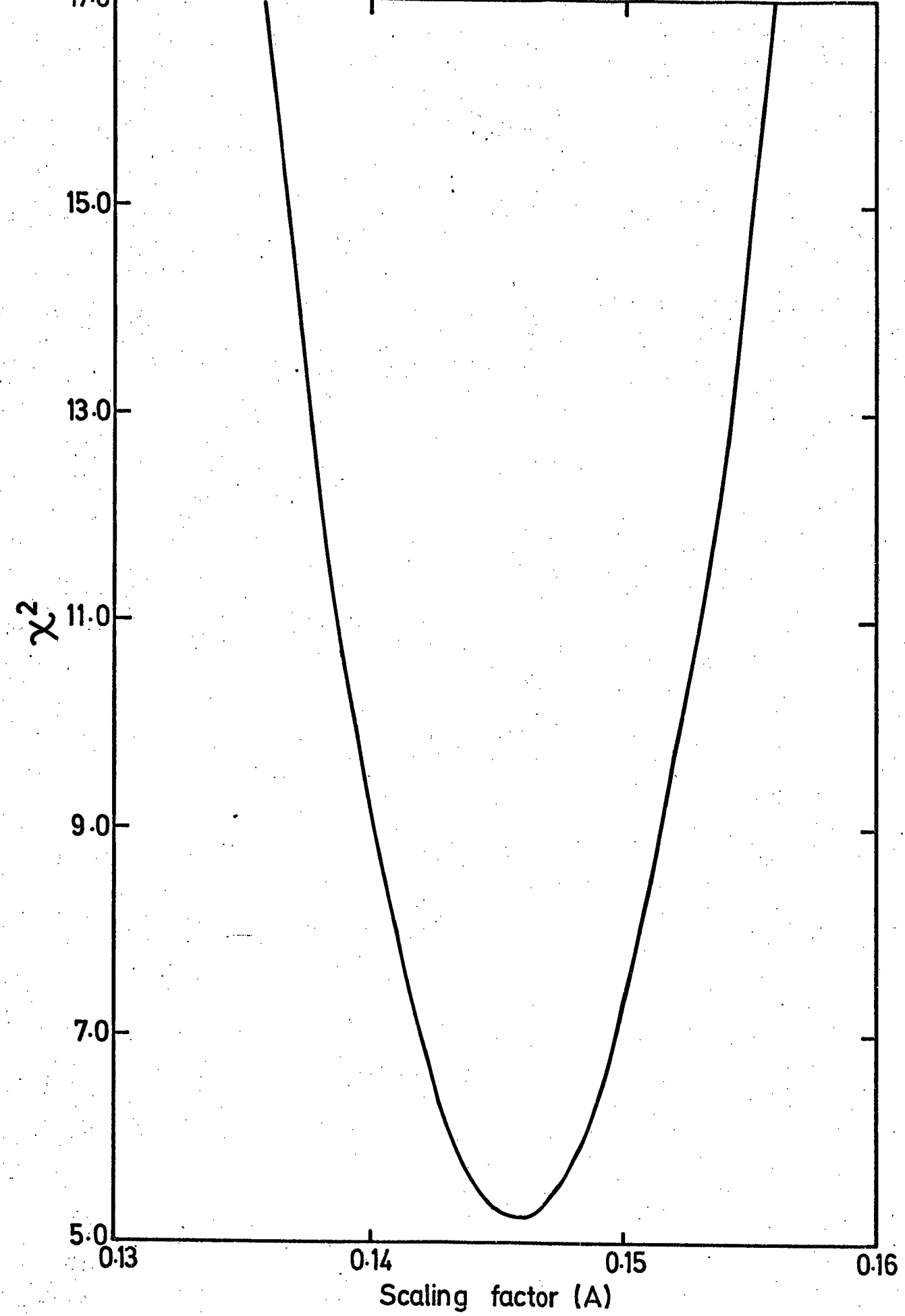

Figure 5.8. The A/χ^2 plot for $\gamma = 2.594$ & $\frac{k}{\pi} = 0.106$

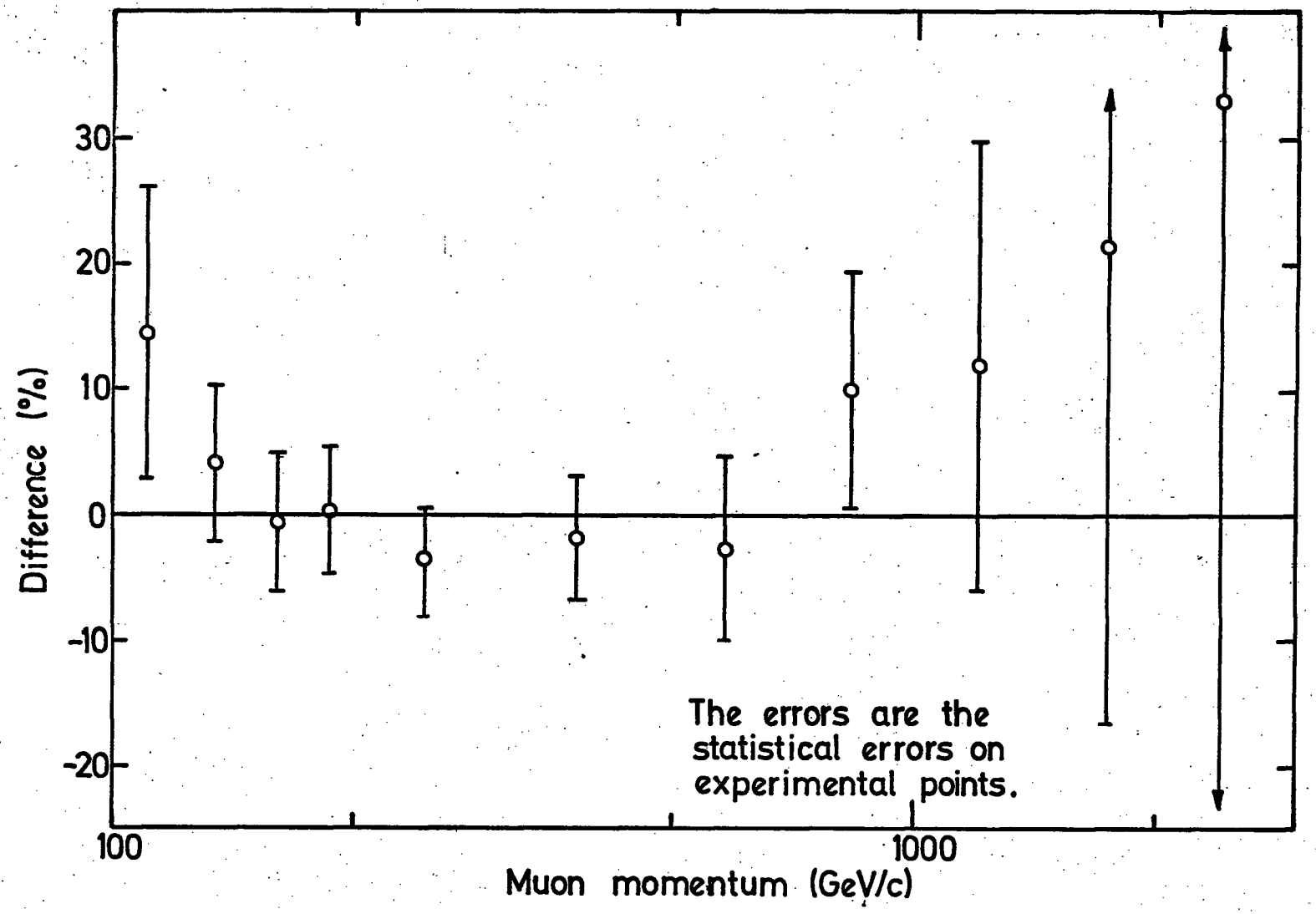

Figure 5.9. Plot of the percentage difference between experimental and best theoretical estimate of the spectrum.

considering the quantity, D, where

$$D = \frac{N_{OBS} - N_{TH}}{N_{OBS}}$$

where N_{OBS} and N_{TH} are the observed and theoretical estimates of the spectrum respectively. This quantity is shown as a function of momentum in figure 5.9. The error bars in this figure are the statistical errors derived from the data. It can be seen from the figure that the theoretical fit is best in the momentum range 150 - 700 GeV/c and it appears that the measured spectrum is flatter than the theoretical spectrum above 700 GeV/c. However the errors on all the points above this energy are large enough to allow the two spectra to be compatible across the whole energy range.

5.9 THE MARK I MOMENTUM SELECTOR DATA

As mentioned previously in this chapter, the Mark I data consists of much fewer events and hence the statistical errors on any measurements of the spectrum derived from these data are very large. These data were used mainly for test purposes involving the computer analysis programme. However, for completeness, the momentum spectrum has been calculated using the Mark I momentum selector data, in the same manner as the spectrum was calculated for the Mark II momentum selector data, (ie including showers and inefficiencies). The total live-time for the collection of this data is 494311 seconds.

For the Mark I momentum selector data there is an additional source of inefficieny, where the computer received no measuring tray flash-tube data for any of the five trays. These events are referred to as 'No Data's and are assumed to be due to electronic faults causing no high-voltage pulse to be applied to the measuring trays. This effect is assumed to be momentum independent and a

flat increase in the overall rate corresponding to the rate of 'no data's is applied to the measured data. The 'no data's recorded are 3.4% of the recorded events.

The data are shown in table 5.14 in terms of the number of trays used and the momentum ranges. The calculated spectrum and charge ratio including all the corrections is shown in table 5.15 and the spectrum is also plotted on figure 5.2. As can be seen from figure 5.2, the data from the Mark I momentum selector is consistent with that obtained using the Mark II momentum selector. The Mark I momentum selector data has not been used in any calculations and will not be used for comparison purposes. The overall charge ratio also agrees with the Mark II momentum selector data and is 1.24 ± 0.16. As can be seen from table 5.15, the errors on the charge ratio are extremely large and no conclusions can be drawn from the results.

5.10 CONCLUSION

In this chapter the data has been used to measure the charge ratio and the momentum spectrum of muons arriving at sea level, and the slope of the pion production spectrum has been estimated. In the following chapter, these results will be compared with those obtained by other workers.

TABLE 5.14

THE MARK I DATA

MOMENTUM RANGE	TRAYS USED			
	3	4	5	ALL
150-175	3	27	17	47
175-200	4	14	15	33
200-300	13	42	52	107
300-500	10	35	38	83
500-700	2	18	11	31
700-1000	1	7	4	12
1000-1500	5	3	5	13
1500-2000	2	2	1	5
2000-3000	0	1	1	2

TABLE 5.15

THE MARK I MOMENTUM SPECTRUM

MOMENTUM RANGE	DIFFERENTIAL INTENSITY $cm^{-2}sr^{-1}sec^{-1}(GeV/c)^{-1}$	DIFFERENTIAL INTENSITY x P^3 $cm^{-2}sr^{-1}sec^{-1}(GeV/c)^{2}$	CHARGE RATIO
150-175	6.83×10^{-8}	0.300	-
175-200	4.34×10^{-8}	0.293	-
200-300	1.92×10^{-8}	0.283	1.38 ± 0.28
300-500	3.21×10^{-9}	0.184	0.98 ± 0.22
500-700	1.00×10^{-9}	0.210	1.90 ± 0.78
700-1000	2.49×10^{-10}	0.147	1.20 ± 0.72
1000-3000	2.38×10^{-11}	0.104	0.75 ± 0.60

CHAPTER 6

COMPARISON WITH THE RESULTS OF OTHER WORKERS

6.1 INTRODUCTION

It is not intended in this chapter to give a complete review of all the results of all the workers in the field covered by the present experiment. However it is intended to consider the results of some recent experiments and to compare them with the results of the present experiment.

The vertical sea-level muon momentum spectrum has been derived by several methods. There have been and are at present several spectrographs operating of a similar type to MARS, most being of the air-gap type. It is the results of these experiments which can best be compared with the results from MARS. The energy spectrum above 1000 GeV has to date mostly been derived from the results of measurements made deep underground. The sea-level muon spectrum is derived from these measurements by considering the range-energy relationship for the rock traversed by the particles before reaching the detector. The uncertainty in this relationship leads to the derived spectra having large errors on all the points.

Another method which has been used is to combine the spectra measured at various inclined directions to derive the vertical spectrum. The spectrum has also been derived from measurements on electromagnetic bursts in local absorbers and from measurement of the γ-ray flux as a function of atmospheric depth.

The starting point for the comparisons made in this chapter will be the results of Hayman and Wolfendale (1962). Earlier measurements have not been considered, as many such results have been superceded by much more detailed measurement especially in the region above 100 GeV/c, the region covered by the present

experiment. The results from each of the main spectrographs will be dealt with in turn, the indirect measurements being discussed at the end of this chapter.

The spectrum which is used in all the comparisons is the best fit spectrum obtained in the previous chapter. For comparison with the actual experimental values reference can be made to figure 5.9, which shows the deviation of the experimental points from the final best fit curve.

6.2 MAGNETIC SPECTROGRAPH MEASUREMENTS IN DURHAM

6.2.1 THE HAYMAN AND WOLFENDALE SPECTRUM

The results of Hayman and Wolfendale (1962) were obtained using an air-gap magnetic spectrograph with Geiger tubes and neon flash-tubes as the track location elements. The authors have fitted a theoretical spectrum similar to the one used in this work in the momentum range 128 to 1640 GeV/c, assuming that the K/π ratio is zero. This yields a value of 2.67 ± 0.10 for γ with the χ^2 test giving a 90% level of significance. The m.d.m. quoted for this apparatus is 657 ± 112 GeV/c. This means that any measurements above such a momentum must be regarded as suspect.

The Hayman and Wolfendale spectrum has been modified by Osborne et al. (1964) to correct for an instrumental bias and this modified spectrum has been combined with the muon spectrum obtained by Duthie et al. (1962) (using the intensity of γ-rays in the atmosphere) in order to extend the high energy limit of the spectrum to 7000 GeV/c.

Aurela and Wolfendale (1967) modified the Hayman and Wolfendale spectrograph by inserting a solid iron plug to increase the measured flux of particles traversing the instrument. This resulted in a spectrum up to 116 GeV/c. However these results were combined with the underground range spectrum of Achar et al. (1965) and the underground

burst spectrum of Vernov et al. (1966) resulting in a spectrum up to 7000 GeV/c.

All these experiments have the drawback of not being absolute measurements, and have all been normalised to the so-called Rossi point at 1 GeV/c (Rossi, 1948). However, recent measurements of the absolute intensity at 1 GeV/c have shown the Rossi value to be approximately 20% too low (Allkofer et al., 1970). All these spectra therefore have to be renormalised to the Allkofer value at 1 GeV/c and these renormalised spectra are shown together with the present result (unnormalised) in figure 6.1.

The Osborne et al. spectrum is seen to be in good agreement with the present results in the momentum range 100 GeV/c to 700 GeV/c. Above this range the present results indicate a much higher intensity of approximately 20% at 1000 GeV/c rising to 50% at 2500 GeV/c. This is probably due to normalisation errors in using the γ-ray data to predict the high energy region of the spectrum.

The Hayman and Wolfendale spectrum is lower in absolute value but when corrected for biases (Osborne et al.) it is in agreement with the present results as mentioned above.

This is again considered to be due to the normalisation errors for the region above 100 GeV/c where indirect methods have been used to derive the muon spectrum. The relative differences between the present data and the several spectra (normalised to the 1 GeV/c point of Allkofer) are shown in figure 6.2.

6.2.2 PREVIOUS RESULTS USING THE MARS SPECTROGRAPH

The momentum spectrum has been measured using only the momentum selector trays of MARS up to approximately 700 GeV/c. These results

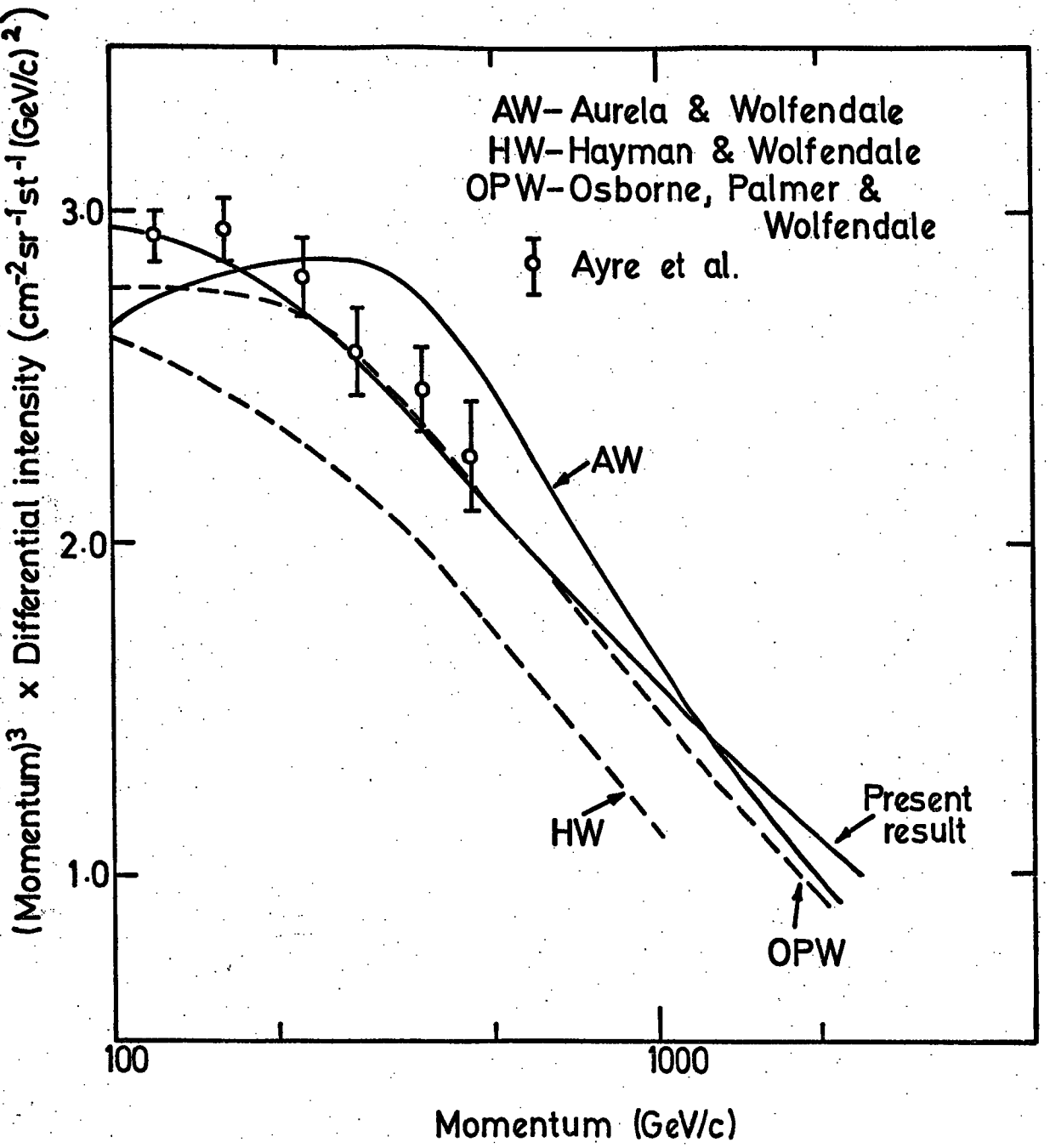

Figure 6.1. The spectra of the previous Durham Experiments.

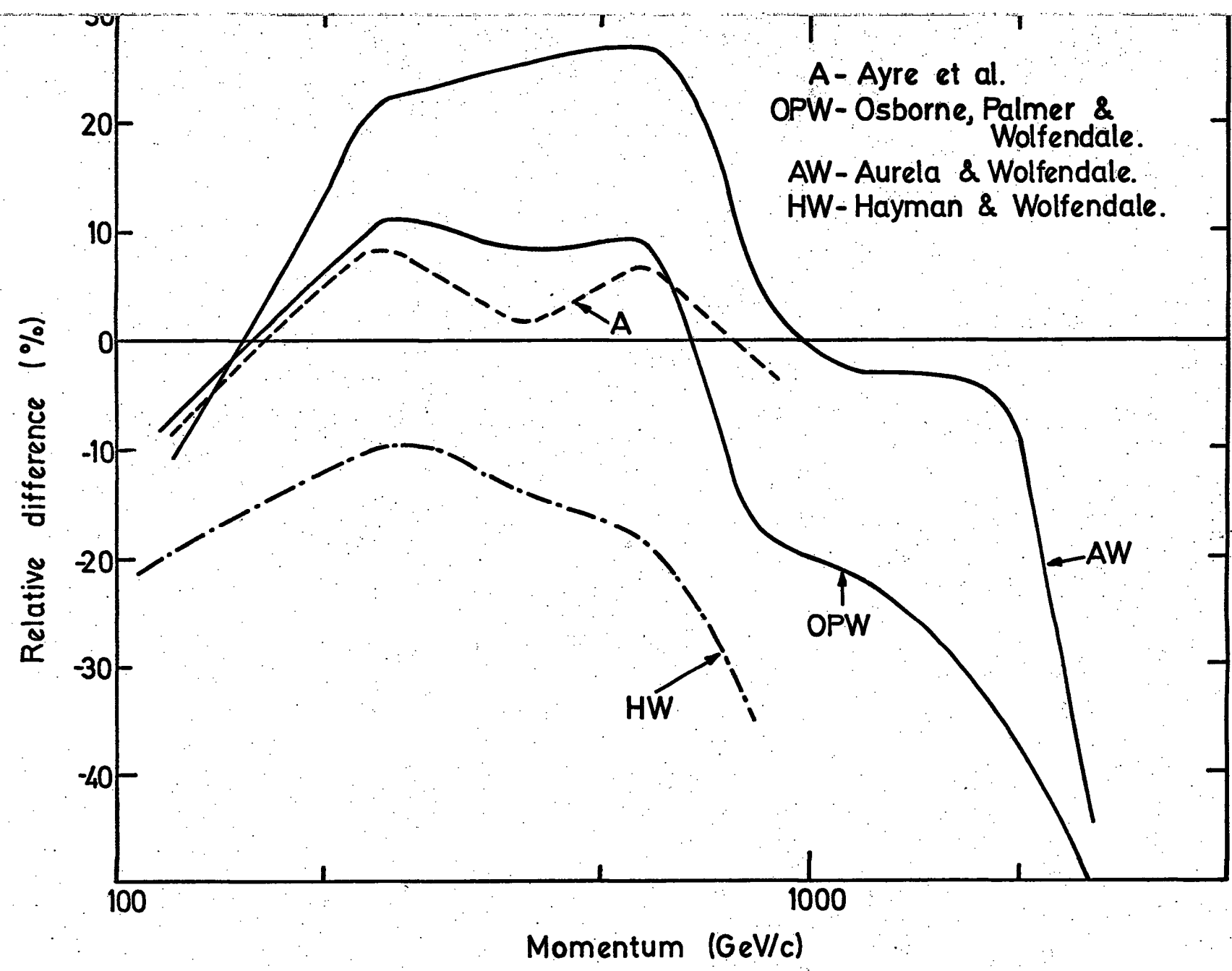

Figure 6.2. The comparison of the data from previous Durham experiments with the present data.

are given by Ayre et al. (1975a) and Whalley (1974). This spectrum is also shown in figure 6.1 and the relative difference from the present results is shown in figure 6.2. It can be seen from the figure that the results of this experiment are in good agreement with the present results, the maximum difference being approximately 9%. Such a difference is covered by the statistical error on the points of both sets of data. It should also be noted that the errors which do not affect the shape of the spectrum are not necessarily in the same sense for both sets of data.

These data from MARS have also been used to predict the pion production spectrum in the momentum range 20-500 GeV/c (Thompson and Whalley, 1975). The results give

$$\gamma = 2.540 \begin{matrix} + 0.039 \\ - 0.036 \end{matrix} \text{ for } 100 \text{ GeV/c} < E_{\pi} < 700 \text{ GeV/c}$$

using a K/π ratio of 0.085. If, for the present data, the K/π ratio were taken to be 0.085, the γ required to give the best fit would be approximately 2.58. Thus the present data gives a slightly larger value of γ than the previous results obtained from MARS, although it must be noted that the present data extends over a much larger energy range (100-3000 GeV/c) than the previous results (100-700 GeV/c).

6.3 THE RESULTS FROM SPECTROGRAPHS IN OTHER PARTS OF THE WORLD

There are several other spectrographs from which data have been obtained on the muon spectrum above 100 GeV/c. Most of the results suffer from large statistical uncertainties, due mainly to the small acceptances of the instruments. However, the overall results from some of these spectrographs are discussed.

The results from Durgapur, India have been reported by Nandi and Sinha (1972). The solid iron spectrograph has an acceptance of 11.6 $cm^2 sr$ and a quoted m.d.m. of 985 ± 25 GeV/c. The results

are shown in figure 6.3. The authors have fitted the usual theoretical model and obtained the value for γ of 2.61 $\pm$ 0.03, with a K/π ratio of zero. This compares with γ = 2.54 for the best fit to the present experiment with K/π = 0. However there is no discrepancy between the experimental points and the present best estimate of the spectrum. These results have been normalised to the Allkofer point at 1 GeV/c.

There have been many measurements of the muon spectrum made at Kiel, Germany, the most recent results using the Kiel spectrograph being reported by Allkofer et al. (1971a). Again the results are shown in figure 6.3. The best fit value for γ and the K/π ratio are 2.63 and 0 respectively. These results again give a high value for γ and a low value for the K/π ratio compared with the present experiment. There is however no discrepancy between the experimental points and the present data. These data points have been combined with the results from the smaller spectrograph and with the absolute intensity measurement at 1 GeV/c to obtain the absolute spectrum over the whole momentum range 0.2 GeV/c to 1000 GeV/c.

The spectrograph at Nottingham has produced two main sets of results, the first being reported by Baber et al. (1968) and the second by Appleton et al. (1971). These are both shown in figure 6.3. The usual best fit spectra give 2.65 $\pm$ 0.03 and 2.73 $\pm$ 0.02 as the values for γ for K/π equal to zero, and the latter gives γ as 2.745 for a K/π ratio of 0.20. These results are both lower in absolute intensity than most of the other measurements and the spectra are also somewhat steeper. A possible source of such differences is the event rejection in the analysis procedure. However, it is difficult to envisage a 20% loss of events above 100 GeV/c, even though rejection of events becomes increasingly likely due to bursts accompanying the muon, with increasing momentum.

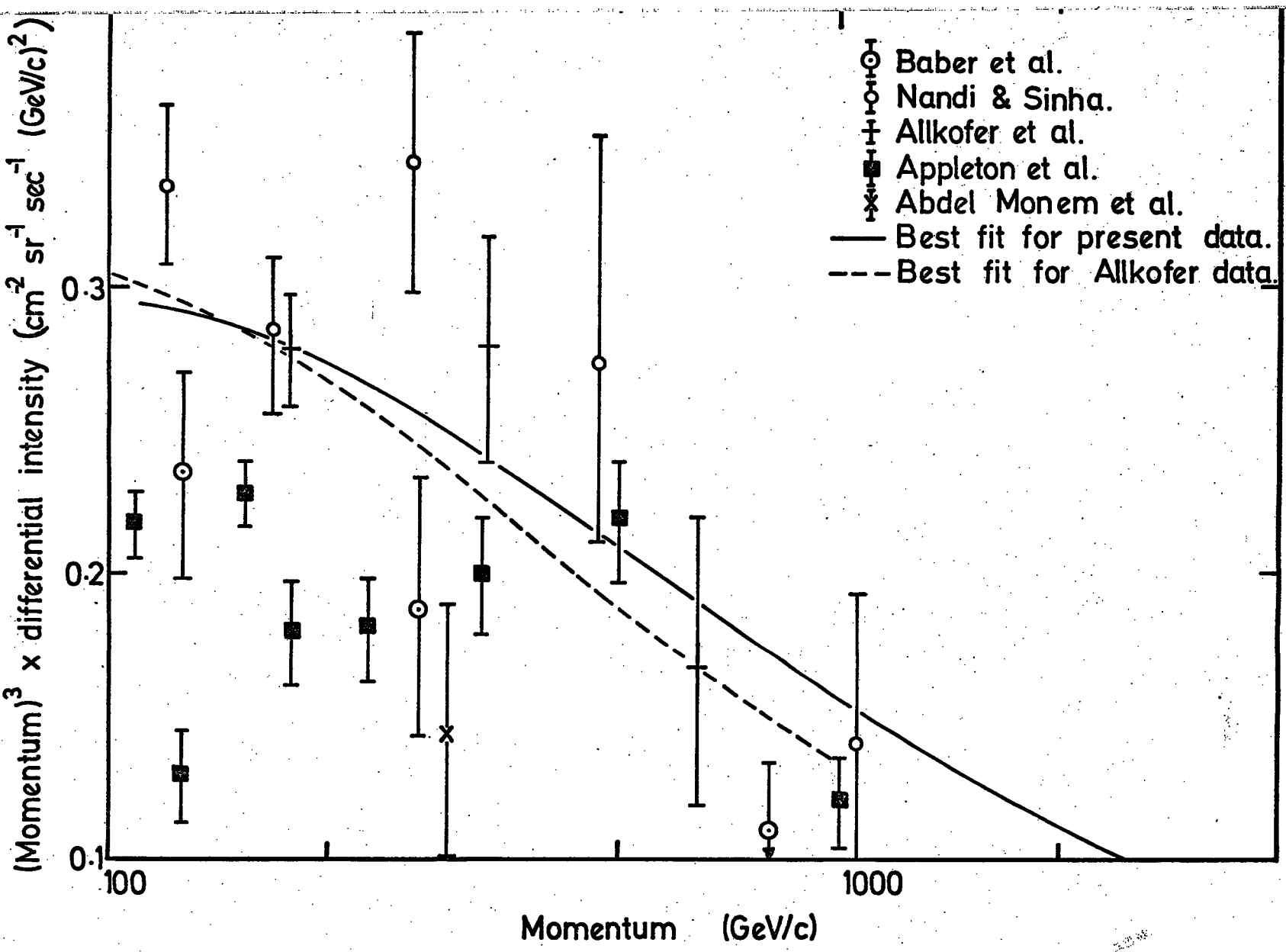

Figure 6.3. The momentum spectra of various workers.

The spectrograph at College Station, Texas, has been used to derive the spectrum up to 1000 GeV/c and the results have been reported by Abdel-Monem et al. (1973). However, since there is only one data point above 100 GeV/c it is difficult to give much weight to such a spectrum. The usual theoretical model was fitted, giving γ as 2.67 and using the K/π ratio as zero, and extrapolated to give the spectrum up to 1000 GeV/c. For completeness the one data point is shown in figure 6.3.

6.4 THE BURNETT ET AL. SPECTRUM

The spectrum derived by Burnett et al. (1973) using the UCSD spectrograph at San Diago, California, deserves special mention. The spectrograph has an overall acceptance of 1500 $cm^2 sr$ and has an m.d.m. of 2500 GeV/c. The solid iron magnet has been used at eight angles from 0^o to 82^o to the vertical. The spectrum at each angle has been measured and the results combined to give a vertical spectrum with small statistical errors. These results have been increased by 15% to allow for the effects of resolution and multiple scattering, from the data in the original paper. The results are shown in figure 6.4 from which it can be seen that the absolute intensity is still approximately 15% lower than the present results. The slope of the production spectrum (using a slightly different method from that mentioned in chapter 5 of this work) is given as 2.715 ± 0.15. The relatively lower intensity might be due to the approximations used in combining the spectra measured at each angle and the high value of γ is considered not to be very significant, especially since different models were used to calculate γ in the present and the Burnett et al. spectra. However it is considered that more work is required in this field as it might be possible to derive the vertical spectrum from the results of the many horizontal spectrographs now in operation.

6.5 INDIRECT METHODS OF MEASURING THE SPECTRUM

As mentioned previously there are three main methods of measuring the muon spectrum. The measurement of γ-rays in the atmosphere has been used by Osborne et al. as discussed previously. The other two methods of burst measurements in absorbers and intensity measurements deep underground will be discussed in more detail.

Burst experiments are usually made by sandwiching detectors between absorbers so that the development of electron-photon showers can be studied. From measurements on the numbers of particles in such a shower the muon energy can be estimated, using the theory of electromagnetic interactions. However the problem of fluctuations due to the non-continuous Bremsstrahlung energy loss makes detailed calculations difficult. Such problems have been discussed by several workers (eg Kiraly et al., 1972).

Measurements underground also require detailed knowledge of the nuclear interactions and electromagnetic interactions, in this case in the rock above the detector. This is not straightforward due to the difficulty of obtaining geological data on the rock. Again fluctuations in the energy loss due to Bremsstrahlung radiation causes difficulties. The effect of this has been estimated by means of Monte-Carlo type simulations by several workers and the results are also discussed by Kiraly et al. Detailed knowledge of nuclear interactions is also lacking, especially at high energies, hence making spectrum derivations difficult.

Two recent surveys on the indirect measurements on the muon spectrum have been made by Ng et al. (1973) and Wright (1973). The results of these surveys are shown in figure 6.5, together with the present best fit spectrum, in the form of an integral spectrum multiplied by the momentum squared. The present spectrum appears

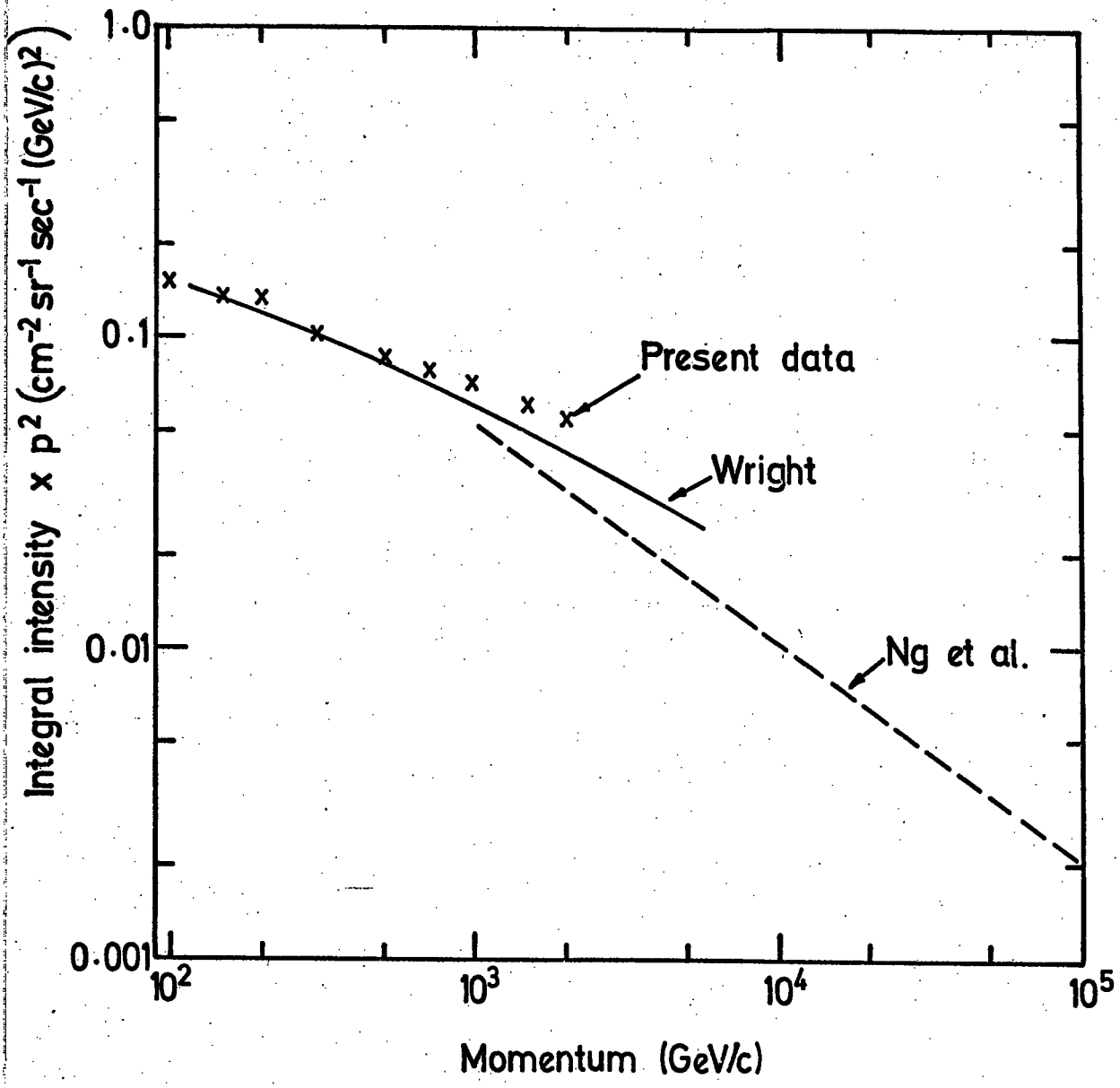

Figure 6.5. The results of two recent surveys on the results of indirect measurements of the muon momentum spectrum.

to give a higher intensity than the underground measurements from the survey of Ng et al. for muons with momenta greater than 300 GeV/c. The best fit value for γ is quoted as 2.69 $\pm$ 0.03 for energies greater than 300 GeV/c. This value of γ is somewhat higher than that predicted by the present results. The survey of Wright is chiefly concerned with the momentum range 5-1000 GeV/c and these results are in good agreement with the present results, giving a slightly higher absolute intensity than those of Ng et al.

6.6 THE CHARGE RATIO

The charge ratio calculated from the present data is shown in figure 6.6. Also shown in this figure is the data from some of the experiments previously mentioned in this chapter. The present data has large statistical errors, but the data is in good agreement with that of other workers (Ashley et al., 1975, Baxendale et al., 1975, Allkofer et al., 1971 (b)) and would appear to be constant over the momentum range 100-2000 GeV/c.

6.7 CONCLUSION

The comparisons with most of the other experiments, both direct and indirect, show that the value of γ obtained in the present experiment is smaller by approximately 2% to 4% excluding the previous results from MARS. The previous MARS data have been fitted to two production spectra, with two different values of γ for $E_\pi > 70$ GeV and $E_\pi < 70$ GeV. All other data has been fitted over the whole momentum spectra from energies of the order of 1 GeV/c and as such the low energy points will give much greater weight to any derived production spectra. Thus if there is indeed a change in slope in the production spectrum at approximately 70 GeV/c then data fitted over the whole momentum range from 5 to 1000 GeV/c will have larger values of γ than data fitted over the range 100 to 1000 GeV/c. It is also interesting to note

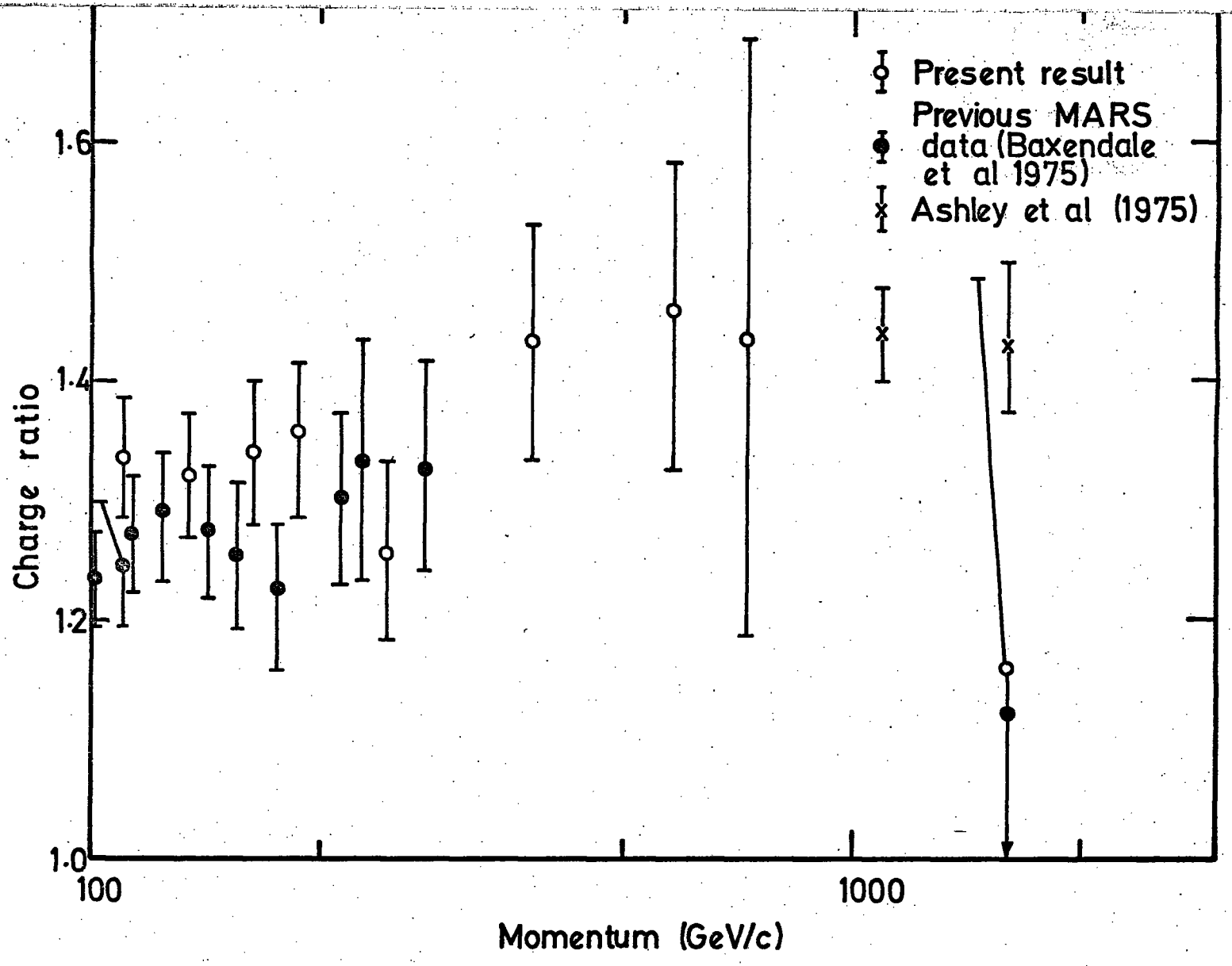

Figure 6.6. The charge ratio as obtained from some recent experiments.

that all the present experimental points above 700 GeV/c lie above the fitted spectrum. This would probably indicate an even smaller value of γ for the present experiment. It is difficult to compare data from other spectrographs due to large experimental errors on the data points above 100 GeV/c for the other spectrographs. The only data being of similar statistical accuracy to the present experiment is the spectrum of Burnett et al. obtained by combining the spectra at various angles.

It is also difficult to compare the data from indirect measurements of the spectrum since the difficulties involved in deriving such spectra from the data are great. It is concluded that more measurements are required using magnet spectrographs in the region 100-5000 GeV/c, yielding data points with more statistical accuracy. MARS is at present still collecting data and such data will provide more accurate measurements up to 3000 GeV/c.

CHAPTER 7

CONCLUSION

7.1 CONCLUSIONS

A short summary of the results obtained in the work is given here. The main conclusions drawn from the present results are that the slope of the pion production spectrum and the muon spectrum is flatter than has been suggested by other workers. This, it is concluded, is due to fits being made to the whole muon spectrum from momenta of approximately 7 GeV/c up to 1000 GeV/c. It is thought that this is incorrect and there appears to be a change of slope in the pion production spectrum at about 100 GeV/c. Thus the results of other workers are biased towards the slope below 100 GeV/c whereas the present experiment only uses data above 100 GeV/c. Thus the results of the present experiment support the previous results obtained using MARS (Ayre et al., 1975) in predicting a flatter production spectrum.

The absolute intensity of the present results are in agreement (within statistical accuracy) with the results of other spectrograph experiments. However the survey of Ng et al (1973) of indirect measurements gives a much lower absolute intensity above momenta of 1000 GeV/c. It is therefore concluded that more work is required to resolve these differences. The analysis of the remainder of the data obtained from MARS will improve the statistical accuracy of the present results, especially in the region above 1000 GeV/c.

7.2 FUTURE WORK

The MARS spectrograph is still collecting data which, as mentioned previously, will improve the statistical accuracy of the present results. The data is to be analysed in the same manner as described in this work. The amount of data collected to date will approximately

halve the statistical errors (see figure 5.2). Using these results it should be possible to determine a value for the K/π ratio which was not possible using the present data due to large statistical errors on all the data points.

For the purposes of this work many potentially useful events were rejected, and then corrected for in order to obtain the absolute spectrum. Such events include three and four tray fits with m.d.m.s for their particular tray combination above the smallest m.d.m. for a three and four tray fit. Thus if the expected number of each particular tray combination is predicted then some of these events can be used, thus decreasing the corrections which must be applied to the data to compensate for such rejected events. This was not possible in the present experiment due to the small numbers of events above 700 GeV/c in each tray combination. However with the new MARS data, the number of events should be increased fourfold and hence such a procedure as mentioned above should be possible to enable a more accurate determination of the spectrum to be made.

It may also be possible to extend the measurements above the theoretical m.d.m. of 3000 GeV/c by using the 'best fit' events, that is those events with low option fits to the tray data in each of the five trays. The m.d.m. for such events is higher than 3000 GeV/c. However the number of these events is very small and it is possible that too few events of this type may be collected to enable such a procedure to be used successfully.

ACKNOWLEDGEMENTS

The author wishes to thank Professor G.D. Rochester F.R.S. and Professor A.W. Wolfendale for the provision of the facilities for this work, and for their interest in the experiment, particularly to his supervisor Professor A.W. Wolfendale for his help and guidance given throughout the project.

The MARS group leader Dr. M.G. Thompson is sincerely thanked for his many helpful and useful discussions. Members of the MARS research group, in particular Dr. C.A. Ayre, Mr. J.M. Baxendale, and Dr. M.R. Whalley are thanked for their help both in discussion and running of the apparatus. In addition Dr. B.J. Daniel is thanked for his work in running the computer efficiently.

The members of the technical staff of the Physics Department are all thanked for their help, particularly Mr. K. Tindale, the group technician, and Mrs. A. Gregory for her patience in drawing many of the diagrams for this thesis.

The staff of the University Computer Unit are also thanked for the provision of the computing facilities.

The author is grateful to his wife for all her help in typing this thesis, drawing some of the diagrams and her constant encouragement throughout this work.

Finally the Science Research Council is thanked for providing a Research Studentship.

REFERENCES

Abdel-Monem, M.S., Benbrook, J.R., Osborne, A.R., Sheldon, W.A., Duller, N.M., and Green, P.J., 1973, P.I.C.C.R., Denver, 3, 1811.

Achar, C.V., Narasimham, V.S., Ramana Murthy, P.V., Creed, D.R., Pattison, J.B.M., and Wolfendale, A.W., 1965, Proc. Phys. Soc. 86, 1305.

Adair, R.K., 1974, Phys. Rev. Lett., 33, 115.

Allkofer, O.C., Dau, W.D., and Kokisch, H., 1970, Proc. 6th Interamerican Seminar on Cosmic Rays, La Paz, 937.

Allkofer, O.C., Carstensen, K., and Dau, W.D., 1971a), P.I.C.C.R., Hobart, 4, 1314.

Allkofer, O.C., Carstensen, K., Dau, W.D., Fahnders, E., Heinrich, W., and Jokisch, H., 1971b), P.I.C.C.R., Hobart, 4, 1319.

Allkofer, O.C., Carstensen, K., Dau, W.D., Jokisch, H., Frohlich, A., Seidman, A., and Yeiven, Y., 1971c), P.I.C.C.R., Hobart, 4, 1596.

Anderson, C.D., 1932, Science, 76, 238.

Appleton, I.C., Hague, M.T., and Rastin, B.C., Nucl. Phys., B 26, 365.

Ashley, G.K., 1975, Private Communication.

Aurela, A.M., and Wolfendale, A.W., 1967, Ann. Acad. Sci. Fenn., A 6, 226.

Ayre, C.A., and Thompson, M.G., 1969, Nucl. Inst. and Meth., 69, 106.

Ayre, C.A., 1971, Ph. D. Thesis, University of Durham.

Ayre, C.A., Hamden, M.A., Hume, C.J., Stubbs, F.W., Thompson, M.G., Wells, S.C., and Whalley, M.R., 1972a), Nucl. Inst. and Meth., 102, 12.

Ayre, C.A., Hamden, M.A., Hume, C.J., Nandi, B.C., Thompson, M.G., Wells, S.C., and Whalley, M.R., 1972(b), Nucl. Inst. and Meth.,102, 29.

Ayre, C.A., Baxendale, J.M., Hume, C.J., Nandi, B.C., Thompson, M.G., and Whalley, M.R., 1975(a), J. Phys. G. Nucl. Phys., 5, 584.

Ayre, C.A., Baxendale, J.M., Daniel, B.J., Goned, A., Piggott, J.L., and Thompson, M.G., 1975(b),Nucl. Inst. and Meth., 124, 335.

Baber, S.R., Nash, W.F., and Rastin, B.C., 1968, Nucl. Phys., B4, 539.

Barrett, P.H., Ballinger, L.M., Cocconi, G., Eisenberg, Y., and Greisen, K., 1952, Rev. Mod. Phys., 24, 133.

Baxendale, J.M., Daniel, B.J., Hume, C.J., Thompson, M.G., and Whalley, M.R., 1975, J. Phys. G. (in press).

Bothe, W., and Kolhorster, W., 1929, Zeits. Phys., 56, 751.

Bull, R.M., Nash, W.F., and Rastin, B.C., 1965, Nuovo Cim., 40 A, 365.

Burnett, T.H., Masek, G.E., Maung, T., Miller, E.S., Ruderman, H., and Vernon, W., 1973, P.I.C.C.R., Denver, 3, 1764.

Clay, J., 1932, Koninklijke Akadamie van Wetenschappen te Amsterdam, Proc. Sec. Sciences, 35, 1282.

Cocconi, G., Koerster, L.J., and Perkins, D.H., 1961, Lawrence Radiation Lab. High Energy Physics Study Seminars No. 28 pt. 2.

Conversi, M., and Gozzini, A., 1955, Nuovo Cim.,2, 189.

Cooke, W.J., Disney, M.J., and Taylor, D.J., 1969, Nature, 221, 525.

Duthie, J., Fowler, P.H., Kaddours, A., Perkins, D.H., and Pinkou, K., 1962, Nuovo Cim.,24, 122.

Erlykin, A.D., Ng, L.K., and Wolfendale, A.W., 1974, N.A.T.O. Institute Durham.

Feynman, R.P., 1969, Phys. Rev. Letts., 23, 1415.

Ginzburg, V.L., and Syrovatsky, S.I., 1964. "The Origin of Cosmic Rays" (London: Pergamon).

Hansen, J.S., 1975, Private Communication.

Hayman, P.J., and Wolfendale, A.W., 1962, Proc. Phys. Soc., 80, 710.

Hess, V.F., 1912, Phys. Zeitschr., 13, 1084.

Hume, C.J., 1975, Ph. D. Thesis, University of Durham.

Johnson, T.H., 1933, Phys. Rev. 43, 834.

Kiraly, E., Kiraly, P., and Osborne, J.L., J. Phys. A, 5 (1972) 444.

Kulikov, G.V., Fomin, Y.A., and Khristiansen, G.B., 1969, Zh. Eksp. Teor. Fiz. 10, 347.

Millikan, R.A., and Cameron. G.H., 1926, Phys. Rev. 28, 851.

Morrison, J.L., and Elbert, J.L., 1973, P.I.C.C.R., Denver, 3, 1833.

Nandi, B.C., and Sinha, M.S., 1972, J. Phys. A : Gen. Phys., 5, 1384.

Ng, L.K., Wdowczyk, J., and Wolfendale, A.W., 1973 (a), P.I.C.C.R., Denver, 3, 1781.

Ng, L.K., Wdowczyk, J., and Wolfendale, A.W., 1973 (b), Internal Communication, University of Durham.

Osborne, J.L., Palmer, N.S., and Wolfendale, A.W., 1964, Proc. Phys. Soc., 84, 911.

Rochester, G.D., and Butler, C.C., 1947, Nature (London), 160, 855.

Rossi, B., and Greisen, K., 1942, Rev. Mod. Phys., 13, 240.

Rossi, B., Rev. Mod. Phys., 20, 537.

Said, S.S., 1966, Ph. D. Thesis, University of Durham.

Skobelzyn, D., 1929, Z. Phys., 54, 686.

Smith, J.A., and Duller, N.M., 1959, J. Geophys. Res., 64, 2297.

Thompson, M.G., and Wells, S.C., 1972, Nucl. Inst. and Meth., 102, 35.

Thompson, M.G., and Whalley, M.R., 1975, J. Phys. G: Nucl. Phys., 1, 48.

Vernov, S.N., Khristiansen, G.B., Nechin, Y.A., Vedeneev, O.V., and Khrenov, B.A., 1966, P.I.C.C.R., London, 952.

Wells, S.C., 1972, Ph. D. Thesis, University of Durham.

Whalley, M.R., 1974, Ph. D. Thesis, University of Durham.

Wolfendale, A.W., 1973, Cosmic Rays at Ground Level, (Institute of Physics: London).

Wright, A., 1973, P.I.C.C.R., Denver, 3, 1709.

(P.I.C.C.R. = Proc. Int. Conf. on Cosmic Rays).